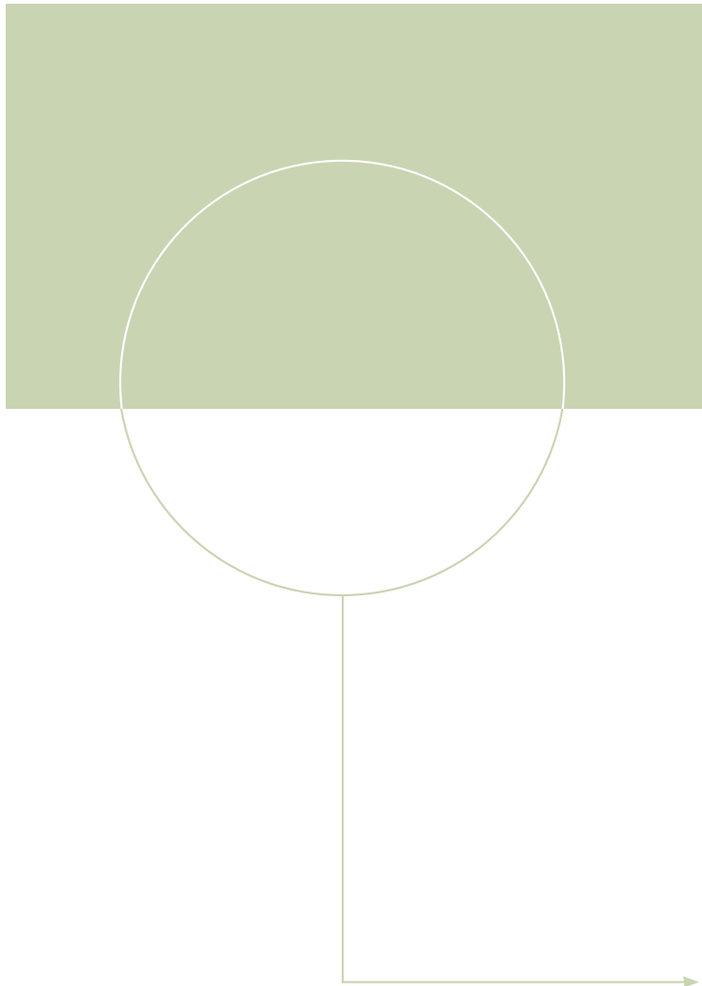

Master's thesis

2019

Ofeliya Ibrahimli

**NTNU**
Norwegian University of
Science and Technology
Faculty of Engineering
Department of Geoscience and Petroleum

Ofeliya Ibrahimli

# Time-shift analysis in the overburden and reservoir zones from 4D studies across the Norne field

June 2019

NTNU
Norwegian University of
Science and Technology

NTNU
Norwegian University of
Science and Technology

NTNU
Norwegian University of
Science and Technology

# Time-shift analysis in the overburden and reservoir zones from 4D studies across the Norne field

Ofeliya Ibrahimli

Petroleum Geoscience and Engineering
Submission date: June 2019
Supervisor: Kenneth Duffaut

Norwegian University of Science and Technology
Department of Geoscience and Petroleum

# Abstract

4D seismic is a powerful tool, mainly used for monitoring the changes in the reservoir and overburden zones that might occur due to hydrocarbon production or EOR-related changes. The observed changes on 4D seismic can be correlated with the data acquired from the wells and the analysis could be performed. Identification of hidden oil and gas pockets, pressure barriers and effects of water injection on 4D can be helpful in implementation in reservoir models and when planning new wells, thus, increasing well success rates and reducing the risks of well-drilling problems.

This master thesis is focused towards time-shift analysis in overburden and reservoir zones over Norne field, using time-lapse seismic dataset from 2001 and 2006. The main aim is to prove if quantified travel-time changes across overburden and within reservoir section correlate, appear consistent and are real and not random noise.

The data was analyzed using Method 1, Method 2 and cross-correlation technique. In Method 1, the seafloor is kept constant as a reference horizon and time-shifts and relative time-shifts are calculated from seafloor down to each interpreted horizon. In Method 2, the time-shifts and relative time-shifts are calculated from one interpreted horizon to another one. Cross-correlation technique was used to define the similarity between two seismic volumes and to inspect the reservoir and overburden zones. Overall, it could be concluded that the latter is best to use to examine the regional change in travel-time, whereas Method 1 and Method 2 are more convenient to observe local changes.

C-, E- and G- segments in Norne field were analyzed and it was presumed that more than one 4D effect (pressure and saturation changes) has an impact on the seismic response, which makes the interpretation of the time-shift behaviour more complicated. Decrease and/or increase of pore pressure, gas going out and coming back to oil, water injection effects in different segments of reservoir zone are affecting the velocities and, thus, time-shifts. These physical changes disturb the stress field of the rocks surrounding the reservoir interval and propagate to overburden and underburden, resulting in velocity and travel-time variations.

# Acknowledgements

This master thesis is written as part of the course TPG4925 - Petroleum Geosciences, Master's Thesis at the Norwegian University of Science and Technology (NTNU), Department of Geoscience and Petroleum.

I would like to express my utmost respect and gratitude to my supervisor Associate Professor Kenneth Duffaut for introducing me to the topic and guiding me through the final year of my study. His patience in explanations, constructive feedback and fruitful discussions helped in completion of this work. Also, I would like to thank PhD candidate in Geoscience, Dicky Harishidayat, for support in Petrel software. Thanks to Equinor and their license partners, and Center of Integrated Operations (IOC) at NTNU for providing the real field data and permission to use it. Finally, my endless gratitude goes to my parents and husband for giving me the opportunity to study abroad and constant support.

Trondheim, 18.06.2019

# Table of Contents

# List of Tables

# List of Figures

# Abbreviations

| | | |
|---|---|---|
| Symbol | = | definition |
| AVO | = | Amplitude Versus Offset |
| CMP | = | Common Mid Point |
| DHI | = | Direct Hydrocarbon Indicator |
| EOR | = | Enhanced Oil Recovery |
| Fm | = | Formation |
| GOC | = | Gas Oil Contact |
| GOR | = | Gas Oil Ratio |
| GIIP | = | Gas Initially in Place |
| HSE | = | Health, Safety, Environment |
| MD | = | Measured Depth |
| MSL | = | Mean Sea Level |
| NRMS | = | Normalized Root-Mean-Square |
| OWC | = | Oil Water Contact |
| OIIP | = | Oil Initially in Place |
| PDO | = | Plan for Development and Operations |
| QC | = | Quality Control |
| RKB | = | Rotary Kelly Bushing |
| $\mathrm{Sm}^3$ | = | Standard cubic meter |
| SRME | = | Surface Related Multiple Elimination |
| TDR | = | Time-Depth Relationship |
| TVD | = | True Vertical Depth |
| TWT | = | Two-Way Travel-time |

Chapter 1

# Introduction

Pressure depletion as a result of hydrocarbon production will create distortion in stress and strain fields of the rock material both within the reservoir interval and outside of it. Decrease in pore pressure in reservoir rock will increase the effective stress, resulting in shrinkage of the rock, which in turn leads to compaction of the reservoir. This compaction may cause the extension of the overburden and the subsidence at the seabed or land surface (Fjær et al., 2008). The velocity of seismic waves propagating through these intervals is also altered due to changes in stress and strain fields and travel-time is also affected by the variations in layer thicknesses (Hatchell and Bourne, 2005b).

Travel-time changes that originate due to increased pore pressure will lead to velocity decrease and increase in travel-time. Travel-time changes that originate due to pressure depletion have different responses inside and outside of the reservoir. The decrease in reservoir layer thickness and the corresponding increase in velocity of seismic wave will cause reduction in travel-time within the reservoir. However, outside of the produced reservoir, the rock is stretched, which results in increased thickness and lower velocity. This in turn yields increases in travel-time (Hatchell and Bourne, 2005b).

The degree of reservoir compaction depends largely on the type of rock material constituting the reservoir zone and the amount of reservoir pressure depletion. For example, compaction of reservoir sections, which consist of sandstone generates smaller times-shifts than that of chalk, since the rock stiffnesses are different. For this reason it is harder to observe travel-time changes in sandstone reservoirs than in chalks (Røste et al., 2015). Overburden time-shifts induced by reservoir compaction are more visible in chalk fields as well. Fayemendy et al. (2012) observed overburden time-shifts in some places at Snorre field and 1D simulation model was built in order to investigate the reasons for time-shift presence. The initial assumption was that the overburden time-shifts are the result of reservoir compaction or gas exsolution from the water leg, nevertheless, they were not built into the model and could not justify the nature of time-shifts.

Since compaction of the reservoir zone can result in seabed subsidence which in turn may damage casing and tubing it is necessary to be aware of these processes in time. It was documented by Barkved and Kristiansen (2005) that at the Vallhall field the seabed

subsidence value is more than 5.4 m and the subsidence is growing for 0.25 m every year. The identification of reservoir compaction and its consequent influence on overburden changes and seabed subsidence is important for a number of reasons described below (Røste et al., 2015):

- Delineating reservoir compaction zones provides information about depletion which is helpful in well planing
- Reservoir modelling which includes reservoir compaction may help in proper field development and future improvement of recovery factor
- Detecting compaction of the reservoir or subsidence at the seabed helps to avoid health, safety and environmental problems (HSE), such as flooding in land operations or platform safety concerns in offshore production

Time-lapse seismic, also known as 4D seismic, is a powerful tool used by the oil industry to monitor overburden and reservoir changes and they are recorded either as travel-time changes or amplitude changes. The major benefit of time-shift measurement is that it detects both velocity and thickness changes within the layer of interest (Røste et al., 2006) and gives a direct quantitative result by being proportional to the change in pay thickness (Landrø et al., 1999). Guilbot and Smith (2002) conducted a 4D study over Ekofisk field and detected 12-16 ms time-shift between 1989 and 1999. These time-shift were associated with compaction values of 6 m for the reservoir chalk formation. 4D tomographic inversion method was used to separate velocity and thickness changes by implementing the velocity-porosity relationship for the reservoir chalk layer. Later, Landrø and Stammeijer (2004) introduced two new techniques for detecting reservoir compaction and velocity change without necessity of using empirical relationship, such as velocity-porosity relationship. One technique is related to measured seismic prestack travel-time changes, another is based on postack travel-time and amplitude changes. The error in their results is linked to the uncertainties in travel-time and amplitude measurements, which in turn are directly linked to the quality and repeatability of 4D seismic data. Mathematically, the relative time-shift for a single layer may be expressed as the difference between fractional changes in thickness and velocity (Equation 1.1). Here layer thickness and velocity are assumed to have very small changes, such that $\triangle z/z \ll 1$ and $\triangle v/v \ll 1$ (Landrø and Stammeijer, 2004)

$$\frac{\triangle t}{t} \approx \frac{\triangle z}{z} - \frac{\triangle v}{v} \tag{1.1}$$

where $t$ is defined as vertical two-way travel-time, $z$ is thickness and $v$ is vertical P-wave velocity.

Another important factor in 4D seismic reservoir monitoring and AVO is the seismic response to fluid saturation. Rocks saturated with less compressible (reciprocal of bulk modulus) fluids show higher P-wave velocities and impedances. The compressibility of gas is higher than that for oil and water, and the compressibility of oil, in turn, is higher than that for water. For instance, in a water-driven process, water displaces oil and the water saturation increases. This will lead to increase in P-wave velocity and therefore

travel-time decreases. Temperature, also, has an impact on seismic properties. As temperature increases, oil viscosity decreases, loosening up the grains of the rock, so that the bulk modulus decreases. This results in velocity decrease, and, thus, travel-time slows down (Wang, 2001).

This master thesis is focused towards time-shift analysis across the Norne field using time-lapse seismic data acquired in 2001 and 2006. The main objective is to prove if quantified travel-time shifts across the overburden and within the reservoir section correlate, appear consistent and are real and not random noise. The first challenge is to accurately identify and interpret formations of interest in highly faulted reservoir zone in Norne field, followed by interpretation of formations located in overburden zone. The next step is to calculate time-shifts and relative time-shits for all interpreted formations using two methods with different input parameters. In Method 1 seabed is kept constant and the calculation is performed from seabed down to each interpreted horizon. Method 2 calculates the incremental change between individual horizons. Also, two surveys (2001 and 2006) were cross-correlated to reveal the discrepancies between seismic traces and observe the changes in travel-time regionally. The generated time-shift maps using this cross-correlation technique will give an image of what kind of 4D effects had an impact on reservoir and overburden zones. The areas where wells were drilled in different segments of Norne field should be inspected carefully.

Chapter 2

# Geological Setting

## 2.1 Area of investigation: Norne field

The Norne field is located in the southern part of the Nordland II area in the Norwegian Sea, blocks 6608/1 and 6608/1 (Figure 2.1). The distance to shore is about 200 km, and the water depth is ranging between 370 and 390 meters. The field was discovered by Statoil (present Equinor) exploration well 6608/10-2 in 1991 and further appraised by well 6608/10-3 in 1993. The license partners are Petoro AS and Vår Energy AS companies (Figure 2.2). From the results of these two wells, it was decided to examine the economical potential of the field and to prepare a Plan for Development and Operations (PDO) (Gjerstad et al., 1995).

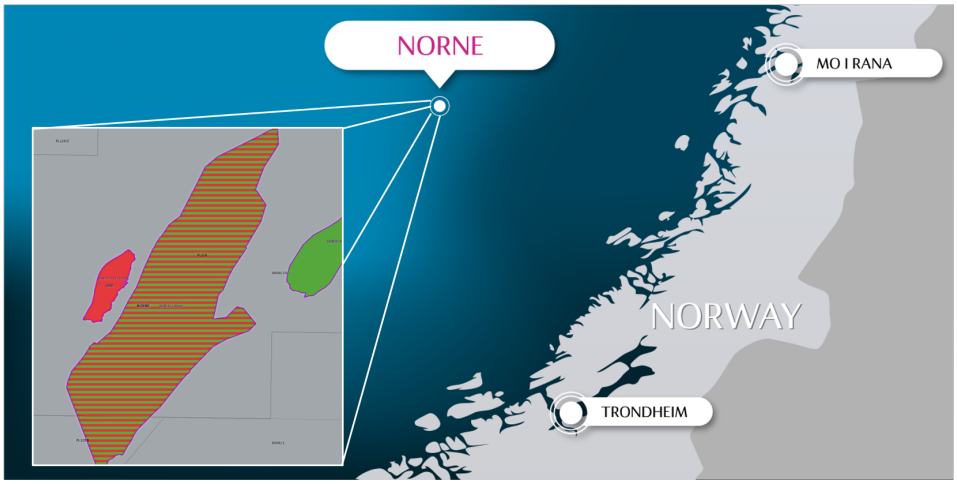


**Figure 2.1:** Location of the Norne field (NPD factpages, 2019; Equinor ASA, 2019)

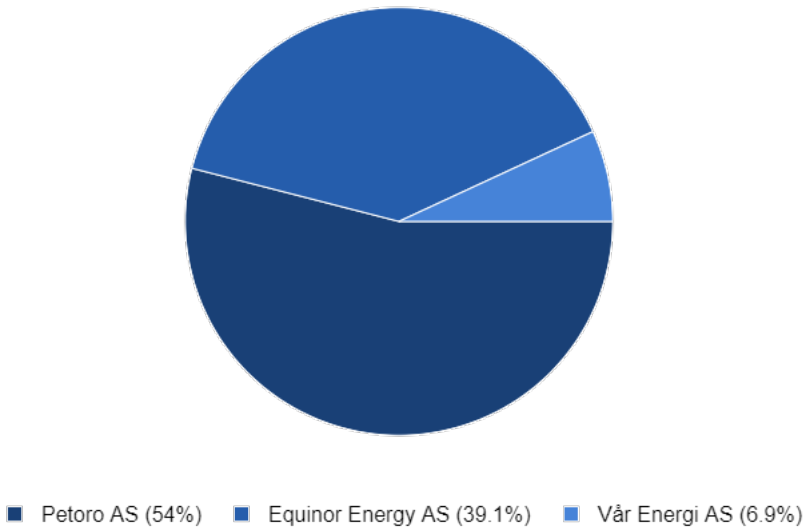


**Figure 2.2:** Equinor Energy AS is operator of the Norne Field with 39.1% interest. Petoro AS and Vår Energy AS are the partners with 54% and 6.9% interest (Norwegian Petroleum, 2019)

Table 2.1 shows the recoverable reserves of hydrocarbons, produced volume of hydrocarbons, remaining and original in place volumes in Norne field. The in-place volume estimates are 157 $\mathrm{MSm}^3$ oil in place (OIIP) and 29.8 $\mathrm{BSm}^3$ gas in place (GIIP). Until 2018, almost 90.8 $\mathrm{MSm}^3$ of oil and 7.5 $\mathrm{BSm}^3$ of gas have been produced. Total recoverable reserves estimates from January 2018 are 93.82 $\mathrm{MSm}^3$ Oil and 12.81 $\mathrm{BSm}^3$ gas. Remaining recoverable reserves are 3.04 $\mathrm{MSm}^3$ oil and 5.35 $\mathrm{BSm}^3$ gas respectively (NPD factpages, 2019). This gives an estimated oil recovery factor of 59.7%, which makes Norne one of the highest recovery fields on the Norwegian continental shelf.

| | Oil [million $\mathrm{Sm}^3$] | Gas [billion $\mathrm{Sm}^3$] |
|---|---|---|
| Orig. recoverable | 93.82 | 12.81 |
| Remaining | 3.04 | 5.35 |
| Produced | 90.78 | 7.46 |
| Orig. inplace | 157.00 | 29.80 |

**Table 2.1:** Hydrocarbons volume in the Norne field (NPD factpages, 2019)

### 2.1.1 Geological Information

The reservoir interval in the Norne field consists of formations which belong to Båt and Fangst Groups deposited during Lower to Middle Jurassic period. The formations comprising Båt Group are Tilje and Tofte formations, whereas formations from Fangst Group are Ile, Not and Garn (Figure 2.3) (Verlo and Hetland, 2008).

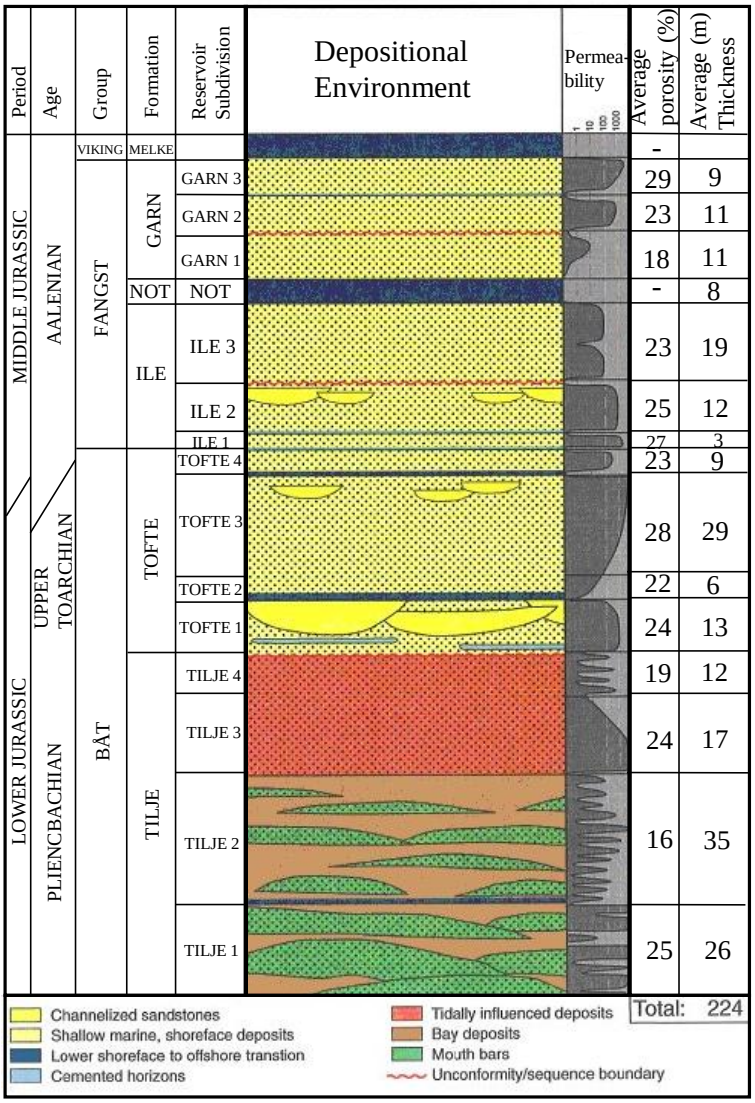


**Figure 2.3:** Stratigraphical subdivision of the Norne reservoir (Statoil, 2001)

The reservoir sandstones, buried at depth of 2500-2700 m, contain fine-grained and well to very well sorted sub-arkosic arenites. The main process which reduces the reservoir quality is mechanical compaction, however most of the sandstones are good reservoir rocks with porosity ranging from 25 to 30% and permeability 20-2500 mD. The whole thickness of the reservoir, from Top Garn to Top Åre Formations is different across the field because of increasing erosion to the north. In the southern part it reaches the thickness of 260 m, whereas in the northern part it decreases to 120 m (Figure 2.6) (Verlo and Hetland, 2008).

Two main source rocks are Spekk formation of the Late Jurassic and Åre formation of Early Jurassic age. The cap rock sealing the reservoir and preventing hydrocarbons from escaping is Melke formation. Another formation which acts as a sealing layer and blocks the communication between two hydrocarbon bearing formations (Garn and Ile) is Not formation (Verlo and Hetland, 2008).

Figure 2.4 gives an overview of the lithostratigraphy of the Norwegian Sea shelf area.

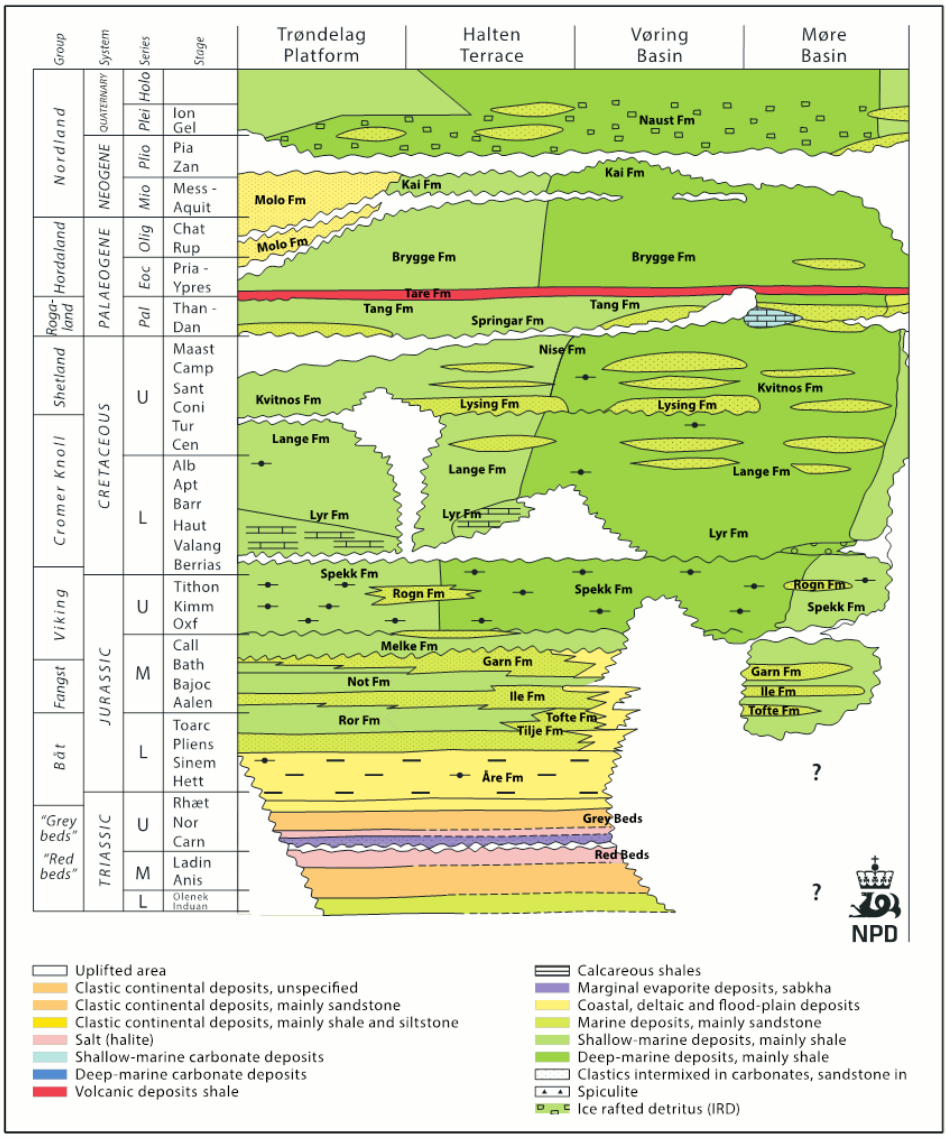


**Figure 2.4:** Lithostratigraphic chart of the Norwegian Sea shelf area (NPD factpages, 2019)

The Norne field is formed by horst structure, approximately 9x3 km, and is comprised by two compartments, namely the Norne Main Structure (Norne C-, D- and E- Segment) containing 97% of initial hydrocarbon reserves, and the North-East Segment (Norne G-Segment) with the remaining 3% of the reserves (Figure 2.5) (Statoil ASA, 2004).

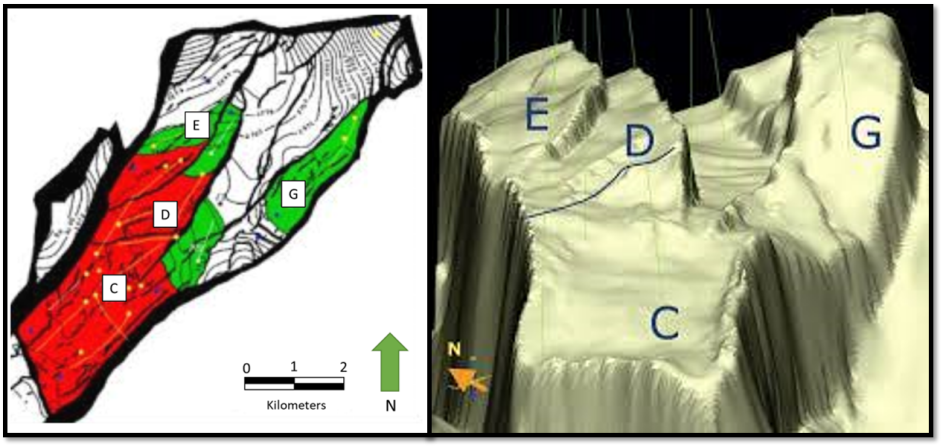


**Figure 2.5:** Norne horst block with four segments in cross-section top view on the right and 3D view on the left.The red area represents the gas cap overlaying the oil, while the green stands for oil (Statoil ASA, 2004)

#### 2.1.1.1 Norne Stratigraphy and Sedimentology

***The Garn Formation*** (Bajocian to Bathonian) is interpreted in terms of deposition and progradation of braided delta lobes over the mud dominated Not Formation. The Garn Fm is present over the central part of the Halten and Dønna Terrace and the Trøndelag Platform, except over structural highs (Nordland Ridge) where the entire formation may be eroded. Depositionally, the sandstones of the Garn Fm are interpreted in terms of a wave-dominated sediments deposited towards the south and the north. The formation consist of medium to coarse-grained, moderately to well-sorted sandstones with the presence of mica-rich zones. This formation is divided into three reservoir zones. Garn 1 is a sandstone unit which is coarsening upwards, the lower part is muddy and bioturbated, because it is the continuation of the Not Fm. On the contrary, the upper part has increased sand content, which includes ripple lamination and thin layer of coarser grained sandstones. The deposits of this bed are considered as beach deposits from the maximum regression period. Garn 2 is a deposition of transgressive environment and consist of fine grained sandstones, which are either bioturbated or laminated. At the Top of formation a calcareous cemented sandstone unit is found, which represents maximum flooding surface. This layer is predicted to be continuous across the field and behave as a local barrier to vertical fluid flow. The upper part of Garn 3 consist of low angled cross-bedded and fine-grained sandstones. The Top of Garn 3 is made up of coarse graided bed, which is characteristic for erosional surface from maximum regression (Dalland et al., 1998; NPD, 2019).

***The Not Formation*** (Aalenian to Bajocian) is developed as a mudstone dominated se-

quence coarsening upwards into bioturbated fine-grained sandstones deposited in lagoons or sheltered bays. The coarsening upwards indicates deposition during regression. The Not Fm thickness is around 10 m. The mudstones of Not Formation are acting as a seal and prevent reservoir communication (Dalland et al., 1998).

***The Ile Formation*** (Upper Toarcian to Aalenian) is defined at the base of generally upwards coarsening sequence from siltstone to sandstone, often associated with more carbonated beds. The sediments of Ile Fm are deposited in tidal or shoreline environments. The upper boundary is defined by the mudstones of the Not Fm. The Ile Fm is present over most of Haltenbanken, with a general thickening to the west and marked thinning to the northeast. The thickness of Ile Fm is ranging between 30-60 m. The Ile Formation consist of three reservoir zones. Ile 1 and Ile 2 both consist of fine to very fine grained sand which is coarsening to the north. Ile 3 is upward fining bioturbated bed which is located above the sequence boundary. The Ile 1 and Ile 2 are separated by a calcareous layer, which is most likely the results of flooding events during regressive period. Ile 2 and Ile 3 are divided by a sequence boundary, indicating the change from regressive to transgressive environment. The general quality of Ile formation is good in regressive depositions, however the properties are decreasing towards the top of the formation (Dalland et al., 1998; Verlo and Hetland, 2008).

***The Tofte Formation*** (Pliensbachian to Toarcian) is composed of moderately to poorly sorted coarse-grained sandstones which were deposited by eastwards prograding fan deltas reflecting tectonic uplift to the west. The sandstones wedge out eastwards and interfere with the Ror Formation. Tofte Fm is found only on the western part of Halten terrace with the mean thickness of 50 m. The Tofte Formation is divided into three reservoir zones. Tofte 1 is composed of medium to coarse grained sandstones with steep dipping lamina, which suggest that the source area for the sediments was located to the north or northeast of the field. The distribution of Tofte 1 is limited in the east-west or northeast-southwest direction. Tofte 2 is muddy, fine-grained sandstone unit with the evidence of bioturbation. Floating clasts can be found in the lowermost part of the section, which is coarsening upward. Tofte 3 comprises very fine to fine grained sandstone, where almost none of the depositional structures are visible because of bioturbation. There is a coarser grained bed representing a sequence boundary at the top of the unit, which is the Upper Toarcian-Aalenian boundary (Dalland et al., 1998; Verlo and Hetland, 2008).

***The Ror Formation*** (Pliensbachian to Toarcian) is defined by the abrupt transition from the sandstones in the Tilje Fm into mudstones, indicating an erosive base. The formation does not occur over large areas on the Nordland Ridge due to erosion and non-deposition. The thickness is not exceeding 8.5 m. The depositional environment was most likely in a lower shoreface with low sediment supply. At the top of the formation a calcareous shells has been dissoleved and cemented, creating a calcareous cemented unit, which considered as a barrier to vertical fluid flow (Dalland et al., 1998).

***The Tilje Formation*** (Sinemurian to Pliensbachian) is defined at the top of a mudstone interval and consists of more sandy sediments deposited in near shore to intertidal environments with increased thickness of individual sandbodies. The source of the sediments was located west of the Norne area (Swiecicki et al., 1998). The thickness of the formation is decreasing to the north because of decreased subsidence rate during deposition, along with increased erosion to the north/northeast at the base of the overlying Tofte Formation. An

unconformity was found at the top of the Tilje Formation, which is the result of the uplift followed by subaerial exposure and erosion. It defines the clear change from heterolitic sediments of the Åre and Tilje Formations into thicker marine sandstones of the overlying formations. The thickness of the formation is in the order of 100-150 m. The Tilje Formation is divided into four reservoir zones based on biostratigraphic events and similarities in log pattern. Tilje 1 is believed to consist of two sequences of sand that is coarsening upward and a more massive sand at the top. Tilje 2 has a heterolitic composition consisting of sandstone layers of variable thicknesses, heavily bioturbated shales, laminated shales and conglomeratic beds. Tilje 3 consists of fine grained sand which has a low degree of bioturbation. Tilje 4 is a fine grained, bioturbated and muddy sandstone in the lower parts, while upper parts have conglomeratic beds interbedded with thin sandstone and shale layers (Verlo and Hetland, 2008).

***The Åre Formation*** (Rhaetian to Pliensbachian) is the lowest formation within Båt Group and represents delta plain deposits (swamps and channels) at the base with up to 8 m thick individual coal seams. Mainly consist of channel sandstones which are 2-10 m thick and alternating with mudstones, shales and coals. Generally, where the coal bearing sequences are thinner, the sandstones are coarser grained. The thickness of the Åre Fm varies between 300 to 500 m, with a maximum thickness of 780 m in the eastern part of the Halten Terrace (Heidrun area). (Dalland et al., 1998; NPD, 2019)

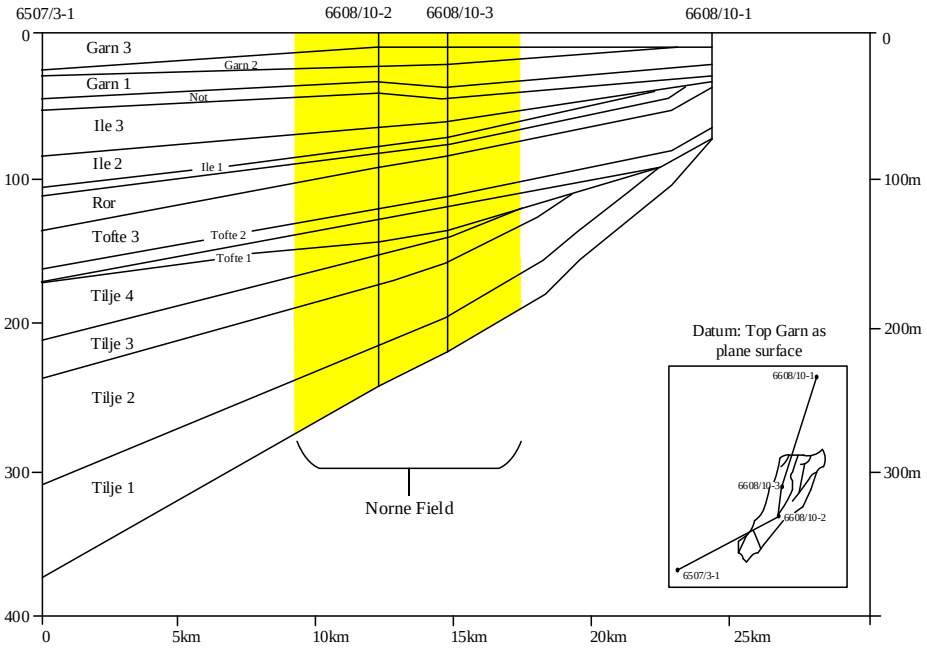


**Figure 2.6:** Cross-section through reservoir zone isochores. Yellow highlighted area indicates location of the Norne field. Note the truncated Ile and Tilje Formations due to erosion (Verlo and Hetland, 2008)

#### 2.1.1.2 Reservoir Communication

Two types of barriers, such as structural and stratigraphic, affect the vertical and lateral flow within the reservoir in the Norne field. Faults which are related to structural barriers can be seen and interpreted on seismic. The sealing major faults which extend over the whole reservoir thickness are considered as traps and hold the hydrocarbons in place. However, if it is intra-reservoir sealing fault (fault displacement is less than the reservoir thickness) it impacts and restricts the reservoir communication.

Stratigraphic barriers are found within the field in the Tofte, Ile and Garn formations. Three continuous calcareous cemented layers act as barriers to vertical flow. Their thickness and lateral extent are evaluated using cores and logs and varies from 0.5 to 3 meters. Also, Not formation with the thickness of 7-10 m affects the vertical and lateral flow. All barriers which block the reservoir communication are described below (Figure 2.3) :

- Garn 3/ Garn 2 - Carbonated cemented layer at top Garn 2
- Not Formation - Claystone Formation
- Ile 3/ Ile 2 - Carbonate cementations and increased clay content at base Ile 3
- Ile 2/ Ile 1 -Carbonate cemented layers at top Tofte 4
- Tofte 2/ Tofte 1 - Significant grain size contrast
- Tilje 3/ Tilje 2 - Claystone Fromation

### 2.1.2 Wellbores and Drainage Strategy

Different drive mechanism have been evaluated for the Norne field, which include (Gjerstad et al., 1995):

- Pressure depeltion
- Gas injection
- Water injection
- Combined gas/water injection

The main purpose of such evaluations have been to create a drainage strategy which optimized the ultimate recover and maximized the net present value of the field development (Gjerstad et al., 1995).

The Norne Field is being developed with a floating production and storage vessel, which is connected to six subsea wellhead templates named B, C, D, E and K, as seen in Figure 2.7. The K template has 4 slots available, 3 of them is used for production and 1 for injection or production. Oil was produced from all 12 slots in 2006, and all 8 injection wells were used for water injection. Nowadays, the field is developed with horizontal producers. The initial vertical producers, which were drilled to accelerate the build-up of well potential until plateau production was reached, have been sidetracked to horizontal producers.

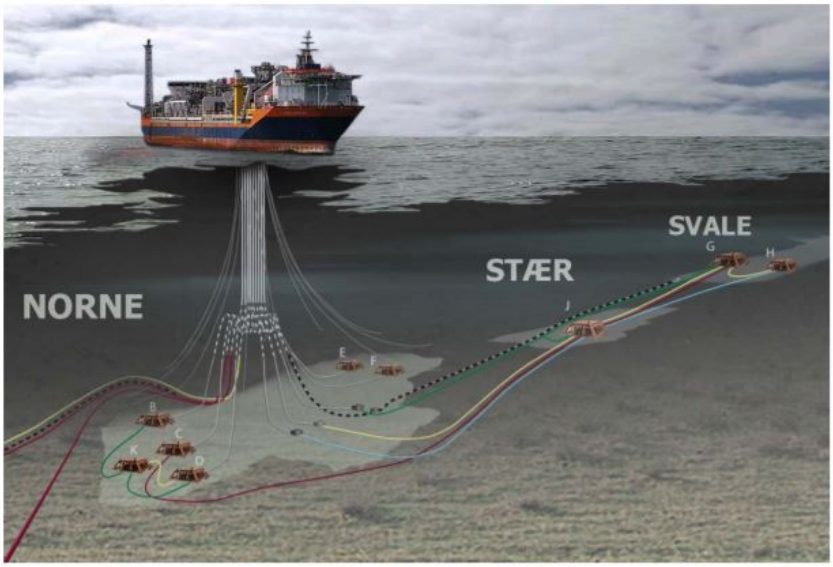


**Figure 2.7:** The development of the Norne field with the storage vessel and six subsea wellhead templates (Statoil ASA, 2004)

The initial strategy to maintain reservoir pressure was to re-inject produced gas into the gas cap and water into the water zone Figure 2.8. But since the gas cap had high pressure and was sealed off by the Not formation, the gas was injected into the water zone and the lower part of the oil zone. This lead to more complicated and uncertain prediction of gas flow in the reservoir. A higher GOR than expected caused the production to be restricted by gas handling capacity. It was decided to start gas export in order to obtain a balanced gas- and water injection strategy, and prevent further increase in GOR.

Also the drainage strategy supposed to be converted from vertical to flank sweep, because the vertical communication in the Norne reservoir is poor. It was achieved by locating the water injectors towards the flanks. In addition to that good areal distribution of the water injectors should be considered in order to maintain a steady rise of the water level and hence good areal sweep. The water was injected into the lower part of the oil zone from Tilje 3 up to Ile 3. Since Tilje 1 consist of unconsolidated sand and is located below tight, laterally extensive shale in Tilje 2, it is not suited for water injection.

In total 58 wells were drilled in the Norne field, but only 3 of them are used in this thesis and described below:

- Well 6608/10-2 was the first exploration well that discovered oil and gas in the Norne field in 1991 and is located in segment C. The goal was to test the hydrocarbon potential of the Fangst Group of Middle Jurasssic age. It was planned to drill a near to vertical well into the rocks of Triassic age at total depth of 3225 m. While drilling it was discovered that the Triassic Formations were located deeper than expected and the total depth of the hole ended at 3678 m. Oil and gas were encountered in both the Båt and Fangst Groups from Lower and Middle Jurassic. The hydrocarbon

column was 135 m, out of which 110 m was oil and the rest was overlying gas cap. Electric log data and FMT pressure plot revealed the fluid contacts positions: GOC at 2605 m and OWC at 2713.5 m. The well was permanently plugged and abandoned on 1992. (Statoil, 1992)

- The next exploration well 6608/10-3 was drilled in the Norne field in 1993 and is located in segment E. The objective was to evaluate the accumulation of oil in the Båt and Fangst Groups in the Northern Fault Block in the Norne field. The total depth reaches the Lower Jurassic Formation (2921 m). Hydrocarbons were found both in Båt and Fangst Groups. GOC in this well is at 2598.5 m and OWC is at 2713 m. The well was suspended as an oil and gas appraisal well in 1993. A re-entry of the well was performed in 1995, and the well was permanently plugged and abandoned as an appraisal well later that year. (Statoil, 1993)

- Well 6608/10-F-1-H was the fourth water injector and drilled in the northern part of the Norne E-segment. This well was drilled vertically through Garn, Ile, Tofte, Tilje and Åre Formations. Injection started in 1999 and it was designed to inject water in the water leg in the northern part of the field. Pressure testing from the well has proved good communication between Ile and Tofte (Verlo and Hetland, 2008)

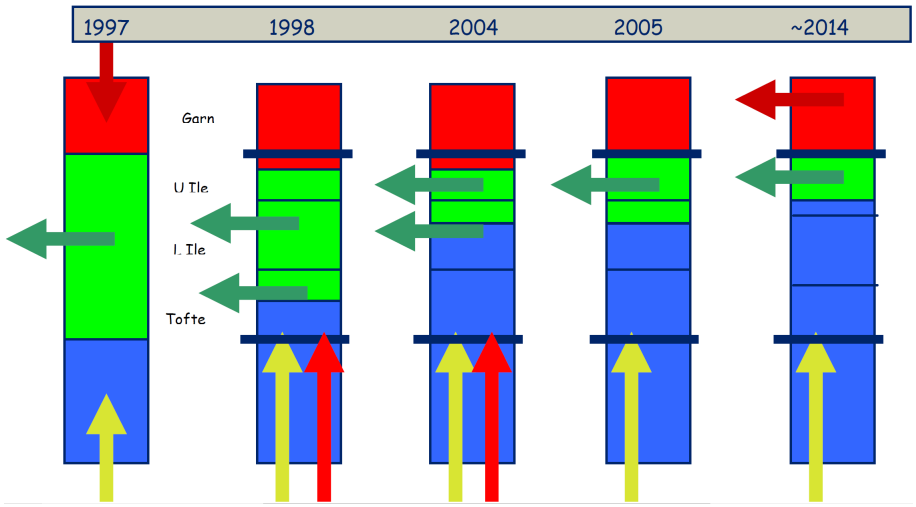


**Figure 2.8:** Drainage strategy of the Norne Field. Vertical arrows represent injection streams, horizontal arrows represent production streams. Blue stands for water, green = oil, red = gas (Statoil ASA, 2006)

### 2.1.3 Time-lapse seismic over Norne field

Overall, 5 seismic surveys were conducted over the Norne field. The main objective of 4D program across the Norne field was to identify and map the displacement of fluid contacts in the reservoir after almost two years of production and to collect fluid and rock properties information to understand the variations in reservoir interval (Goto et al., 2004). In this master thesis the 4D seismic is used to perform time-shift analysis and to monitor the behaviour of reservoir and overburden zones due to production related events, such as changes in pore fluid type, localized compaction or stretching and fracturing and changes in temperature and pressure. The 2001 seismic dataset is used as a baseline survey and 2006 seismic dataset is the monitor survey.

#### 2.1.3.1 Acquisition

The first seismic survey was acquired in 1992 using a dual source and three streamers separated by 100 m. The next four monitor surveys were collected with WesternGeco Q-marine system, which helped to precisely locate the streamers for acquiring reliable repeat surveys (Statoil ASA, 2006). A single source and six steerable streamers separated by 50 m were used for these surveys.

The first Q-survey (ST0113) was shot in 2001, considered as a time-lapse survey and compared to a dataset from 1992. Also it was the base Q-survey and all the following surveys repeated its geometry with maximum possible accuracy (Osdal et al., 2006). Second survey (ST0305), covered 85 $\mathrm{km}^2$ and was acquired in 2003. Year later, in 2004 third survey (ST0409) was shot and covered larger area (146 $\mathrm{km}^2$) (Figure 2.9). The fourth Q-marine survey (ST0603) was acquired in 2006. In all years, several undershoot lines were acquired to generate coverage beneath the Norne production vessel. The same undershoot vessel and source were used in 2001 and 2003, but a different one in 2004 and 2006. All these vintages allowed to perform 4D study and identify time-lapse changes over the Norne field (WesternGeco, 2007).The acquisition parameters for all the seismic surveys can be found in Figure 2.10.

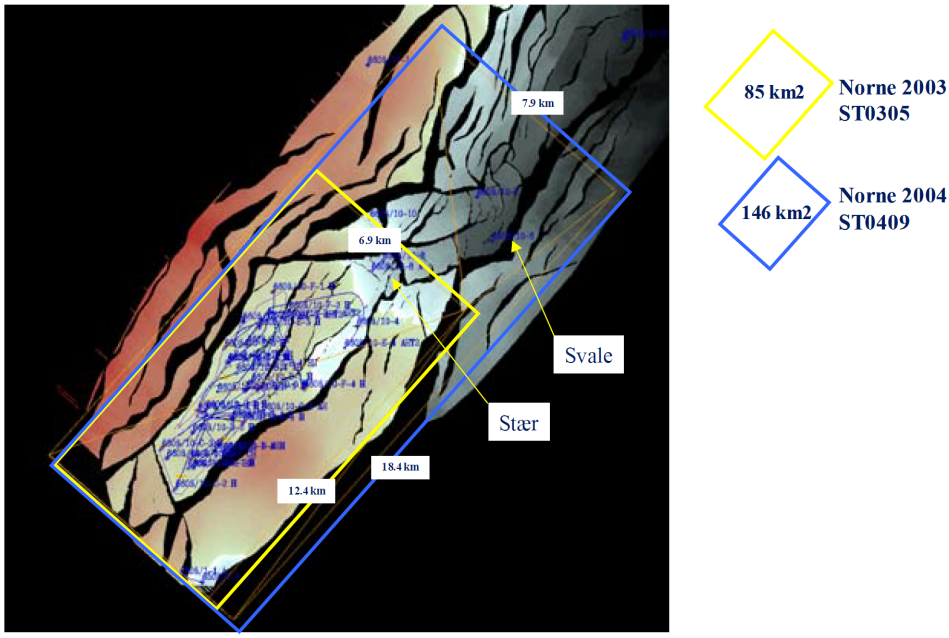


**Figure 2.9:** Seismic survey areas (2003,2004) in the Norne Field (Statoil ASA, 2006)

| | | | | |
|---|---|---|---|---|
| **Company** | WesternGeco | **Vessel** | | Geco Topaz |
| **Survey date** | August/Sept. 2001, June 2003, July 2004, 2006 | **Survey type** | | 3D |
| **Instruments** | Triacq 5 | **Tape format** | | SEG-D |
| **Filter settings** | **High cut** | 200 Hz | **Slope** | |
| | **Low cut** | 3 Hz | **Slope** | |
| **Record length** | 6144 ms | **Sample rate** | | |
| **Timing delay** | 64 ms | **Filter delay** | | |
| **Source array** | 1 x 5085 cu.in. airgun array, operating at 2000 psi | | | |
| **Source depth** | 6 m | **Shotpoint interval** | | |
| **Receiver array** | 6 x 3200 m streamer, 240 groups per streamer | | | |
| **Cable depth** | 8 m | **Group interval** | | |
| **Inline offset** | 122 m | | | |
| **Source separation** | n/a | **Cable separation** | | |
| **Configuration** | 254 trace, 64 fold, 6 lines per boat pass, 25 m line spacing | | | |
| **Polarity convention** | Positive pressure at hydrophone recorded as negative number | | | |

**Figure 2.10:** The acquisition parameters for the ST0113 (2001), ST0305 (2003), ST0409 (2004), ST0603 (2006) surveys (WesternGeco, 2007)

#### 2.1.3.2 Processing

The processing algorithms should be tested on all seismic vintages available over the Norne field in order to analyze and compare 4D difference displays (Osdal et al., 2006). The pre-stack and post-stack portions of the processing flow which was applied to 2006 seismic survey can be found in Figure A.2 and Figure A.1.

During acquisition of the baseline survey in 2001 two adjacent swaths were repeated. By analyzing the data it was observed that the 2001 seismic dataset could be closely repeated and by applying deterministic processes the results will contain low 4D noise levels. While testing, the NMRS value was calculated and showed good repeatability level with the number of 13%. NRMS (normalized Root-Mean-Square) is the parameter that helps to estimate seismic repeatability between different surveys and will be discussed in details in section 3.1. This results revealed that the monitor survey can be processed independently of the baseline survey, which accelerated the delivery of 4D processing (Goto et al., 2004).

In Figure 2.11 the effect of Radon and tau-p deconvolution processing methods can be seen on 4D data. This step helps to clear the multiples, however it also disrupts the effect of rising OWC. Also, the data should undergo multiple attenuation and several passes of Radon deconvolution because a lot of diffracted multiples are present in the Norne data. The effective solution which removed the multiples and preserved the 4D signal was to apply 2D SRME, even though it is adaptive process (Figure 2.11 (c)) (Osdal et al., 2006).

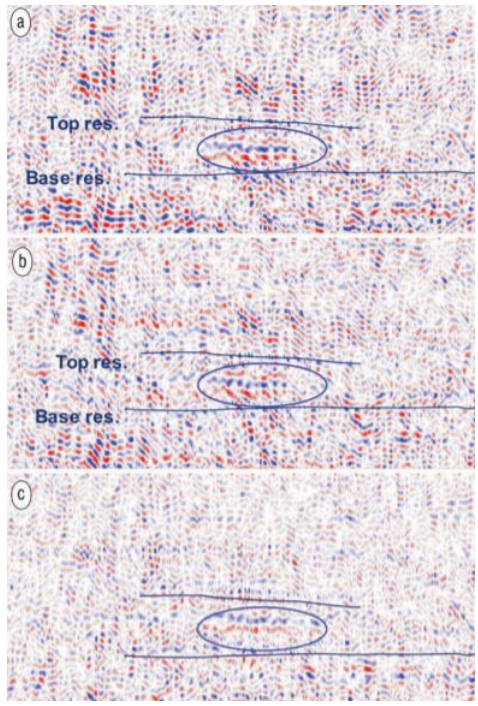


**Figure 2.11:** (a) Radon stack; (b) Radon and tau-p deconvolution; (c) Radon and 2D SRME. Blue circle indicates the 4D effect of a rise of the OWC (Osdal et al., 2006)

Chapter 3

# Basic Theory

## 3.1 Introduction to 4D seismic analysis

4D seismic, also known as time-lapse seismic or repeated seismic, is a term used to describe a seismic data set that is acquired over the same area or field at different points in time. The main purpose is to monitor the changes in the reservoir and/or overburden intervals that might occur due to hydrocarbon production or enhanced oil recovery-related (EOR) changes, such as injection of water/gas, steam, etc., into the reservoir . Also, there are other applications of time-lapse seismic listed below (Landrø, 2015):

- monitoring the underground storage of $CO_2$
- monitoring seasonal changes in the near-surface layers
- mapping hidden oil and gas pockets in reservoir
- assessing the impact of earthquakes, volcanoes and landslides
- monitoring and separating saturation and pore pressure changes
- identifying and mapping the displacement of OWC or GOC

When the hydrocarbons are produced from the reservoir interval, the parameters such as pore pressure, fluid saturation, temperature and layer thickness (compaction or stretching) are mostly affected and changed. During 4D studies the link between these reservoir parameters and seismic parameters (usually velocity and density) is established by applying knowledge from rock physics discipline. Theoretical rock physics models and laboratory experiments are used as an input to 4D seismic analysis (Landrø, 2015).

The two most common techniques that are used for 4D analysis are based on amplitude changes and travel-time changes. Generally, fluid saturation and pore pressure changes lead to acoustic impedance changes, which in turn result in amplitude anomalies and is

captured by amplitude analysis method. Time-shift measurement captures the pull up or push down effects representing the changes in travel-time (Landrø et al., 2001). Amplitude analysis method detects the variations near the interface (local feature), whereas time-shift method evaluates the average changes over one or several layers. Although the amplitude measurement is more widely integrated in the 4D study, the travel-time analysis method becomes more and more popular as the accuracy of 4D seismic improves. The biggest advantage of the latter is that the travel-time changes are proportional to the changes in pay thickness (i.e thickness of the layers that are saturated with hydrocarbons) (Landrø, 2015). Furthermore, the travel-time is less dependent upon the uncertainties in acquisition or processing than amplitude, therefore, in the case where changes in reservoir characteristics alter travel-time, the time-shift method is more reliable (Dimri et al., 2012).

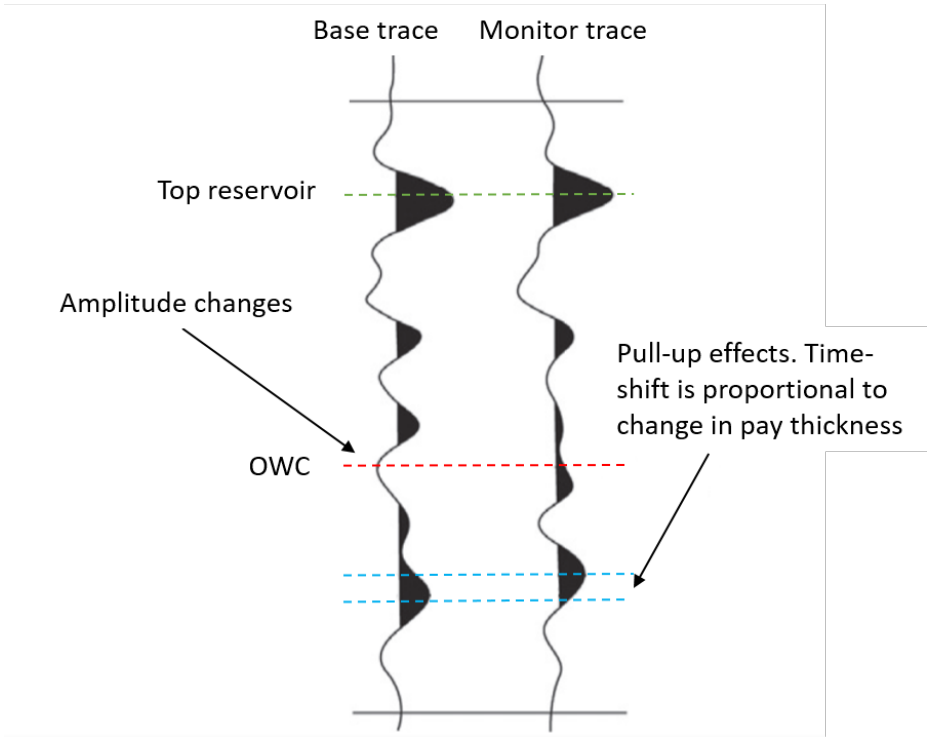


**Figure 3.1:** Two 4D analysis techniques. Red dotted line represents top reservoir, where no amplitude change is observed between base and monitor traces, while at OWC (green dotted line) big amplitude change might be noticed. Below the OWC, there is change in travel-time which is associated with pay thickness change (blue dotted line). Figure is modified after Landrø (2015)

One of the challenges that rise during time-lapse seismic analysis is the distinction between pressure and saturation changes. Because of the different nature in responses it is possible to separate between pressure and saturation changes by applying the time-lapse AVO technique suggested by Landrø et al. (1999) and Tura and Lumley (1999). In order to derive direct expressions for estimating the saturation and pressure related changes Landrø

combined rock physics relation (based on Gassmann and ultrasonic core measurement) with common AVO (amplitude versus offset) equations. The input that is used in this methodology is near and far offset amplitude changes obtained from the base and monitor 3D seismic cubes. This approach was successfully tested on real field data, Gulfaks oil field, North Sea (Landrø, 2001).

The factor that plays a huge rule in ability to detect the reservoir parameters changes is the repeatability of 4D seismic which must be of sufficient high quality. The quality itself is dependent on several factors such as the complexity of the reservoir and overburden, although the repeatability of acquisition is equally important. Several parameters that affect acquisition should be taken into consideration in order to reach high quality and accurate 4D seismic data-set (Landrø and Amundsen, 2018):

- changing positions of source and receiver
- different sea water temperature
- tidal effects
- changing weather conditions
- Possible noise from the vessel or in surrounding area
- Varying source signals
- Different acquisition system (e.g. new vessel, cables, sources, receivers and etc.)
- Changes in shot generate noise (from the previous shot)

The majority of these factors can be controlled by acquisition planning and performance. The parameter that helps to estimate seismic repeatability is normalized Root-Mean-Square (NRMS) and is calculated by using Equation 3.1 (Kragh and Christie, 2002):

$$NRMS = 2\frac{RMS(a-b)}{RMS(a)+RMS(b)} \tag{3.1}$$

and the RMS operator is obtained from Equation 3.2:

$$RMS(a_t) = \sqrt{\sum_{t_1}^{t_2}(a_t^2)/N} \tag{3.2}$$

Here $a$ is the trace from the monitor (repeated) seismic survey taken within the given window $t_1 - t_2$, $b$ is the trace from base (reference) seismic survey taken within the given window $t_1 - t_2$, $N$ is the number of samples in the time interval $t_1 - t_2$. Usually, NRMS is assessed over a time window where no changes in production are observed and is measured in percentage. The number 2 in Equation 3.1 comes from taking the average of the monitor and base RMS values (Landrø and Amundsen, 2018).

A quantity of NRMS is not specifically bounded to the range of 0% to 100%. If there is some random noise in two traces then the NRMS error is 141%, if both of the traces anti-correlate (i.e. if one trace consists only from zeros and the other is 180°out of the phase) the NRMS increases even more and reaches the value of 200%, if one trace is half amplitude of the other the NRMS error is 66.7% (Kragh and Christie, 2002). Usually the value of less than 60% is counted as preferable for the analysis (Dimri et al., 2012). The common values of NRMS for early 4D studies are ranging between 60% and 80% as in the case with Gullfaks 4D study (Landrø et al., 1999), whereas for 4D studies where steerable streamer technology is applied NRMS value might range between 10% and 30% (Goto et al., 2004). Moreover, for land data, the NRMS value is frequently higher because of the inaccuracies in acquisition or seasonal changes in near-surface layers (Dimri et al., 2012).

The complexity of the field geometry, especially the reservoir interval, highly affects the business value of time-lapse seismic surveys (Landrø, 2015). Monitoring the reservoir interval is used to determine the amount and location of reserves that have not been extracted yet, whereas the changes detected in the overburden mostly help to overcome problems associated with drilling or HSE (health, safety, environment), as well as to understand the nature of the changes in the reservoir zone (Røste et al., 2015). Consequently, if the configuration of the reservoir is much simpler it means that the number of hydrocarbon pockets is less and the advantage of using 4D seismic is lower (Landrø, 2015). In general, it could be said that 4D seismic is a valuable tool in reservoir management, since its ability to identify hidden oil and gas pockets, detect gas exsolution, identify displacement of OWC and GOC and etc. impacts the infill drilling and reduces the risks of well-drilling problems. Thus, the well success rates increases, making time-lapse seismic one of the EOR techniques (Jack, 2017).

## 3.2 Amplitude changes

Comparing amplitudes before and after production or other changes gives a clue about the processes that take place in the reservoir and/or overburden zones in 4D seismic analysis (Landrø and Amundsen, 2018). In order to create amplitude difference map between two seismic vintages the amplitude map of monitor survey is subtracted from amplitude map of baseline survey. Figure 3.2 shows the amplitude change from 2001 to 2006. The negative amplitude difference anomaly could be noted in the G-segment. In C-, D-, and E- segments a mixture of positive and negative amplitudes could be observed. The variations on the Top Garn Fm shows that either rock or fluid properties are changing across this horizon. Assuming that the rock framework does not change much, it can be said that changes are induced due to differences in the fluid saturation. The acoustic impedance in a porous media will decrease with increasing oil saturation. On the amplitude difference map this will mean more negative amplitude response in the hydrocarbon-filled segments compared to the water-filled zones (Aschjem, 2013).

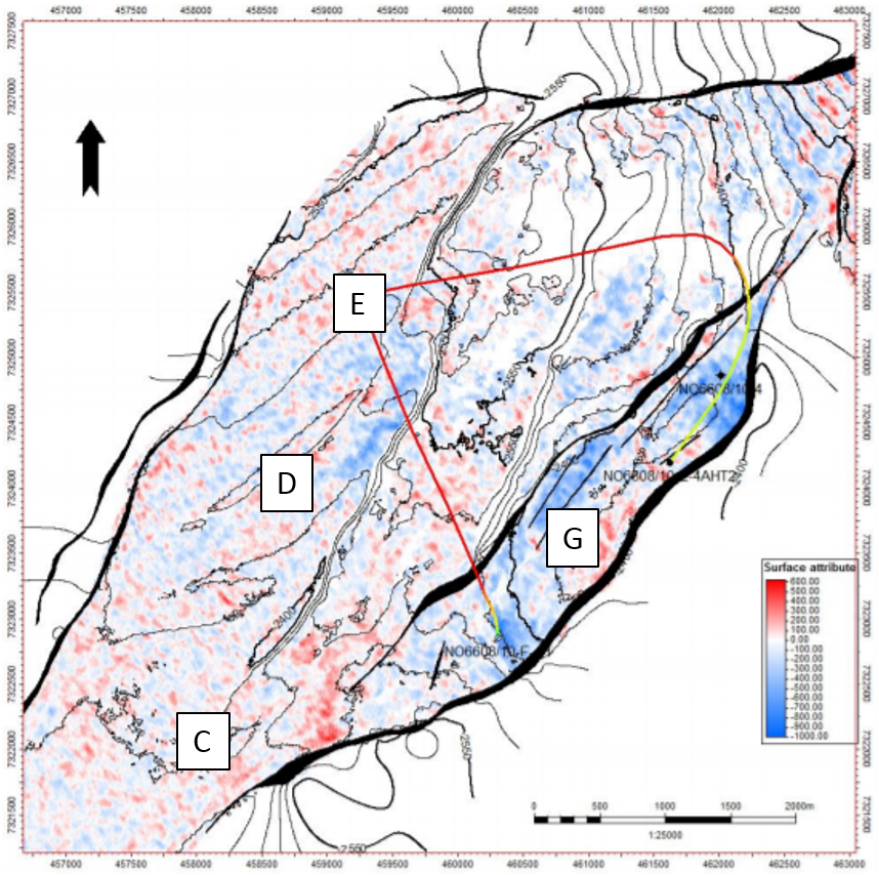


**Figure 3.2:** 4D amplitude difference map (2001 to 2006) over Top Garn Fm in the Norne field (Aschjem, 2013)

## 3.3 Time-lapse time-shifts

The variations in travel-time that are commonly observed in the 4D analysis are called time-lapse time-shits (Hatchell and Bourne, 2005a). The causative sources for these time-shifts are divided into three types: production induced stress and strain deformation both inside and outside of the reservoir, pore-pressure or strain changes within the reservoir zone and changes in fluid properties (MacBeth et al., 2018).

Injection or production of hydrocarbons from the reservoir interval creates displacements in stress and strain fields both in the reservoir itself and also in the rocks bounding the reservoir. For instance, pressure depletion due to production of fluids will cause reservoir compaction and corresponding overburden and underburden extension along with some amount of seabed subsidence (MacBeth et al., 2018; Hatchell and Bourne, 2005a). Therefore, the layer thicknesses change in the reservoir and outside of it and with that the seismic velocities are changed which lead to different travel-times before and after pro-

duction. Production-induced time-shifts have different gradients in the reservoir itself and outside of it. When the reservoir compacts, the layer thickness is reduced and the seismic velocity increases. This yields decreased seismic travel-time over this layer (negative time-shifts or speed-up). The compaction of reservoir causes the overburden to stretch. The thickness of the expanded overburden is increased and seismic velocities propagate slower, which increases the travel-time (positive time-shift or slow-down) (Hatchell and Bourne, 2005b). Consider small changes in thickness and velocity over the layer, such that $\triangle z/z \ll 1$ and $\triangle v/v \ll 1$. Then the changes in travel-time could be expressed as (Landrø and Stammeijer, 2004):

$$dt = (\frac{\delta t}{\delta z})_v dz + (\frac{\delta t}{\delta v_p})_z dv \tag{3.3}$$

Evaluation of the partial derivatives for $t = 2z/v_p$ leads to:

$$dt = \frac{2dz}{v_p} - \frac{2zdv_p}{v_p^2} \tag{3.4}$$

Dividing by t = $2z/v_p$ results in:

$$\frac{dt}{t} = \frac{\frac{2dz}{v_p}}{\frac{2z}{v_p}} + (-\frac{\frac{2zdv_p}{v_p^2}}{\frac{2z}{v_p}}) \tag{3.5}$$

Simplifying the equation above gives:

$$\frac{dt}{t} \approx \frac{dz}{z} - \frac{dv}{v} \tag{3.6}$$

where $dt$ is the 4D timing difference between two reflectors, $t$ is the original travel-time between them, $dz$ is the change in thickness, $z$ is original thickness, $dv$ is the 4D change in velocity and $v$ is the original velocity in the layer between two reflectors. This equation shows the relationship between subsurface parameters and changes in travel-time. The fractional change in travel-time is the difference between fractional change in thickness and velocity (Hatchell and Bourne, 2005b). For this geometry, the fractional change in thickness is equal to the average vertical strain across the layer, $\epsilon_{zz}$. In order to calculate time-shifts both strain and velocity change must be known, however they compete with each other. It was suggested both by Hatchell and Bourne (2005b) and Røste et al. (2006) at the same time to connect fractional change in velocity to the fractional change in thickness (or vertical strain) so that

$$\frac{dv}{v} = -R\epsilon_{zz} \tag{3.7}$$

The dimensionless value, R, is a factor that is dependent on the rock properties, magnitude of the relative thickness change and spatial coordinates (Røste et al., 2006). Inserting Equation 3.7 into Equation 3.6 and re-arranging it gives:

$$\frac{dt}{t} = (1 + R)\epsilon_{zz} \tag{3.8}$$

This relationship gives an opportunity to connect the seismic and geomechanical domains (MacBeth et al., 2018). Therefore, travel-time changes, seafloor subsidence and reservoir compaction can all be linked and calibrated to each other (Hatchell and Bourne, 2005b).

Changes in pore pressure induced by production causes the reservoir to compact due to changes in the effective stress field and results in changes in travel-time (Hatchell et al., 2005). Although the travel-time changes could also be induced by fluid substitution and even temperature changes, it is important to compute velocity changes triggered by stress and pore-pressure changes alone (Holt et al., 2005). The change in the effective stress field is given as :

$$\Delta\sigma^{eff} = \Delta S - \alpha\Delta P \tag{3.9}$$

where $\Delta\sigma^{eff}$ is the effective stress tensor, S is the total stress tensor, $\alpha$ is the Biot coefficient, which controls deformation of a linearly elastic rock and is usually close to 1, and P is the fluid pressure (Hatchell et al., 2005). The vertical element of Equation 3.9 will be described by the equation below:

$$\Delta\sigma^{eff}_{ZZ} = \Delta S_{ZZ} - \alpha\Delta P = (\gamma - \alpha)\Delta P \tag{3.10}$$

The $\gamma$ is the stress-arching coefficient and is used to describe the relation of change in total vertical stress to the change in reservoir pressure (Hatchell et al., 2005). This relation is strongly dependent on the reservoir geometry, size, depth, Young's modulus and Poisson's ratio (Fjær et al., 2008).

Based on all this, it is possible to perform laboratory measurements and construct geomechanical models to predict changes in pore pressure and stress, and therefore quantify changes in seismic velocities, as, for instance, was done by Holt et al. (2005).

The indication of reservoir saturation-caused time-shifts is a zero response above the top of reservoir followed by linear increase within the reservoir zone and maintenance of this value as a constant below the base of reservoir. This kind of time-shift responses are often observed in time-lapse seismic studies due to water or gas flooding, steam injection into heavy oil reservoirs and when gas is released from a solution. The geomechanical effects either boost or reduce these time-shifts within the reservoir zone. For example, increase in both gas saturation and pressure signals generate a slowdown, while increase in water saturation and pressure signals compete with each other (MacBeth et al., 2018).

The modeling the effects of fluid on rock velocity and density is widely practised to establish the impact of pore fluids on seismic data. Gassmann (1951) equations are extensively used to compute seismic velocity changes resulting from different fluid saturation in reservoir. These equations frequently applied in the analysis of direct hydrocarbon indicators (DHI), such as bright spots, AVO and time-lapse reservoir monitoring (Han and Batzle, 2004).

Chapter 4

# Methodology

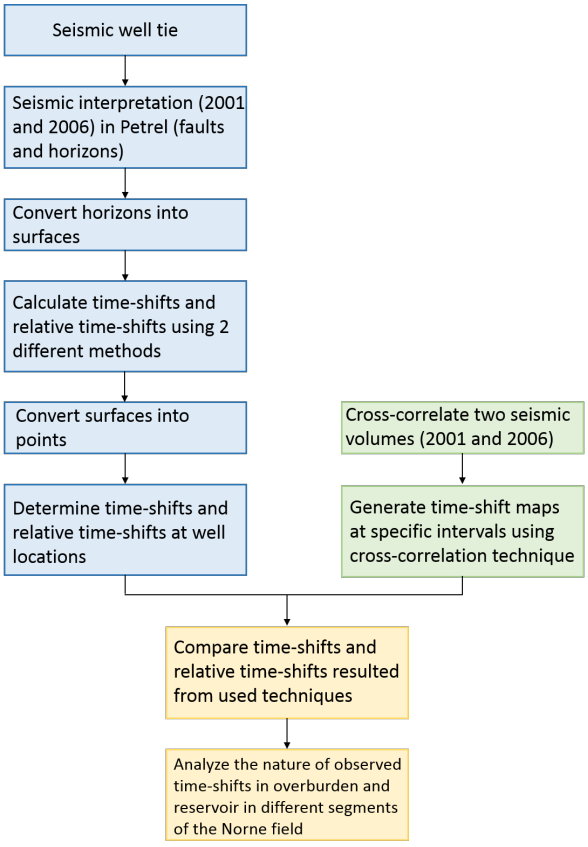


**Figure 4.1:** Flowchart displaying the steps performed in this thesis

The following chapter describes the methodology used in this master thesis to further obtain the results and perform time-shift analysis. Figure 4.1 summarizes all the steps completed in this work. The work was done using Petrel software, which was provided by Schlumberger.

## 4.1 Seismic to Well Tie

Well tie is a procedure which establishes the connection between seismic data and well log data, since the latter are measured in depth and seismic data are usually measured in time. This is done to precisely identify the reflectors on seismic, which have already been determined in the wells as formation tops. Therefore, there is need in the conversion of depth to time (Simm and Bacon, 2014).

The main objectives of performing a well tie are the following (Simm and Bacon, 2014) :

- QC (quality check) data: checking if data are zero phase, and adjusting it if necessary
- Offset scaling: checking if the seismic data have been correctly processed to have the true amplitudes and the right AVO response and adjusting amplitudes if required
- Extraction of a wavelet for use in seismic inversion or modelling
- Accurate identification of reflectors that represent the formation tops

The polarity of the seismic surveys can be identified by analyzing the first strong reflector, which is the seabed. The seabed on 2001 seismic dataset is illustrated by a red reflector or peak, suggesting an increase in acoustic impedance, whereas the decrease in acoustic impedance is represented by a blue reflector or trough (Figure 4.2a and Figure 4.2b). Following this convention, it can be stated that the data displays the normal (also called positive) polarity.

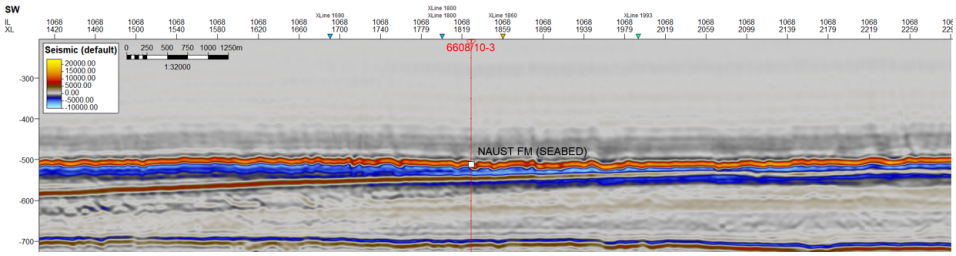


**(a)**

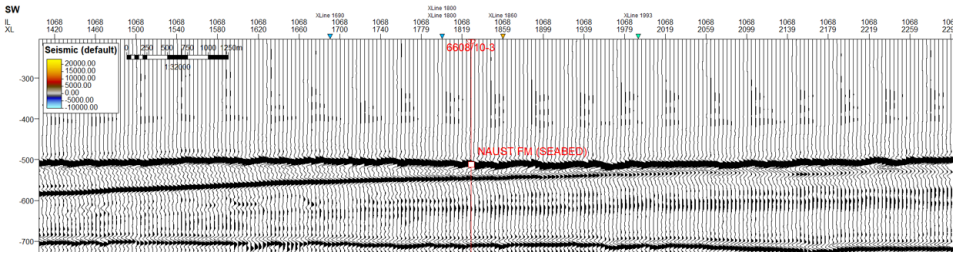


**(b)**

**Figure 4.2:** (a) Seismic data from the Norne field, where the first red reflector represents the seafloor (b) Seismic data displayed in wiggles, from which can be seen that peak is assigned to red color

The SWT is done by creating a synthetic seismogram, using sonic and density logs (or simply acoustic impedance logs), and comparing it with the acquired and processed seismic traces. Since the quality and properties of the data usually change with travel-time, the well tie is generally accomplished over specific time window rather than whole depth extent of the well logs.

In order to get a good seismic to well tie, it is essential to perform a quality control on the checkshot data and also, edit the well logs, where suspiciously high and low readings are corrected. Subsequently, calibration of the sonic log is carried out, followed by generation of a synthetic seismogram. Later, if necessary, this synthetic seismogram can be modified (stretched and squeezed) to match the reflections on processed seismic data. Overall, the procedure for performing SWT is summarized in Figure 4.3.

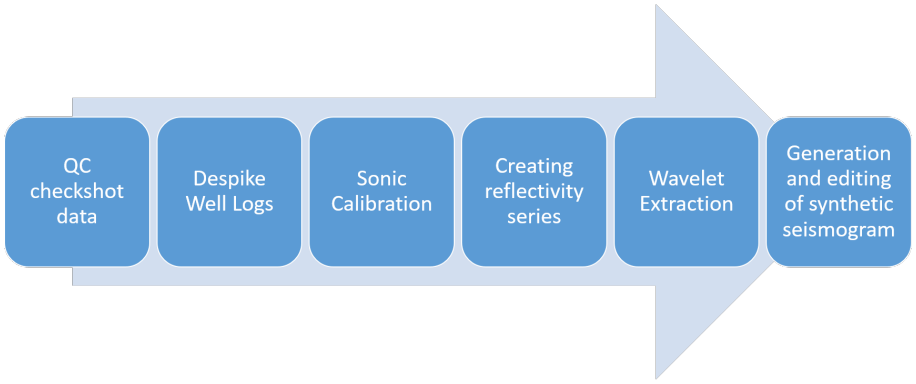


**Figure 4.3:** Order of steps that are essential in achieving seismic to well tie

The quality control step is done by checking all the time values which supposed to be negative. Since all the values below mean sea level are counted as negative, the time values should also be negative. Therefore if the imported checkshot data represents positive time values, it accounts for the fact that the data was loaded incorrectly (Petrel Geophysics, 2016). This step is necessary only when using Petrel, as it is the specifics of the software.

The next step is editing the logs, which are sonic and density logs. This is done to remove defects and improve the quality of the well tie. This process should be performed carefully, because there is a risk of having inconsistent time-depth relationships and false responses in the synthetic, resulting in imprecise calibration. If a spike in the input log is associated with a lithological change which can be verified by a gamma-ray log, then this spike is kept, otherwise it is eliminated.

When the quality control and despiking steps are finalized, checkshots can be applied for sonic log calibration. Sonic logs have to be adjusted to seismic, because values acquired from sonic log (specifically time) vary from those collected by means of seismic pulse. Sonic calibration step allows to compare sonic transit times to checkshot times and correct them to have approximate match (White, 2003). This is achieved by adding/editing knee points over the interval of the sonic log, and achieving a good match to the data between them. It means, fitting the red curve to the black points (Figure 4.4). Drift curve represents calibration of the sonic TDR to match checkshot data. Effect of drift is related to the velocity dispersion between log and seismic frequencies (Stewart et al., 1984). The knee points should be added at big changes in lithology or unconformities where velocity is changed in order to prevent generation of false reflectors. The aim is not to fit all black points exactly, because this will introduce noise and artefacts (Simm and Bacon, 2014).

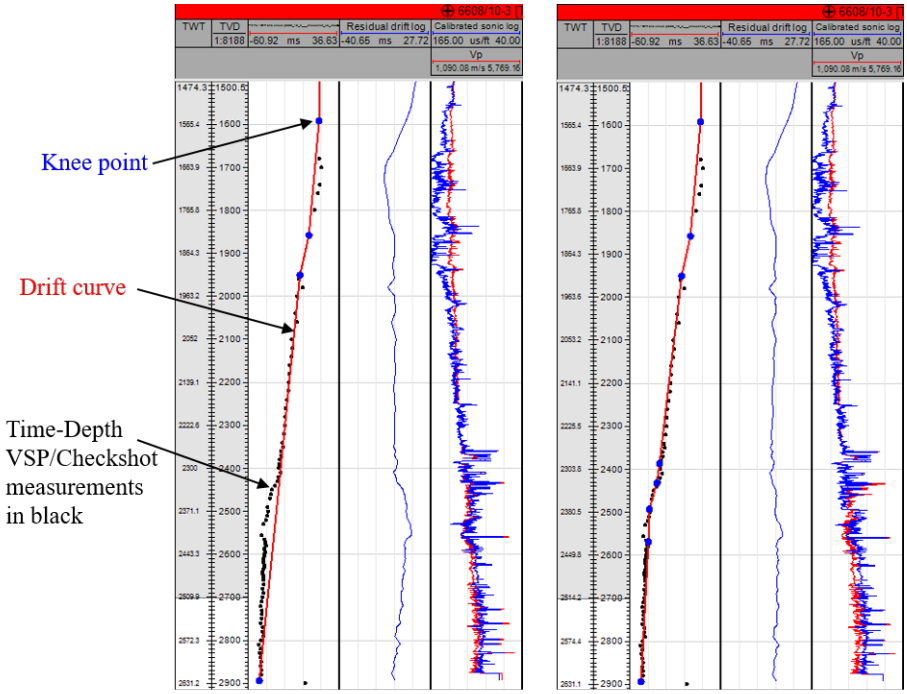


**Figure 4.4:** (a) Initial drift curve (in red) which will be optimised by adding new knee points (blue) during sonic calibration procedure in $6608/10-3$ well; (b) The final calibration of sonic and checkshot data (black)

Generating the synthetic seismogram includes creating reflectivity series[1] in time and convolving it with a wavelet. In order to create reflectivity series it is required to use either a velocity log with the drift applied to it or the initial sonic log values together with the time-depth relationship generated from applying drift to the sonic log (White, 2003).

In order to determine the appropriate wavelet to use for generating synthetic seismogram, it should be extracted from the seismic data on which the well-tie is performed. To perform a robust extraction the log data quality should be good and the time-depth conversion should be precise. This procedure includes extracting wavelet from specific time window of seismic data, which is usually the reservoir zone. The length of the wavelet is generally taken around 500 ms. If the length will be too long there might be uncertainty in phase stability and phase rotation with depth could disturb the final results. The tie accuracy could be negatively affected by short wavelength as well (Simm and Bacon, 2014). Figure 4.5 illustrates the extracted wavelet. The wavelet was extracted in 2320-2620 ms time window, which encompasses the reservoir zone. The phase of this wavelet is 22° which is close to zero-phase and counted as acceptable value. This wavelet shows stable

[1]The reflectivity is the ratio of seismic wave amplitude reflected from an interface to the wave amplitude incident upon it (Kearey et al., 2002).

phase up to 95 Hz after which it starts to gradually decrease.

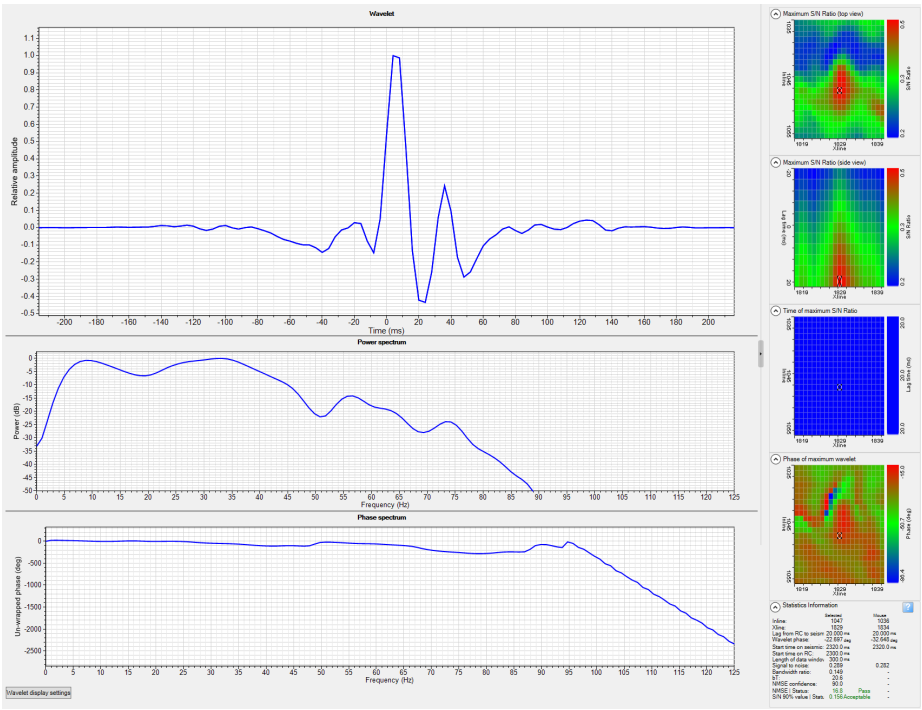


**Figure 4.5:** Extracted wavelet used in well tie with acceptable S/N, bandwidth ratio and stable phase spectrum. Phase is 22°, S/N ratio is 0.289 and bandwidth ratio is 0.149

Finally, the extracted wavelet is convolved with reflectivity series to create synthetic seismogram which is displayed side-by-side with the seismic traces themselves. Generally, after producing synthetic seismogram it is necessary to adjust it to the seismic, by applying bulk shift in the synthetic along with displaying the formation tops, in order to achieve more accurate correlation between the synthetic traces and the reflection seismic traces. Nevertheless, this step should be carried out carefully and potential reasons for mistie should be investigated first (Simm and Bacon, 2014).

In Figure 4.6 some differences might be observed between synthetic seismogram and the seismic, because when one formation top is matched to its reflector, another one might lose its position. This is shortcoming of the well tie, even though it is possible to apply stretch and squeeze option to the synthetic. However, this step was skipped because the initial well tie seems to be good and the position of interested reflectors could be detected avoiding shifting.

Once the well tie procedure is accomplished the stratigraphic boundaries determined from well log data are aligned in time with corresponding reflectors on seismic data. Thus, the horizons of interest can be interpreted confidently. In Figure 4.7 several horizons are displayed and it can be observed that they match the proper reflectors.

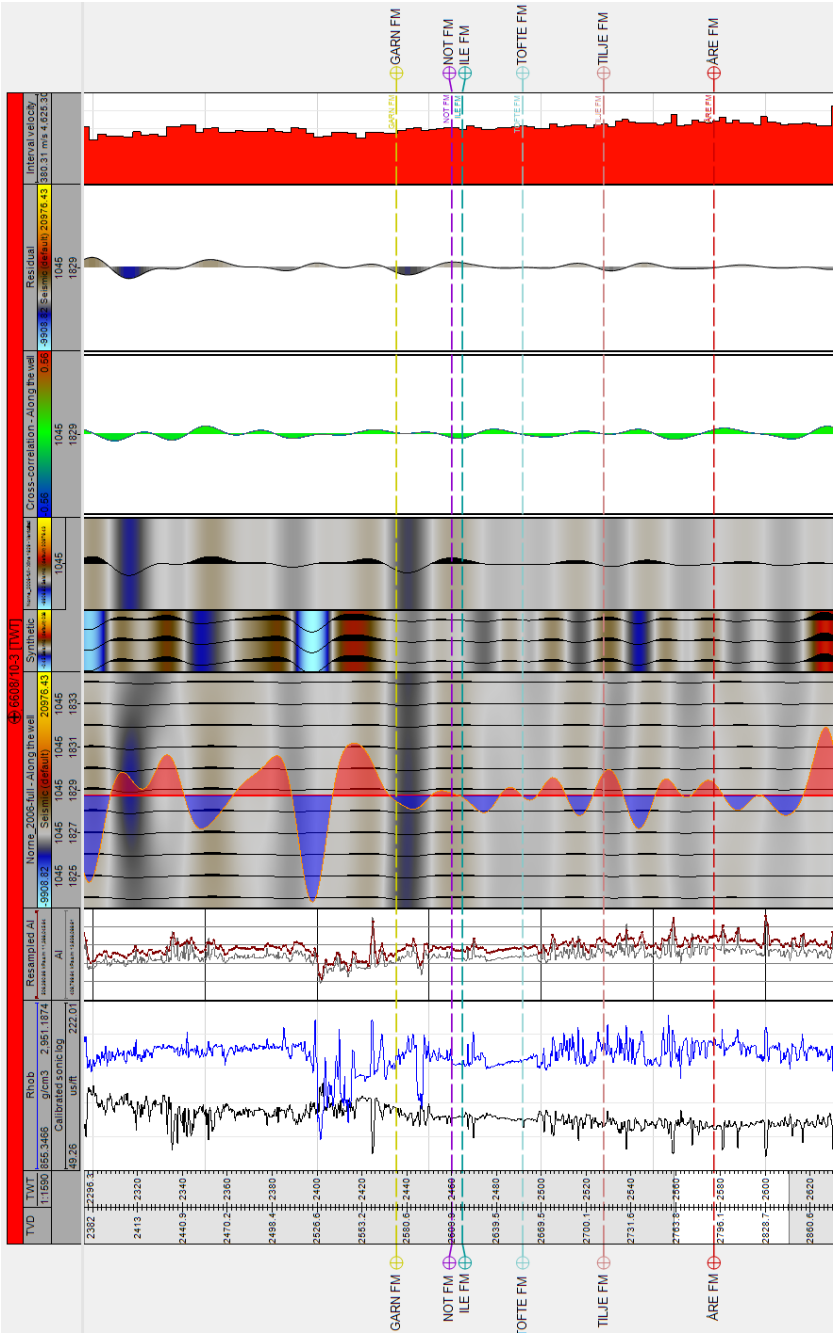


**Figure 4.6:** The example of seismic well tie shown in well $6608/10-3$ with the formation tops

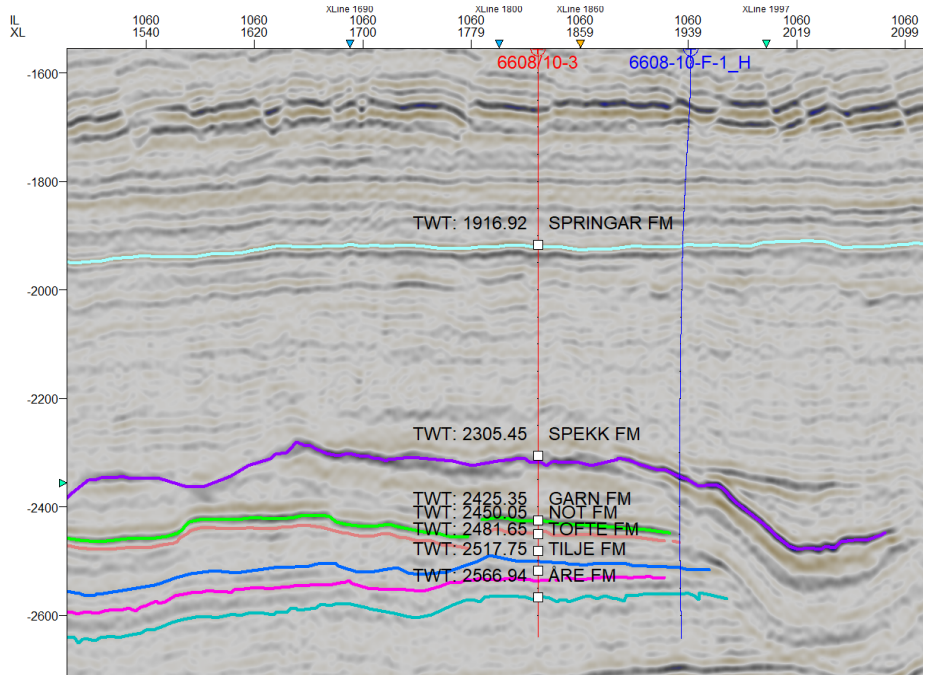


**Figure 4.7:** Inline 1060 from 2001 (base) seismic survey intersecting the well $6608/10-3$ and the formation tops which are aligned on the proper reflectors

## 4.2 Seismic Interpretation

### 4.2.1 Fault Interpretation

The horst block of Norne field consist mainly of normal faults which are oriented in northeast-southwest direction. Since these major faults are sealing, the field is divided into different segments (C, D, E, G). For more accurate delineation of faults on horizon slices and vertical seismic profiles the variance attribute was used to help interpretation.

Variance attribute is an edge method which measures the resemblance of waveforms or traces adjacent over given lateral and vertical windows. This attribute reveals discontinuities in seismic data either related to stratigraphic terminations or structural lineaments. It is widely used in salt dome outlining, gas chimney and mud volcano mapping, detection of faults and channels and etc. (Pigott et al., 2013). Variance method uses the local variance as a measure of signal unconformity, which is found from horizontal slices. If this slice covers continuous reflection layer, the amplitude variance will be small, whereas amplitude variations due to a fault will cause high variance (Randen et al., 2001).

The faults were interpreted either on inline or crossline depending on their orientation and geometry. Horizon slice of Variance cube was a guide in choosing correct orientation of faults and in general QC of fault interpretation (Figure 4.8 and Figure 4.9).

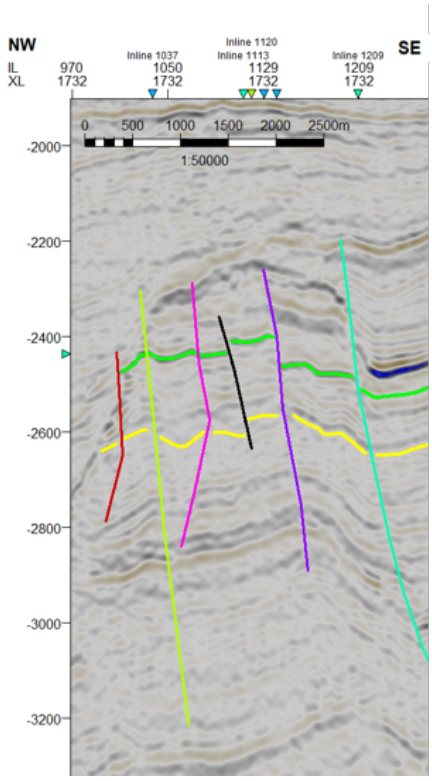


**Figure 4.8:** Interpreted faults displayed on cross-line 1732 from 2001 seismic survey. Green horizontal reflector represents Top Garn FM, lower yellow reflector represents Top Åre FM

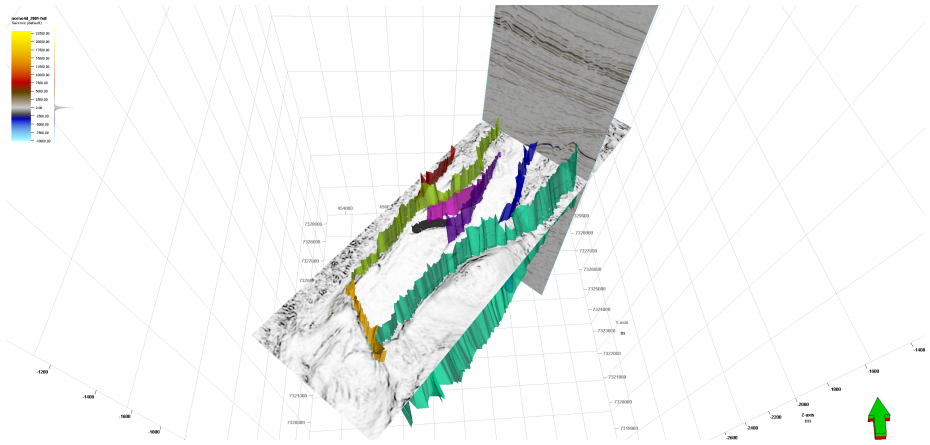

**Figure 4.9:** Faults displayed in 3D view on Z-section -2436 of variance attribute and cross-line 2061. The faults orientation and geometry create reservoir shape of the Norne field

### 4.2.2 Horizon Interpretation

The following formation tops on two 3D seismic surveys from 2001 (base survey) and 2006 (monitor survey) were determined and interpreted for further travel-time shift analysis :

- Top Naust FM (seabed)
- Top Kai FM
- Top Springar FM
- Top Spekk FM
- Top Garn FM
- Top Not FM
- Top Tofte FM
- Top Tilje FM
- Top Åre Fm

The reflectors which have either peak or trough response in the wavelet were interpreted by using the auto tracking option in Petrel software. This option automatically interprets the reflector and demands minimal control from the seismic interpreter. The only thing that needed to be done is choosing the seed points from which the interpretation is accomplished in all directions. When the reflectors have very strong amplitudes and can be easily tracked this option is the most time-saving.

Moreover, in this project the auto tracking was chosen because the interpretation has to be precise on both datasets from 2001 and 2006 years in order to have an accurate analysis of the relative timeshifts. This can be achieved by using auto tracking where input, which can potentially cause irregular discrepancies, from a person will be little.

The interpreted formations from two different wells with corresponding values in seconds and meters are presented in the Table 4.1 and Table 4.2 below .

| Well 6608/10-3 | | | |
|---|---|---|---|
| Horizons | Depth RKB MD (m) | Depth MSL TVD (m) | TWT (ms) |
| Top Naust FM | 715.6 | 685.6 | 819 |
| Top Kai FM | 1368 | 1344 | 1348 |
| Top Springar FM | 1950 | 1926 | 1916 |
| Top Spekk FM | 2407 | 2381.9 | 2306 |
| Top Garn FM | 2571.5 | 2548.5 | 2433 |
| Top Not FM | 2610.5 | 2585.3 | 2458 |
| Top Tofte FM | 2657 | 2631.8 | 2488 |
| Top Tilje FM | 2707 | 2681.8 | 2519 |
| Top Åre Fm | 2791 | 2765.7 | 2568 |

**Table 4.1:** Formations with corresponding values in seconds and meters in the well 6608/10-3 (Statoil, 1993)

| Well 6608/10-2 | | | |
|---|---|---|---|
| Horizons | Depth RKB MD (m) | Depth MSL MD (m) | TWT (ms) |
| Top Naust FM | 724 | 700.5 | 830 |
| Top Kai FM | 1352 | 1327.5 | 1354 |
| Top Springar FM | 1951 | 1927.5 | 1907 |
| Top Spekk FM | 2346.5 | 2323 | 2229 |
| Top Garn FM | 2577 | 2554 | 2406 |
| Top Not FM | 2611 | 2587.5 | 2429 |
| Top Tofte FM | 2668 | 2644.5 | 2466 |
| Top Tilje FM | 2719.5 | 2696.5 | 2498 |
| Top Åre Fm | 2818.5 | 2795 | 2555 |

**Table 4.2:** Formations with corresponding values in seconds and meters in the well 6608/10-2 (Statoil, 1992)

After performing interpretation it was possible to convert the interpreted horizons into surfaces in Petrel software, which allowed to accomplish timeshift analysis from one seismic survey to another. Figure 4.10 shows several interpreted horizons in a 3D view.

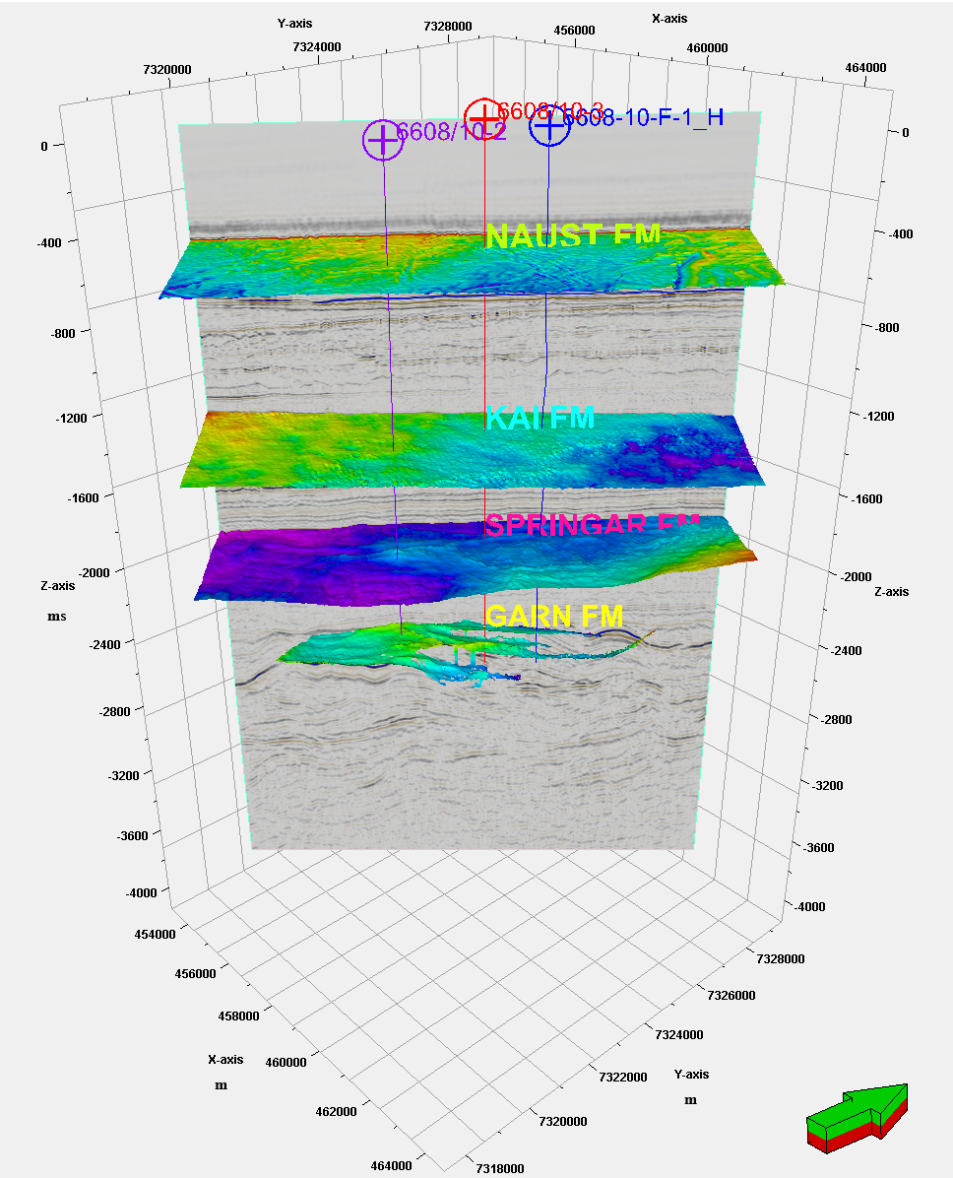


**Figure 4.10:** Several interpreted horizons displayed in 3D with an inline 970 from 2001 seismic survey

## 4.3 Calculation of travel-time changes

Analysis of travel-time changes at Norne field starts with the calculation of time-shifts and relative time-shifts over interested formations using two different techniques, where chosen intervals are defined differently (subsection 4.3.1 and subsection 4.3.2).

When the travel-time is calculated between two chosen intervals, the travel-time $\triangle t$ is determined. For this reason the time-shift is denoted as $\triangle(\triangle t)$. It defines the difference in travel-time from the base to the monitor seismic survey and can be written as shown in Equation 4.1 :

$$\triangle(\triangle t) = \triangle t_{monitor} - \triangle t_{base} = \triangle t_{2006} - \triangle t_{2001} \tag{4.1}$$

The relative time-shift is defined as the fractional change in travel-time from the base-line to the monitor seismic surveys (Equation 4.2) :

$$\frac{\triangle(\triangle t)}{\triangle t_{base}} = \frac{\triangle t_{monitor} - \triangle t_{base}}{\triangle t_{base}} = \frac{\triangle t_{2006} - \triangle t_{2001}}{\triangle t_{2001}} \tag{4.2}$$

In this thesis time-shift analysis was performed at specific locations..... The time-shifts and relative time-shifts were calculated at these sites using the methodologies described below. This analysis helps to interpret how the formations in the overburden and the reservoir zone have deformed at the well locations due to production-induced changes between 2001 and 2006.

### 4.3.1 Method 1

In method 1 the seafloor is set as the reference point and the calculation of time-shift and relative time-shift is performed from the seafloor down to the top of each interpreted horizon. Since the depth is increasing the interval thickness increases as well. The result of these calculations is the accumulated travel-time change. The equations used for the calculation of time-shift illustrated below:

$$\begin{aligned}\triangle(\triangle t)_{horizon_{i+1}} &= \triangle t_{horizon_{i+1},monitor} - \triangle t_{horizon_{i+1},base} \\ &= (t_{horizon_{i+1},2006} - t_{seafloor,2006}) - (t_{horizon_{i+1},2001} - t_{seafloor,2001})\end{aligned} \tag{4.3}$$

$$\begin{aligned}\triangle(\triangle t)_{horizon_{i+2}} &= \triangle t_{horizon_{i+2},monitor} - \triangle t_{horizon_{i+2},base} \\ &= (t_{horizon_{i+2},2006} - t_{seafloor,2006}) - (t_{horizon_{i+2},2001} - t_{seafloor,2001})\end{aligned} \tag{4.4}$$

$$\vdots$$

$$\begin{aligned}\triangle(\triangle t)_{horizon_N} &= \triangle t_{horizon_N,monitor} - \triangle t_{horizon_N,base} \\ &= (t_{horizon_N,2006} - t_{seafloor,2006}) - (t_{horizon_N,2001} - t_{seafloor,2001})\end{aligned} \tag{4.5}$$

where $i = seafloor, 1, 2, ..., N$ and $\triangle(\triangle t)_{horizon_{i+1}}$ expresses the time-shift at some specific horizon in depth, $\triangle t_{i+1}$ expresses the change in travel-time from horizon $i$ to horizon $i+1$ in base and monitor seismic surveys.

Consequently, the relative time-shifts are calculated using the equations below:

$$\frac{\triangle(\triangle t)}{\triangle t}_{horizon_{i+1}} = \frac{\triangle t_{horizon_{i+1},monitor} - \triangle t_{horizon_{i+1},base}}{\triangle t_{horizon_{i+1},base}} = \frac{(t_{horizon_{i+1},2006} - t_{seafloor,2006}) - (t_{horizon_{i+1},2001} - t_{seafloor,2001})}{t_{horizon_{i+1},2001} - t_{seafloor,2001}} \tag{4.6}$$

$$\frac{\triangle(\triangle t)}{\triangle t}_{horizon_{i+2}} = \frac{\triangle t_{horizon_{i+2},monitor} - \triangle t_{horizon_{i+2},base}}{\triangle t_{horizon_{i+2},base}} = \frac{(t_{horizon_{i+2},2006} - t_{seafloor,2006}) - (t_{horizon_{i+2},2001} - t_{seafloor,2001})}{t_{horizon_{i+2},2001} - t_{seafloor,2001}} \tag{4.7}$$

$$\vdots$$

$$\frac{\triangle(\triangle t)}{\triangle t}_{horizon_{N}} = \frac{\triangle t_{horizon_{N},monitor} - \triangle t_{horizon_{N},base}}{\triangle t_{horizon_{N},base}} = \frac{(t_{horizon_{N},2006} - t_{seafloor,2006}) - (t_{horizon_{N},2001} - t_{seafloor,2001})}{t_{horizon_{N},2001} - t_{seafloor,2001}} \tag{4.8}$$

Figure 4.11 gives a visual overview of how a travel-time is estimated from seafloor down to the interested point in depth.

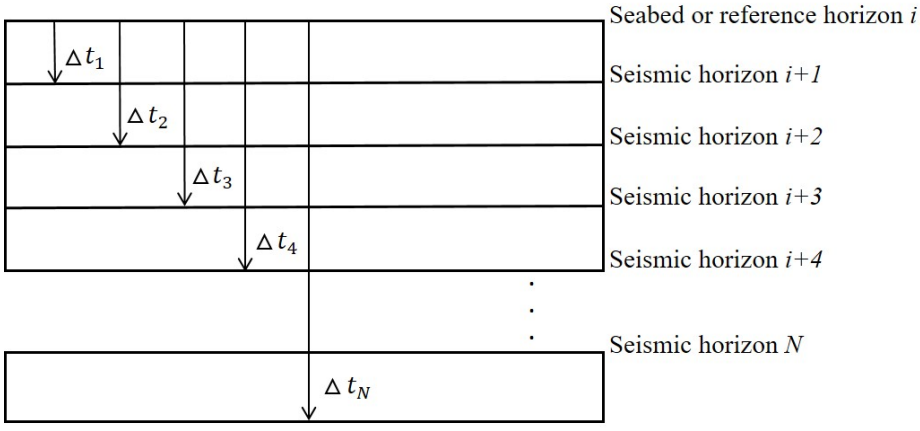


**Figure 4.11:** Visual overview of travel-time calculation using Method 1. Modified after (Erichsen, 2008)

### 4.3.2 Method 2

In method 2 the time-shift and relative time-shift are calculated between each interpreted horizon. Since the interpreted horizons are formation tops, the estimated travel-time change is the change through that particular interval. The result of these calculations is the interval travel-time change and can be found using Equation 4.9-Equation 4.11

$$\begin{aligned}\triangle(\triangle t)_{horizon_{i+1}} &= \triangle t_{horizon_{i+1},monitor} - \triangle t_{horizon_{i+1},base} \\ &= (t_{horizon_{i+1},2006} - t_{i,2006}) - (t_{horizon_{i+1},2001} - t_{i,2001})\end{aligned} \tag{4.9}$$

$$\begin{aligned}\triangle(\triangle t)_{horizon_{i+2}} &= \triangle t_{horizon_{i+2},monitor} - \triangle t_{horizon_{i+2},base} \\ &= (t_{horizon_{i+2},2006} - t_{i+1,2006}) - (t_{horizon_{i+2},2001} - t_{i+1,2001})\end{aligned} \tag{4.10}$$

$$\vdots$$

$$\begin{aligned}\triangle(\triangle t)_{horizon_N} &= \triangle t_{horizon_N,monitor} - \triangle t_{horizon_N,base} \\ &= (t_{horizon_N,2006} - t_{N-1,2006}) - (t_{horizon_N,2001} - t_{N-1,2001})\end{aligned} \tag{4.11}$$

where $i = 1, 2, ..., N$ and $\triangle(\triangle t)_{horizon_{i+1}}$ expresses the time-shift at some specific horizon in depth, $\triangle t_{i+1}$ expresses the change in travel-time from horizon $i$ to horizon $i+1$ in base and monitor seismic surveys.

The relative time-shifts are calculated in a similar fashion:

$$\begin{aligned}\frac{\triangle(\triangle t)}{\triangle t}_{horizon_{i+1}} &= \frac{\triangle t_{horizon_{i+1},monitor} - \triangle t_{horizon_{i+1},base}}{\triangle t_{horizon_{i+1},base}} \\ &= \frac{(t_{horizon_{i+1},2006} - t_{i,2006}) - (t_{horizon_{i+1},2001} - t_{i,2001})}{t_{horizon_{i+1},2001} - t_{i,2001}}\end{aligned} \tag{4.12}$$

$$\begin{aligned}\frac{\triangle(\triangle t)}{\triangle t}_{horizon_{i+2}} &= \frac{\triangle t_{horizon_{i+2},monitor} - \triangle t_{horizon_{i+2},base}}{\triangle t_{horizon_{i+2},base}} \\ &= \frac{(t_{horizon_{i+2},2006} - t_{i+1,2006}) - (t_{horizon_{i+2},2001} - t_{i+1,2001})}{t_{horizon_{i+2},2001} - t_{i+1,2001}}\end{aligned} \tag{4.13}$$

$$\vdots$$

$$\begin{aligned}\frac{\triangle(\triangle t)}{\triangle t}_{horizon_N} &= \frac{\triangle t_{horizon_N,monitor} - \triangle t_{horizon_N,base}}{\triangle t_{horizon_N,base}} \\ &= \frac{(t_{horizon_N,2006} - t_{N-1,2006}) - (t_{horizon_N,2001} - t_{N-1,2001})}{t_{horizon_N,2001} - t_{N-1,2001}}\end{aligned} \tag{4.14}$$

Figure 4.12 gives a visual overview of how a travel-time is estimated for each interpreted horizon.

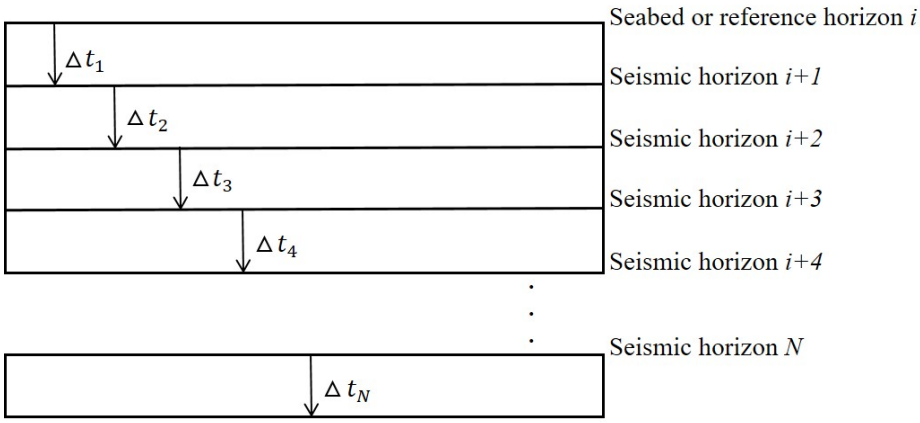


**Figure 4.12:** Visual overview of travel-time calculation using Method 2. Modified after (Erichsen, 2008)

### 4.3.3 Calculation of relative time-shifts at well locations

For better analysis of time-shifts and relative time-shifts over overburden and reservoir intervals, specific well location points are inspected. After calculating time-shifts and relative time-shifts using Calculator option in Petrel software and following the techniques described above, it is required to convert the surfaces into points in order to see which values are assigned to each point close to the well location. Four points around each of the wells are chosen and the mean values are quantified (Figure 4.13).

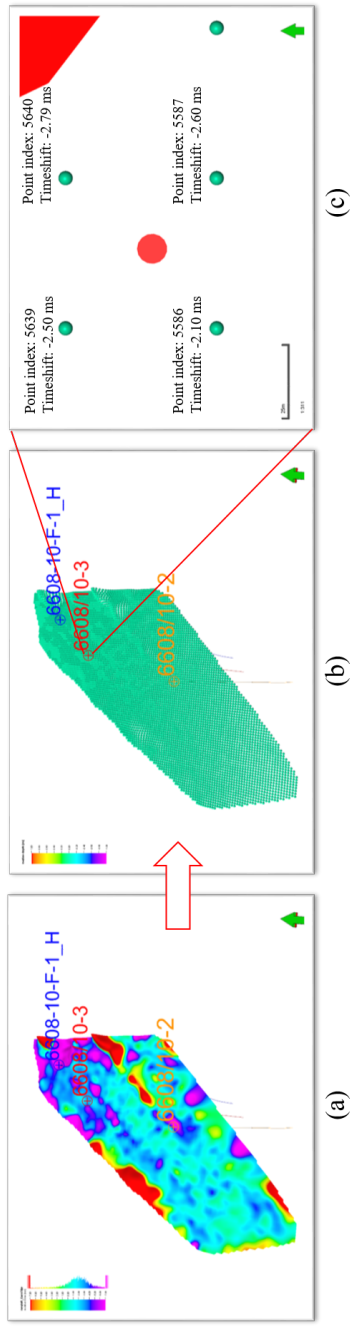


**Figure 4.13:** (a) Time-shift map generated using Method 1 (subsection 4.3.1); (b) The same time-shift map converted into points; (c) Closer view of the points with corresponding values Red dot represents well location

## 4.4 Cross-correlation

### 4.4.1 Principles of cross-correlation

Cross-correlation establishes the similarity between the two traces of the volumes. One set is taken as a reference, corresponding values of two datasets are multiplied together, after that the products are summed to result in the value of the cross-correlation, which will show how much two sets resemble each other (Telford et al., 1990; Yilmaz, 2012). A result of cross-correlation (cross-correlation coefficient) which is equal to 1 indicates that the two traces are identical, whereas 0 represents poor match. If the cross-correlation has a large negative value, it means that the two data sets would be similar if one were inverted (they are similar except that they are out of phase) (Telford et al., 1990)

In the Figure 4.14 the procedure of calculation the cross-correlation function of two signals is shown. Signal g is displayed relative to the signal f, and the corresponding coordinates are multiplied vertically. Then the Signal g is shifted one unit to the right and the multiplication and summation is repeated again. The dot product represent the similarity between two signals. Here, the maximum correlation value occurs at lag of 1 ms, which suggests that if the signal was shifted one sample back in time these two signals would have maximum similarity.

As a measure of similarity, cross-correlation is frequently applied in different data processing procedures. For example, traces in a CMP gather are cross-correlated with a pilot trace to determine the residual statics shifts. Also cross-correlation is used to calculate velocity spectra (Yilmaz, 2012).

### 4.4.2 Application of cross-correlation technique

In this work cross-correlation is used to define how similar two volumes are to each other and to inspect the reservoir interval. It can measure the production caused time changes that correspond to different pressure and temperature, compaction or elongation and etc. It is important to cross-correlate the reservoir interval, as well as zones beneath and above the reservoir, since the changes in the latter most likely would affect the over and under-burden sections.

Cross-correlation is conducted between 2001 and 2006 seismic surveys, where the latter is taken as a reference dataset and 2001 seismic volume is displayed relative to it. It is expected to see the production induced changes within the reservoir zone, and areas close to it beneath and above. For that the window size, its position and lag should be chosen. The lag is taken to be 100 ms, which is the amount of displacement applied on each seismic trace to be cross-correlated. This amount cross-correlates each seismic trace sample from -100 to +100 ms, which makes the total displacement to be 200 ms (Petrel, 2017).

Here the maximum amplitude of the waveform is concentrated at the chosen window position and it should interpreted by 3D autotracking. After that this horizon should be converted to surface so that further calculations could be performed. In order to see the degree of travel-time changes the value for window position which was chosen earlier should be added to the surface. This will result in new surface where time-shift values are

distributed over it and mostly represent the shifts due to production. The changes due to noise can also be present.

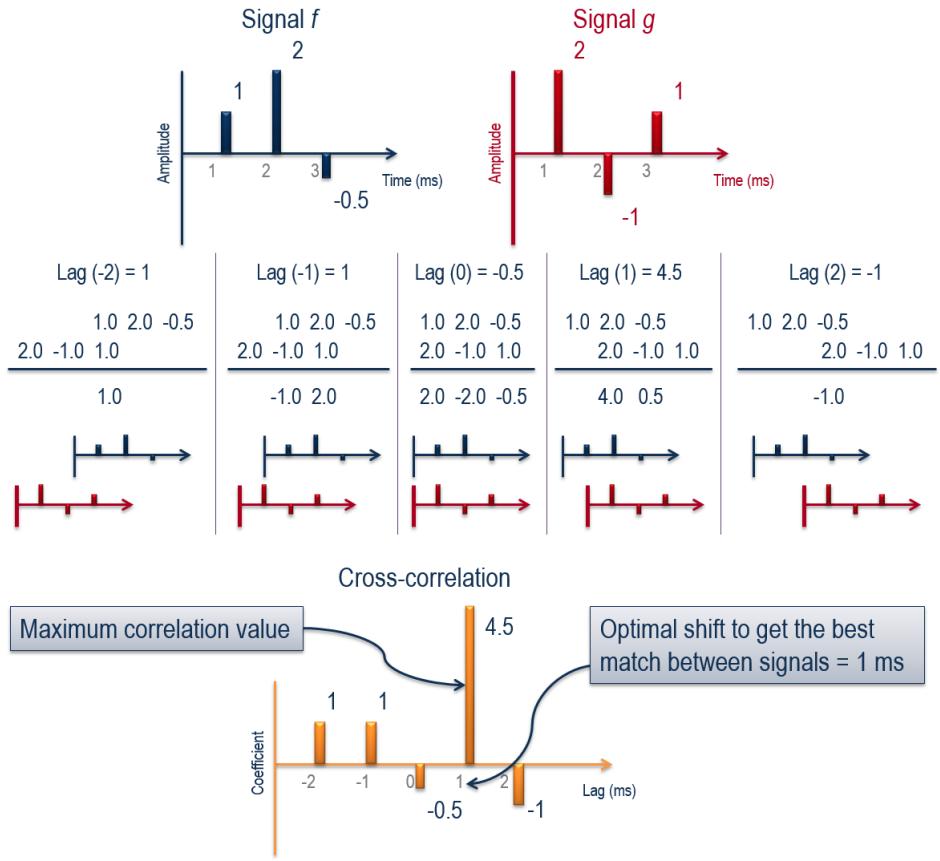


**Figure 4.14:** The procedure of calculating the cross-correlation function of two signals (Petrel, 2017)

Chapter 5

# Results

## 5.1 Time-shifts at specific locations

Time-shift values computed using Method 1 and Method 2 are present in Figures Figure 5.1-Figure 5.6 for wells 6608/10-3, 6608/10-F-1H and 6608/10-2. First two wells are located in segment E, while well 6608/10-2 is drilled in C-segment. Relative time-shift values can be seen in Appendix B and Appendix C.

### 5.1.1 Method 1

Figure 5.1 shows time-shift values for well 6608/10-3. Negative time-shift value can be noted for Seabed - Top Kai Fm interval, which suggests increase in velocity and reduction in thickness. This is the same for Top Springar Fm. At the point where well intersects Top Spekk formation, the time-shifts are positive, suggesting slow-down in travel-time. At Top Garn formation which is the top of reservoir interval time-shift stays positive, although the value decreased in magnitude. The interval from seabed down to the Top Not Fm is also characterized by positive time-shifts, implying the increase in thickness. Intervals from seabed down to the Top Tofte Fm, Top Tije Fm and Top Åre Fm have negative time-shifts, suggesting increase in velocity and decrease in thickness.

Figure 5.2 presents the results which are time-shifts computed for exploration well 6608/10-2. The sign of time-shifts are mostly the same as in well 6608/10-3, but there are still some differences. Interval from seabed down to Top Sprinar Fm has opposite sign and marked with positive time-shifts. This implies slow-down in travel-time and decrease in velocity. Both intervals from seabed to Top Spekk Fm and Top Not Fm differ as well. Here the time-shifts are negative.

Figure 5.3 shows the time-shift values for injector well 6608/10-F-1H. It can be noted that the interval from seabed to Top Not Fm is marked with positive time-shifts, suggesting slow-down in travel-time across the whole interval, including Top Kai, Top Springar, Top Spekk and Top Garn formations. For the last three intervals the time-shifts are negative as in well 6608/10-3.

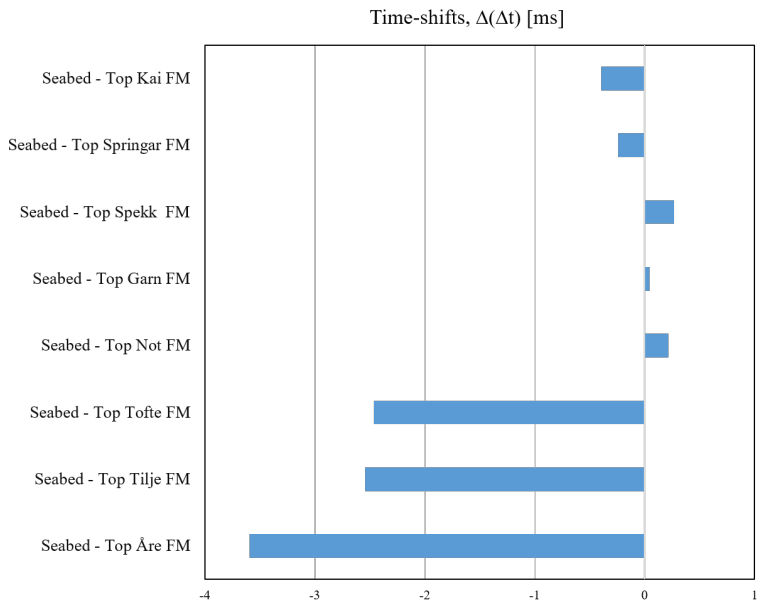


**Figure 5.1:** Time-shift values, calculated using Method 1, for the intervals between seabed and top of each interpreted horizon in well 6608/10-3. Negative values show decrease in interval TWT thickness, while positive values show increase in TWT thickness

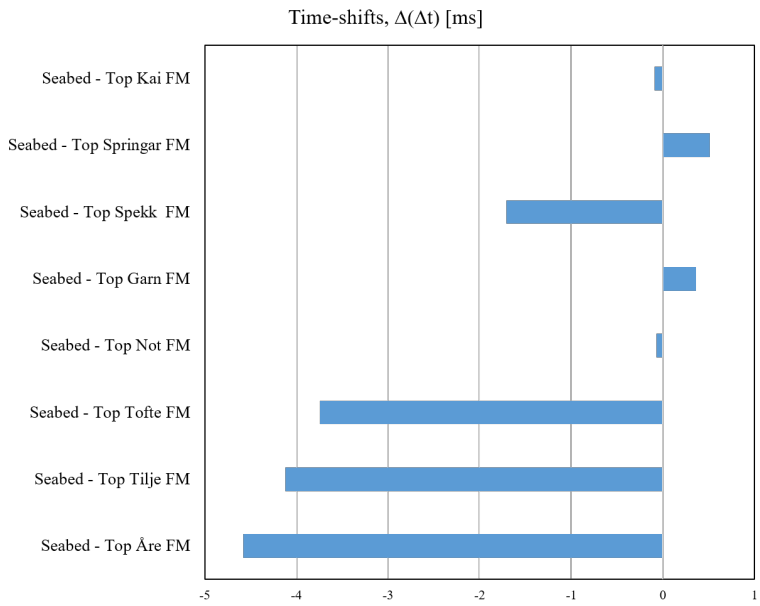


**Figure 5.2:** Time-shift values, calculated using Method 1, for the intervals between seabed and top of each interpreted horizon in well 6608/10-2

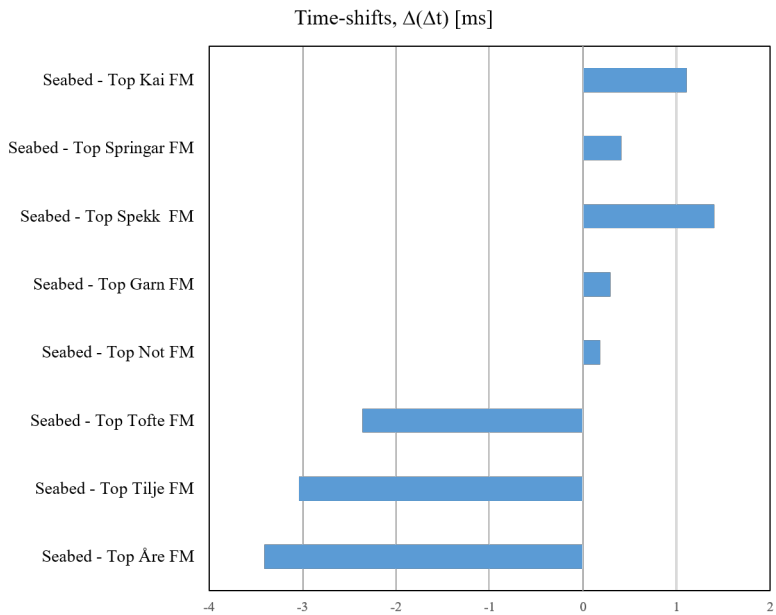


**Figure 5.3:** Time-shift values, calculated using Method 1, for the intervals between seabed and top of each interpreted horizon in well 6608/10-F-1H

### 5.1.2 Method 2

Comparing Method 1 and Method 2 it can be said that the time-shifts, generally, have similar behaviour. In well 6608/10-3 (Figure 5.4) the interval from Top Spekk to Top Garn differs, and, here, time-shifts are negative. In the Top Tilje Fm - Top Åre Fm interval time-shifts, also, have opposite sign, compared to Method 1. In well 6608/10-2 the only dissimilar interval is, again, Top Tilje Fm - Top Åre Fm (Figure 5.5). In well 6608/10-F-1H there are more discrepancies (Figure 5.6). Intervals Top Kai Fm- Top Springar Fm, Top Spekk Fm - Top Garn Fm, and Top Garn Fm - Top Not Fm are marked with negative time-shifts, whereas time-shifts calculated using Method 1 are positive in this well.

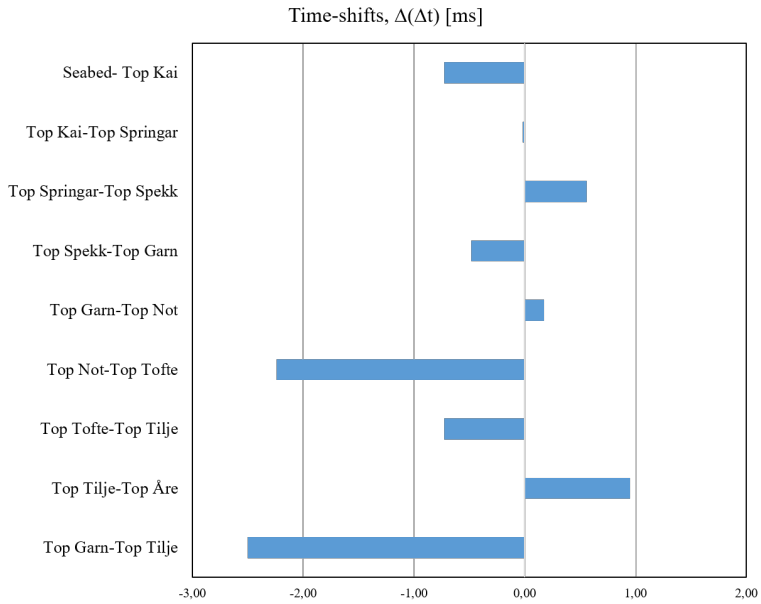


**Figure 5.4:** Time-shift values, calculated using Method 2, for the intervals between individual horizons in well 6608/10-3

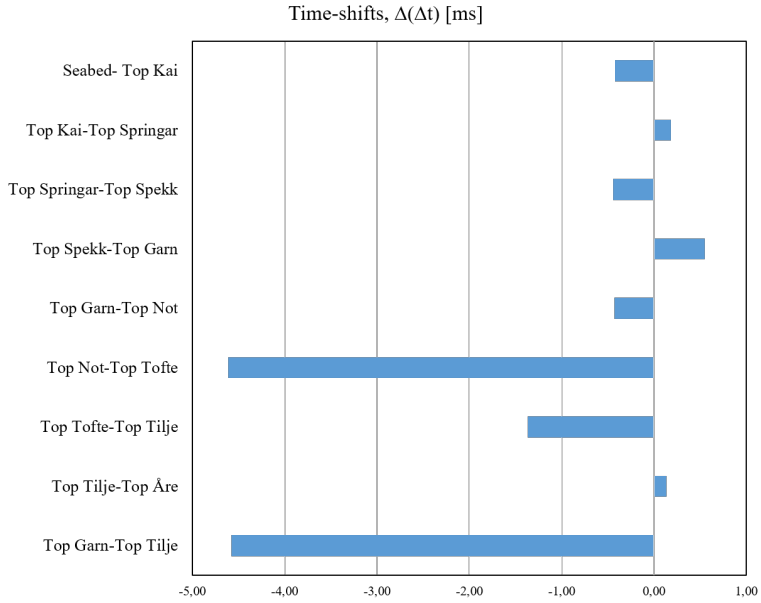


**Figure 5.5:** Time-shift values, calculated using Method 2, for the intervals between individual horizons in well 6608/10-2

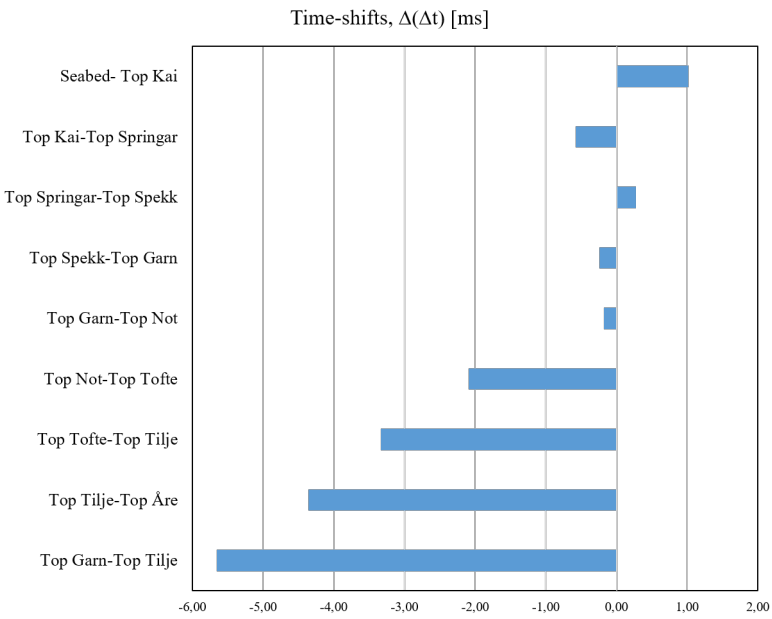


**Figure 5.6:** Time-shift values, calculated using Method 2, for the intervals between individual horizons in well 6608/10-F-1H

## 5.2 Time-shift maps

To present all the figures in a systematic way it was decided to show in Results section only time-shift maps generated using cross-correlation technique. The time-shift maps which were created using Method 1 and Method 2 can be seen in Appendix B and Appendix C

### 5.2.1 Cross-correlation technique

Figure 5.7 shows the time-shifts across the seabed. The negative and positive time-shifts in a form of parallel lines marked with light blue/blue and yellow colors respectively are noted on cross-correlation map. The inline seismic section intersecting the cross-correlation map is shown as an example with differently colored squares which mark the most pronounced time-shifts. In Figure 5.7b the squares show the areas which correspond to these time-shifts. These are the zones where the seabed is disturbed the most and has complex structure.

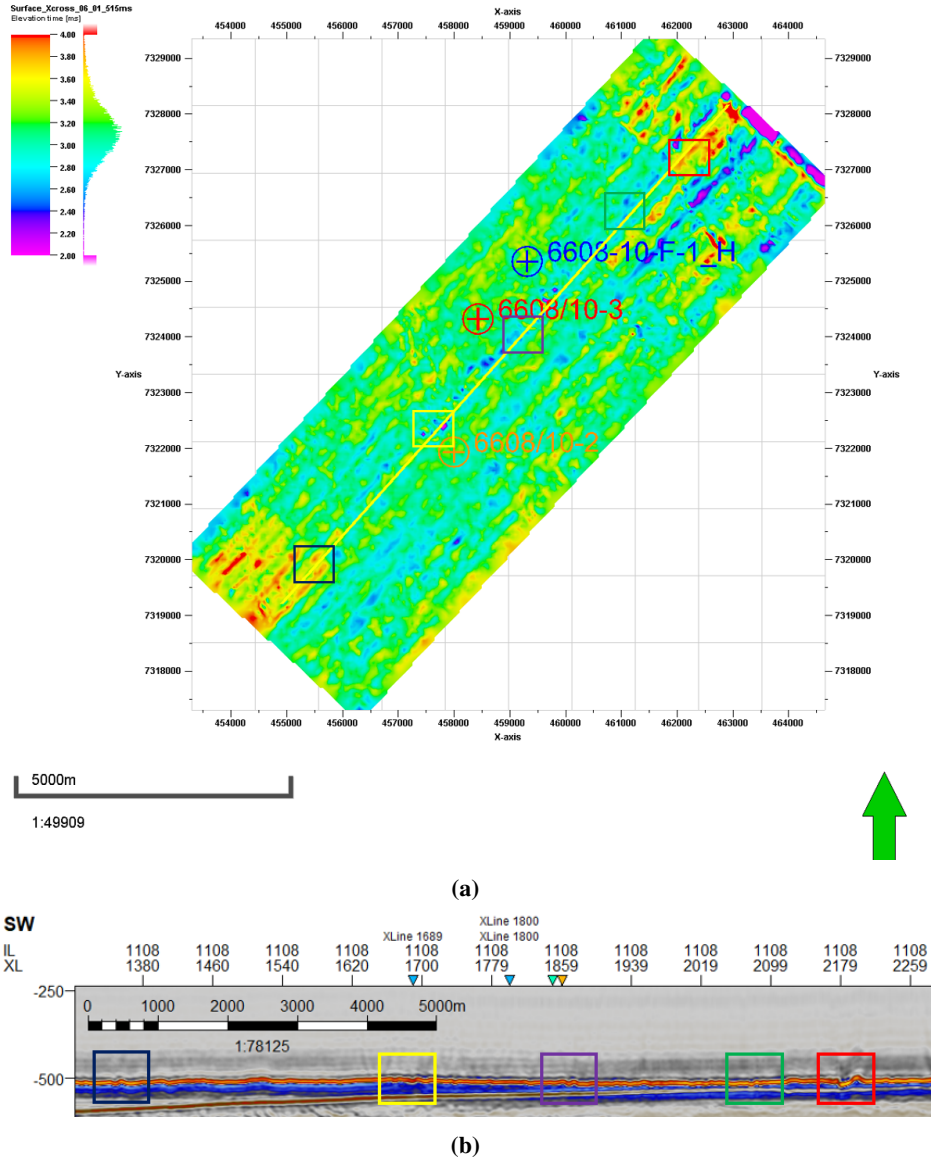


**Figure 5.7:** (a) Cross-correlation map showing the variations in time-shifts across 515 ms level (seabed). Yellow line indicates inline seismic section (Figure 5.7b) intersecting this time-shift map (b) Inline 1108 displaying the seabed. Differently colored squares show the complexity of the seabed and corresponding squares are displayed at cross-correlation map, where time-shifts can be noted specifically at this locations

Figure 5.8 represents the surface at 2300 ms level, which approximately indicates the location of Top Spekk Fm. The time-shifts are ranging from positive to negative across

the whole surface. The reservoir shape marked with black line is displayed to observe how changes in the reservoir zone propagate to overburden and affect it, and if time-shifts in the overburden are correlatable with the time-shifts in the reservoir zone.

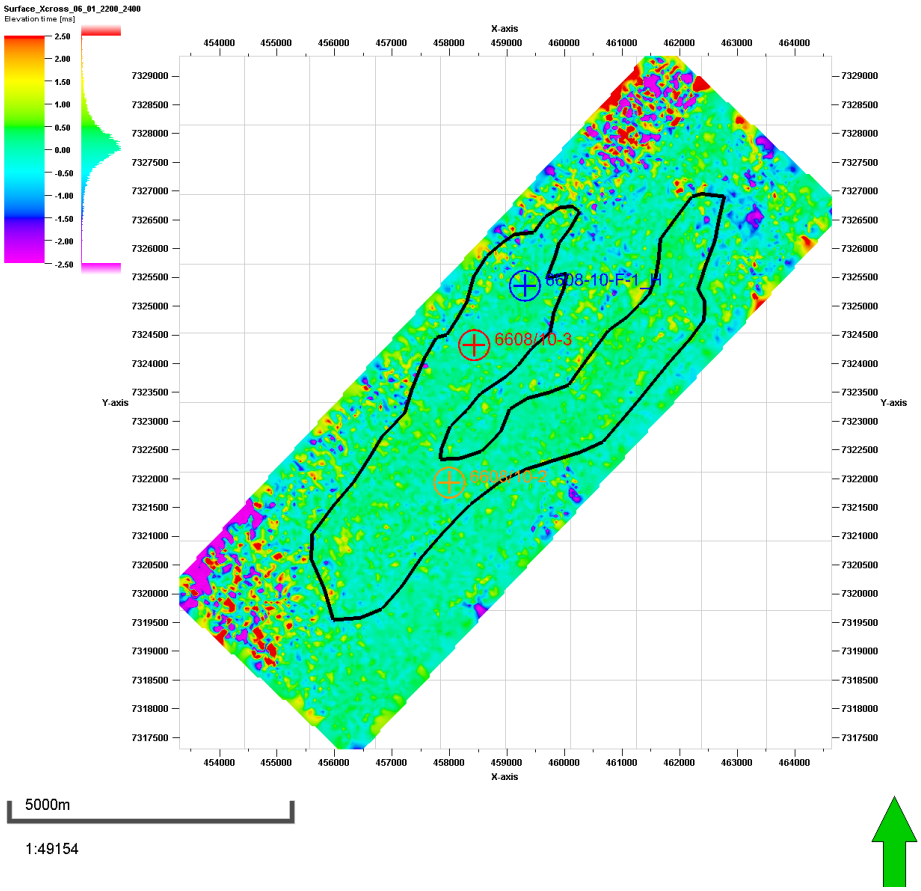


**Figure 5.8:** Top view of time-shift map at 2300 ms level, which corresponds to Top Spekk Fm. Black coloured line delineates the reservoir shape

Figure 5.9 displays the time-shift map at 2425 ms, which is approximate level for the Top Garn formation. The reservoir shape is shown in black color, and it can be observed that the areas around 3 wells are marked with green and yellow colors which indicate positive time-shifts. Area within G-segment contains negative time-shifts (blue and magenta colors) along the eastern part of the field which implies drop in travel-time. Outside of the reservoir shape some noisy areas can be noticed.

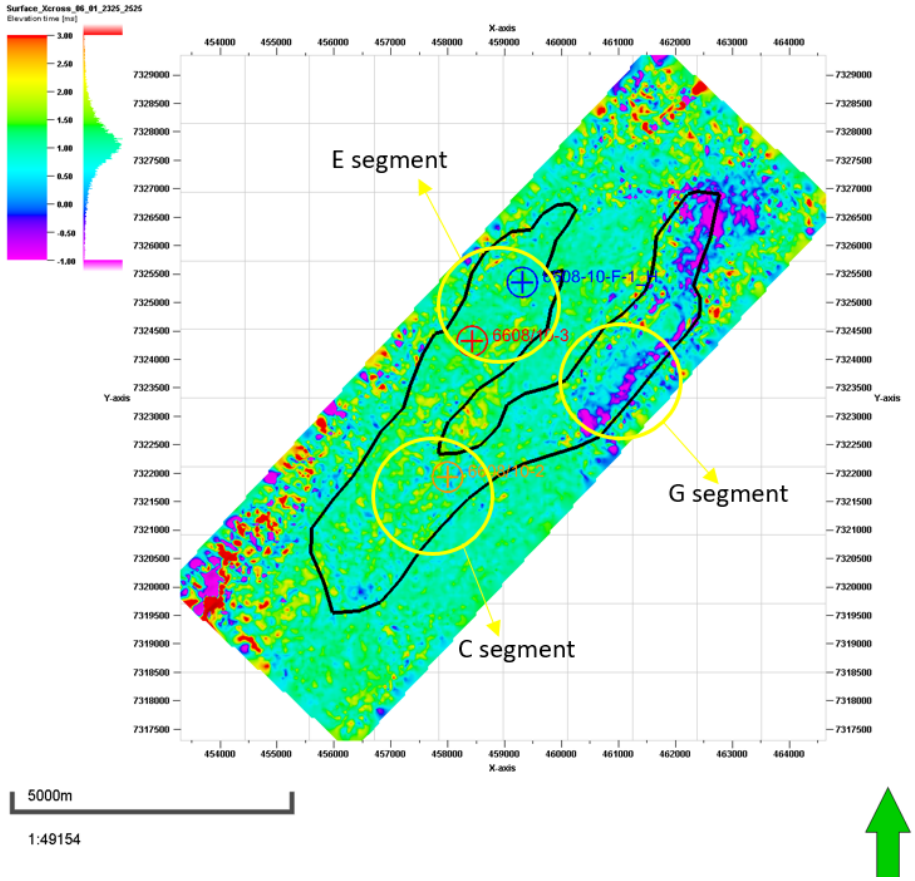


**Figure 5.9:** Top view of time-shift map at level of 2425 ms (approximately Top Garn Fm) generated using cross-correlation technique. Black coloured line delineates the reservoir shape, while yellow circles indicate locations of the segments

Figure 5.10 shows the interval deeper, 2500 ms, related to Top Tofte formation. Here, the negative time-shifts in G-segment become more pronounced, while segments E and C are still dominated by zero to positive time-shifts. Closer to well locations negative time-shifts are more distinct, implying speed up in velocity.

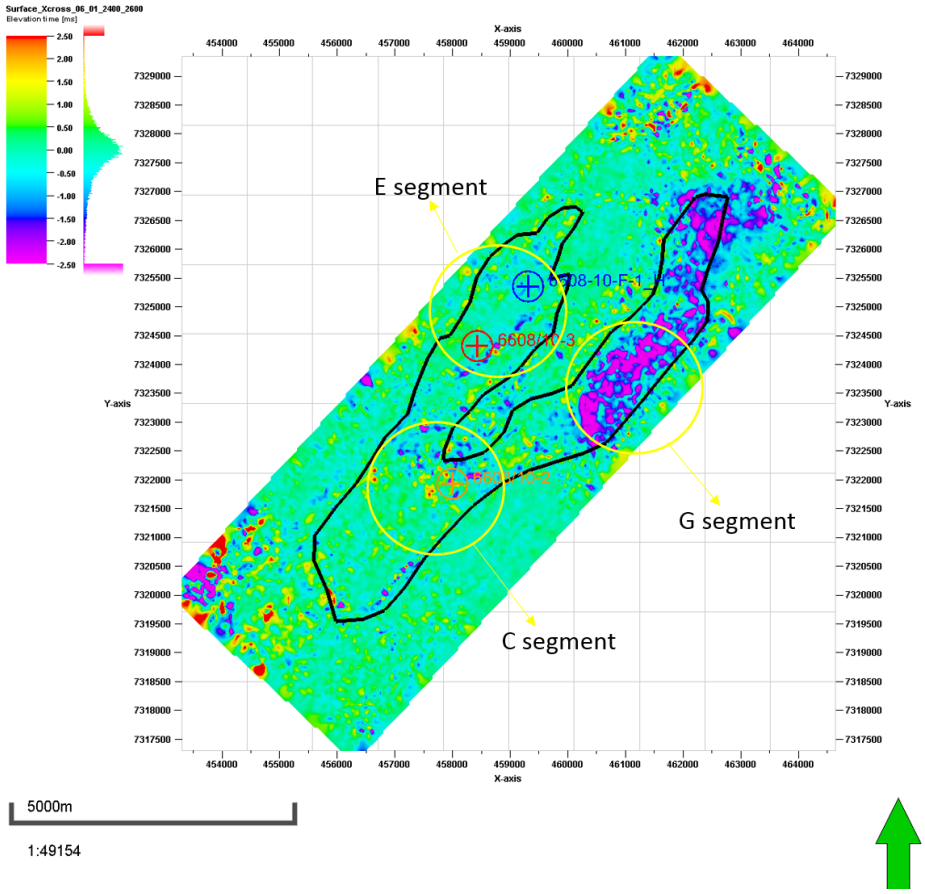


**Figure 5.10:** Top view of time-shift map at 2500 ms level (approximately Top Tofte Fm) generated using cross-correlation technique. Black coloured line delineates the reservoir shape, while yellow circles indicate locations of the segments

Figure 5.11 shows the time-shift map at 2600 ms level which is the base of the reservoir interval (approximately Top Åre FM ). Within the reservoir itself, negative time-shift indicated by blue and magenta colors could be distinguished, suggesting drop in travel-time. The highest negative time-shifts are noticed within the four segments of the Norne field. The area between C- and G- segment, marked with red circle, and the areas outside the horst block show almost zero to positive time-shifts. The switch from negative time-shifts to positive time-shifts fits the shape of the reservoir section delineated by black color.

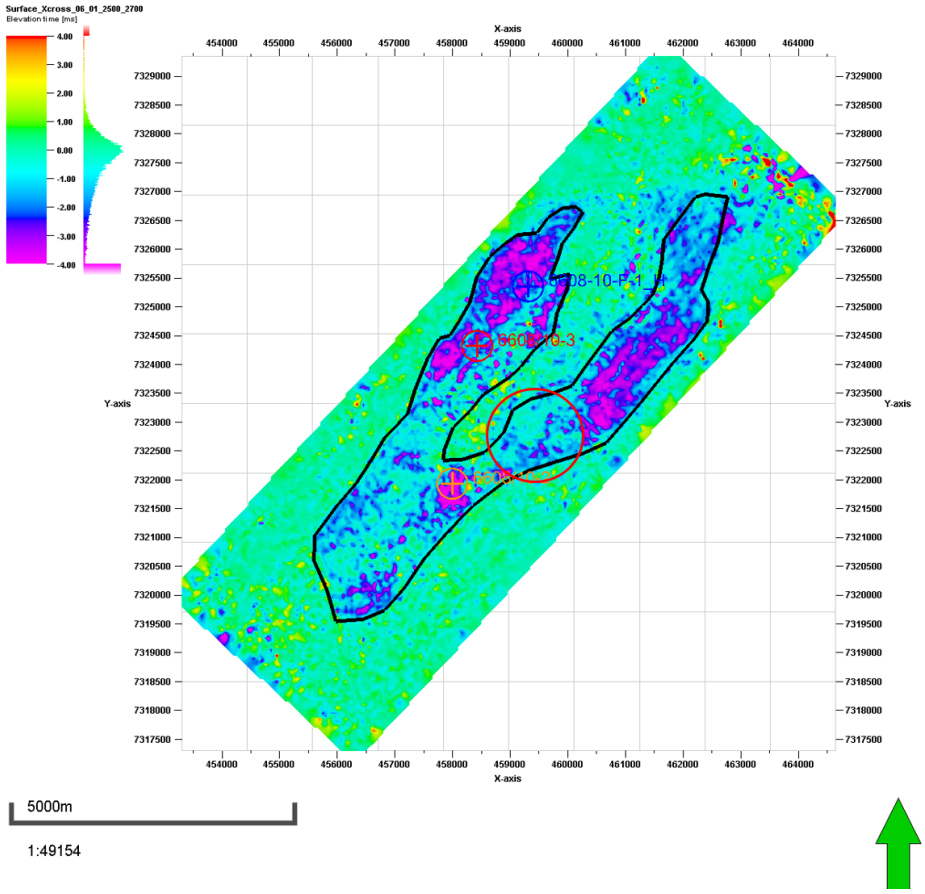


**Figure 5.11:** Top view of time-shift map at 2600 ms level (approximately Top Åre Fm) generated using cross-correlation technique. Black coloured line delineates the reservoir shape, while red circle indicates the area betwenn C- and G- segment

Chapter 6

# Discussion

## 6.1 Comparison of different techniques

In general, the correlation of time-shifts (and therefore relative time-shifts) signs (negative or positive) in both methods match very well in 6608/10-3 and 6608/10-2, while in well 6608/10-F-1H there are discrepancies. The values of time-shifts and relative time-shifts in Method 2 are much higher for reservoir zone (Figures 5.4-5.6 and C.3-C.5). Method 1 calculates the accumulated time-shifts from seabed down to each interpreted horizons, whereas Method 2 calculates the incremental change from one horizon to the next one. Since interpretation of the seismic data is subjected to interpreter's view, and the resolution of the seismic data is decreasing with depth, it is hard to interpret reflectors, especially in the faulted reservoir zone. Therefore, some uncertainty that affects the final computations should be taken into account. This uncertainty in interpretation will affect Method 2 more than Method 1, as the computation error will propagate into obtained outcomes based on Equation 3.6.

Comparing cross-correlation technique with the methods described above it is evident that the lateral distribution of the travel-time change on cross-correlation time-shift maps seems to be more clear than that for Method 1 or Method 2 (For example Figures B.1-B.2 or Figures C.1-C.2). Therefore, to observe the changes in travel-time regionally it is best to use cross-correlation technique, while for local changes Method 1 works better. However, in some cases, there might also be uncertainty in the cross-correlation maps. In Figure 6.1 the geometry of Spekk Fm is indicated by purple line. The window position (yellow stippled line) which was chosen for cross-correlation between two seismic vintages omits the deeper parts of the layer. Even though this has small impact on the results, it does not represent the whole picture and this technique works the best for the layers deposited horizontally with small variations in depth.

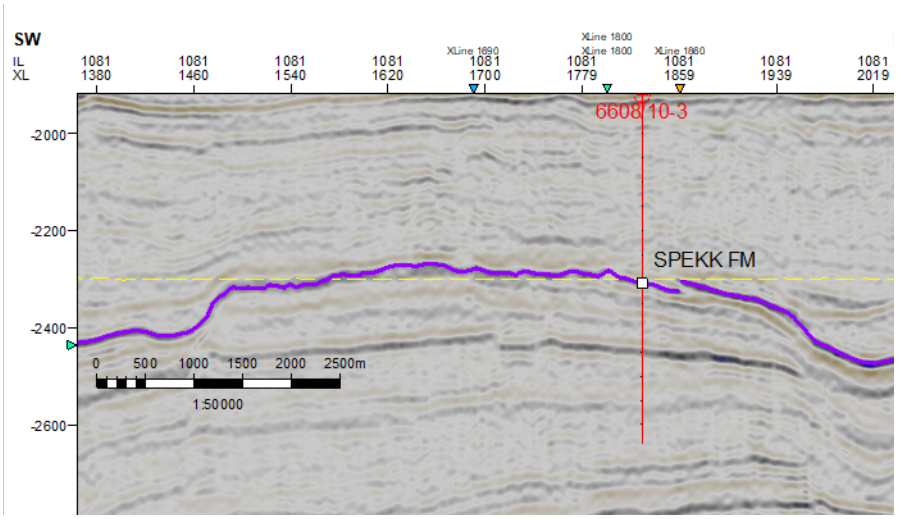


**Figure 6.1:** Inline 1081 intersecting well 6608/10-3. Purple interpreted reflector indicates Top Spekk formation, whereas yellow stippled line shows the chosen window position for cross-correlation between 2001 and 2006 seismic surveys

## 6.2 Time-shift analysis

### 6.2.1 Reservoir zone

The discussion is based on Figure 5.9 and Figure 5.10.

E-segment, where 6608/10-3 and 6608/10-F-1H wells were drilled, is located in the north-western region of the Norne field. Thickness of the Garn Fm in this segment is around 40 m and GOC in the well 6608/10-3 is at the depth of 2598.5 m which includes Garn formation (Statoil, 1993) (see Figure 6.2). After production of hydrocarbons, the pressure drops and gas starts to expand resulting in density decrease. This in turn affects the velocities propagating through the Garn formation and they become slower. The cross-correlation maps show the positive time-shifts in this segment at the Garn level, and a bit deeper, which correlates well with this explanation.

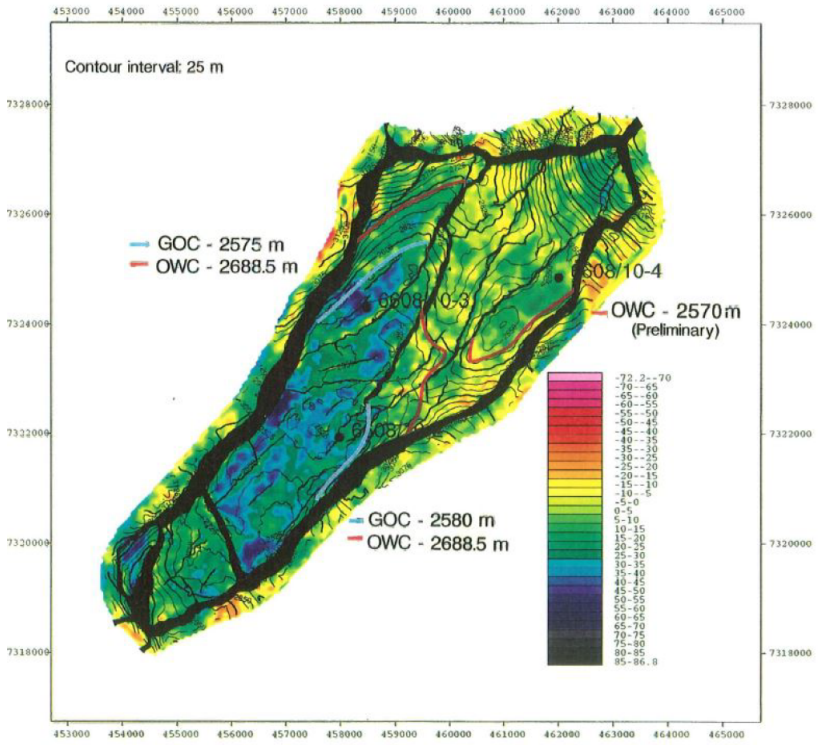


**Figure 6.2:** Top reservoir map showing OWC and GOC for the Norne field in 1994 and well locations

However, as water is injected (well 6608/10-F-1H) to the reservoir it replaces the oil, and the water saturation increases. Meanwhile, pore pressure drops due to production. This will give more distinct 4D effect on cross-correlation maps. Both water saturation increase and pore pressure drop will result in increase in velocities, so that two effects reinforce each other. This process can explain the change from positive to negative time-shifts with the value of 3-4 ms deeper within the reservoir section (Tofte-Tilje Fm).

Well 6608/10-2 was drilled in the C-segment, which is located in the south-eastern part of the Norne field. Here the gas cap (mainly in Garn Fm) overlies the oil in Ile and Tofte formations. There is carbonate cemented barrier between Ile and Tofte Fm. Before acquisition in 2001 the gas was injected in this area. The effect of it can be seen on cross-correlation maps at Garn level with positive time-shifts.

The negative time-shifts observed in the lower part of the reservoir interval could be explained by the fact that very thin (around 20 cm) carbonate cemented barrier might contain small-scale faults that are below seismic resolution and could not be detected on seismic data. This faults allow water to flow to the lower part of Ile formation and replace the oil, resulting in velocity increase and corresponding travel-time speed-up.

According to Osdal et al. (2006) the upper part of the Tofte formation was undrained, and, therefore, a new producer was drilled here in 2005. Before this new producer, a pilot

well was drilled into Tofte formation to confirm OWC and take pressure measurements. The pilot well approved that upper part of the Tofte Fm was undrained and showed gas expansion. However, much of the water flooded into this zone from the north and the effect of water replacing oil overrides the gas expansion effect. Again, the water saturation increase leads to increase in velocities, which in turn results in negative time-shifts.

Even though this work does not describe any well data for G-segment, cross-correlation maps showed pronounced response of negative time-shifts within and outside of the reservoir interval in this segment. Therefore, it is important to analyze the G-segment and discussion will be based on Osdal et al. (2006) and Aschjem (2013).

G-segment is located in the north-eastern part of the Norne field (Figure 2.5) and contains oil only in the uppermost section of Garn Fm with the thickness of 25-30 m. Before production the reservoir was undersaturated, which means that the reservoir was filled with oil and it existed above bubble point[1] without gas cap. After production the pressure depleted and the gas came out of the solution. Due to lack of pressure support, the water injector was drilled downflank in the water zone and this lead to general pressure increase in the segment.

The challenging part of the interpretation of these effects is that the changes in seismic properties (velocity and therefore travel-time) are affected by both saturation and pressure changes. In a water-driven process, the oil saturation decreases, whereas pore pressure, on the contrary, increases. The decreased oil saturation causes the velocity of the wave to increase, while increased pore pressure leads to decrease in the seismic waves (Wang, 2001).

Figure 6.3 shows the change in acoustic impedance from 2001 to 2006. It can be noticed that the impedance is decreased closer to the western main fault, which correlates very well with the positive time-shifts in Figure 5.9. Water injection started in 2001 and as the result pressure increased, which can explain both the decreased impedance and positive time-shifts. Closer to the eastern part, the gas going back to oil causes the increase in acoustic impedance. This opposite effects are observed due to the presence of pressure barrier C. The pressure increase in the eastern part is less than the pressure increase closer to the western main fault. Also, it is know from rock physics that for the higher pore pressures the change in velocity can be higher.

[1] Bubble point is the pressure at a given temperature, at which the first bubble of gas comes out of the solution in oil (Petrowiki, 2019)

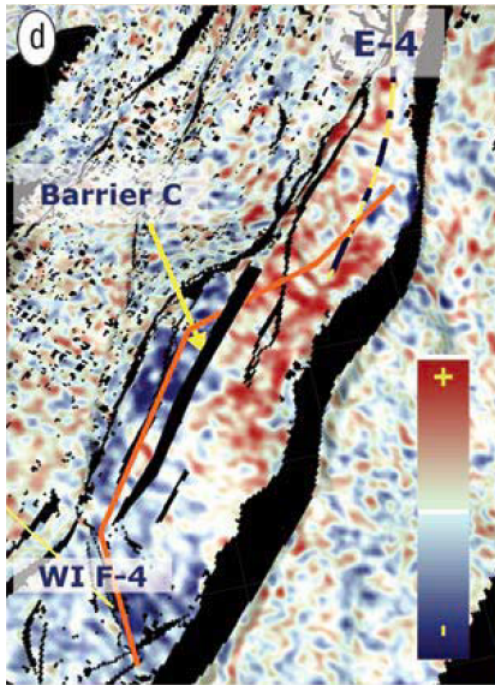


**Figure 6.3:** Change in acoustic impedance from 2001 to 2004. Blue indicates decrease in acoustic impedance related to pressure increase due to water injection. Red is increase in acoustic impedance related to gas going back to the oil phase

For better analysis of the 4D effect in the underburden (Figure 5.11), the Gassmann equation can be used to demonstrate the effect of fluid substitution on velocities (and therefore on time-shifts) from water saturation of 20% to water saturation of 80%. The interval taken for that will be from Garn Fm till Tilje Fm, which is around 126 m. Using Equation 3.4 and assuming small changes in the layer thickness (dz) the equation becomes:

$$dt \sim -\frac{2z dv_p}{v_p^2} \tag{6.1}$$

$dv_p$ is the difference between velocity in 80% water saturated interval and 20% water saturated interval and $v_p$ is the initial velocity in 20% water saturated interval, and $z$ is the thickness of the interval.

In practice, fluid substitution is accomplished by starting with P- and S- waves velocities measured on rocks saturated with the initial fluid or gas and then extracting bulk and shear moduli. After that, the bulk modulus of the rock saturated with new fluid is computed and velocities are recreated. However, if shear velocity is not given then bulk modulus cannot be extracted from velocity, which is the case in this work (Mavko et al., 2009). To solve this problem Mavko et al. (1995) suggested a method that operates on the P-wave modulus, $M = \rho v_p^2$. After using this relation and calculating velocities, the Equation 6.1 could be solved and the time-shifts are established. The value is $-3.5$ ms,

which suggest increase in velocity and reduction in thickness, i.e compaction. This fits the results from cross-correlation time-shift maps and Method 1.

The calculated time-shifts and relative time-shifts in specific well locations using Method 1 and Method 2 also support the outcomes of cross-correlation maps. The magnitude of time-shifts and relative time-shifts are higher for Method 2, and as was discussed previously this is not reliable. The only difference in sign convention is at the Top Åre formation, where in Method 2 it shows positive time-shifts. However, Method 1, cross-correlation analysis and fluid substitution exercise show negative time-shifts, which are considered more robust.

### 6.2.2 Overburden

In general, thickness of the overburden is ranging from one to several kilometers, therefore even very small changes in velocity can be accumulated into noticeable time-shifts at top reservoir. Overburden time-shifts caused by reservoir compaction can be easily distinguished for chalk fields (e.g., Valhall and Ekofisk) and for high-pressure, high-temperature (HTHP) fields (e.g., Elgin and Kristin) (Røste et al., 2015).

However, in case with fields with normal pressure and temperature and sandstone reservoir rock it is more difficult to observe time-shifts changes and typically they are very small. The degree of compaction is dependent on the stiffness (or compressibility) of the rock. The compressibility of a sandstone increases with increasing pore pressure. This causes the compressibility of water-filled sandstone to be greater than that for oil-filled sandstone, which in turn is greater than compressibility of gas-filled sandstone (Mann and Fatt, 1960).

Since the reservoir in Norne field consist of sandstone, the reservoir compaction is likely to be very small and does not have impact on the whole overburden thickness. Nevertheless, this small compaction of the reservoir may affect the stress distribution in the overburden, which might be an explanation for the observed time-shifts in this zone.

Two levels right above Top Garn formation are displayed in Figure 6.4 and their corresponding cross-correlation time-shift maps are shown in Figure 5.8 (yellow stippled line), Figure D.5 (red stippled line).

In Figure D.5 the level right above Top Garn formation at 2350 ms can be seen. The cross-correlation surface displays the time-shifts ranging from positive to zero. This might be explained by the fact that there is gap cap overlying the oil and with production gas may expand. As a consequence of pressure drop in the Garn formation, the stress in the interval at 2350 ms increases and leads to velocity slow-down. This slow-down affects the travel-time change, and positive time-shifts can be observed.

Figure 5.8 shows the time-shifts across 2300 ms level, which was chosen to represent the Spekk Fm. Areas around 6608/10-3 and 6608/10-F-1H, which are located in E-segment are marked with positive time-shifts, while some negative values can be observed around 6608/10-2 well, which is drilled in C-segment. Both Method 1 and Method 2 indicate positive time-shifts in 6608/10-3 and 6608/10-F-1H (Figures 5.1 and 5.3 for Method 1, and Figures 5.4 and 5.6 for Method 2), whereas in well 6608/10-2 (Figure 5.2 and Figure 5.5 for Method 1 and Method 2 respectively) the time-shifts are negative, which fits well with the result from cross-correlation map. The positive time-shifts might be explained in the same manner as the time-shifts across the level at 2350 ms. Negative

time-shifts in C-segment can be interpreted based on the evidence of water flooding and pressure increase effect in this area of reservoir section. Due to changes in the reservoir, stress in Spekk Fm can be increased resulting in velocity speed-up through this formation.

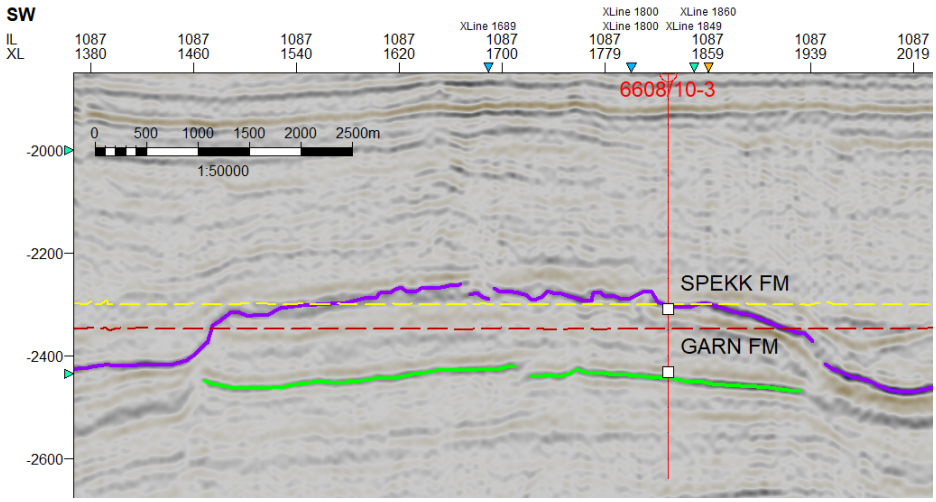


**Figure 6.4:** Three window position for generating cross-correlation time-shift maps are displayed on inline 1087 intersecting well 6608/10-3. Yellow stippled line represents the level at 2300 ms which approximately indicates Top Spekk Fm position (purple horizon), red stippled line is the level at 2350 ms which is the closest to the top reservoir Garn Fm (green horizon)

Going further up from the reservoir zone, in Figure D.4 and Figure D.3 the time-shifts become less observable within the area which delineates the reservoir. In Figure D.4 the surface corresponds to the level, where Springar Fm is approximately located and it is dominated by positive time-shifts regionally, however when calculating time-shifts locally (at well locations) both methods show negative time-shifts in well 6608/10-3 (see Figures 5.1 and 5.4). The Spekk formation might still be affected by the physical changes in Garn Fm, although lithological variation within Spekk Fm (it is mudstone with limestone and sandstone stringers) itself may cause discrepancies in the time-shifts at well locations.

Figure D.3 displays the level at 1650 ms, which is located in the area with polygonal faults. There is a mix of positive and negative time-shifts. The areas where time-shifts with opposite signs outstand correspond to fault locations (Figure 6.5). Mainly, if lateral extension of the reservoir is greater than the thickness, $\Delta\sigma_{horizontal} < \Delta\sigma_{vertical}$ inside the reservoir. Such direction dependent stress is termed differential stress and the development of this stress causes fault reactivation(Mulders, 2003). This might affect the stress distribution specifically at this level of the overburden and due to fault reactivation the layers are a bit shifted, which causes changes in travel-time from 2001 to 2006.

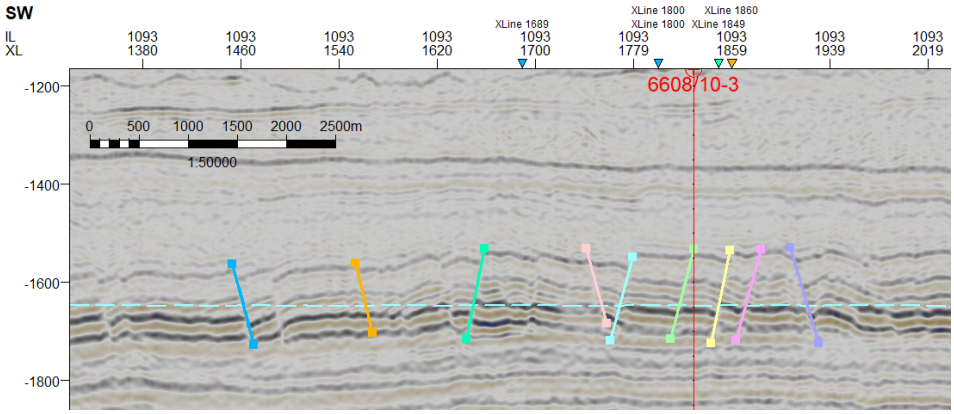


**Figure 6.5:** Inline section 1093 shows the level at 1650 ms, which is the area in the overburden contaminated by the polygonal faults. Vertical colored lines represent the interpreted polygonal faults, while blue stippled line is highlighting the position of the cross-correlation time-shift map displayed in Figure D.3

Figure D.2 represents the level at 1350 ms, where approximately Top Kai Fm is positioned. Again, regionally only zero to positive time-shifts can be observed, whereas the calculation of time-shifts using Method 1 and Method 2 showed negative time-shifts both in wells 6608/10-3 and 6608/10-2 and positive time-shift in well 6608/10-F-1H. Since position of Top Kai Fm is the first strong reflector over the level described above (1650 ms) it might be affected by the physical changes of that layer. The movable layers of that interval might have an impact on Kai formation and stress distribution is changed in it. As can be seen in Figure 6.5 well 6608/10-3 is drilled in the zone with reverse faulting, for which shortening of the rock is common. After fault reactivation the layer could have slightly moved, causing Kai Fm to decrease in thickness, which resulted in negative time-shifts.

Figure 5.7a represents the seabed in Norne field. The seabed in this area is rough and is contaminated by the ice scours in different directions. The variations in time-shifts from positive to negative are associated with the rough seabed and the diffracted energy it induces and causes residual noise on the time-lapse data. The changes increase with the seabed complexity (Figure 5.7b). Also, such sources of non-repeatability like water column variations, mis-positioning and strength of the ice scours produce diffracted energy and contaminate the data even more. In Grude et al. (2013) paper this effects are described and explained in more details.

Chapter 7

# Conclusion

In this master thesis time-shift analysis was performed over Norne field to observe and explain the nature of the changes within and outside of reservoir interval. Decrease and/or increase of pore pressure, gas coming out and going back into the solution and water injection are effects that have changed the rock parameters in the reservoir interval. This in turn creates distortion in stress field of the rocks surrounding the reservoir rock and induces the changes in velocity and therefore in travel-time.

The main results of this work are outlined in bullet points below:

- Method 1 is considered more robust compared to Method 2 because of the different techniques used to calculate the time-shift and relative time-shift values. In Method 1, the reference horizon stays constant at seafloor, and the seismic interpretation uncertainty will have small impact on the time-shift (and relative time-shift) values than for Method 2, where the time-shift magnitudes are computed from one horizon to the next one.

- The regional distribution of time-shift values is best seen in cross-correlation maps, whereas Method 1 and Method 2 could be used to identify local changes in time-shifts and relative-time-shifts.

- Relying on time-shift results it can be concluded that the overburden acts as heterogeneous mass and when the reservoir is produced each layer in overburden reacts individually to these production-induced changes. Hence, it can be said that stress sensitivity varies from one layer to another in the overburden due to difference in lithology and elastic properties of these layers.

- The travel-time changes might be the result of both thickness and velocity changes, however, since Norne field is a sandstone reservoir, the change in thickness is assumed to be very small and therefore has small impact on the overburden. Therefore, it might be presumed that the time-shifts are induced by changes in stress field in the overburden, which, in turn, is the result of changes in reservoir.

- In G-segment, fault close to the western main fault acted as a pressure barrier and isolated higher pore pressure increase from another one, which was lower. This lead to different effects in travel-time changes, i.e. slow-down was observed in the area close to the western fault, while speed-up was noticed closer to the eastern part.
- Both in C- and E- segments the upper zone of the reservoir is dominated by positive time-shifts because of gas injection and gas expansion, while deeper parts are characterized by negative time-shifts due to water injection.

More than one 4D effect has an impact on the seismic response, which makes the interpretation of the time-shift behaviour much more complicated and further detailed study should be carried out. For further work it is suggested to use Landrø (2001) technique for discriminating between pressure and saturation effects, where near- and far-offset stacks for baseline and monitor surveys are used as independent measurements. The direct expressions for saturation and pressure changes are acquired using rock physics relations combined with AVO equations. Furthermore, construction of geomechanical model would help to closely examine the time-shifts in the overburden and better understand its behaviour. Also, these results can be used in simulation model to check if the outcomes would correlate with one another.

# Bibliography

Aschjem, G., 2013. Mapping Reservoir Changes Using 4D Seismic on the Norne G-segment, Norwegian Sea. Master's thesis, Norwegian University of Science and Technology, Norway, Trondheim.

Barkved, O. I., Kristiansen, T., 2005. Seismic time-lapse effects and stress changes: Examples from a compacting reservoir. Geophysics 24, 1244–1248, https://doi.org/10.1190/1.2149636.

Dalland, A., Augedahl, H. O., Bomstad, K., Ofstad, K., 1998. The Post-Triasic succession of the Mid-Norwegian shelf. In: Dalland, A., Worsley, D., Ofstad, K. (Eds.), A lithostratigraphic scheme for the Mesozoic and Cenozoic succession offshore mid- and northern Norway. NPD-Bulletin NO 4, pp. 3–65.

Dimri, V., Srivastava, R., Vedanti, N., 2012. Chapter 4 - Seismic Reservoir Monitoring. In: Dimri, V. P., Srivastava, R. P., Vedanti, N. (Eds.), Fractal Models in Exploration Geophysics. Vol. 41 of Handbook of Geophysical Exploration: Seismic Exploration. Pergamon, pp. 65 – 88, https://doi.org/10.1016/B978-0-08-045158-9.00004-X.

Equinor ASA, 2019. Equinor website. https://www.equinor.com/en/what-we-do/norwegian-continental-shelf-platforms/norne.html, Last accessed on 2019-03-30.

Erichsen, L. L., 2008. Estimation of Timeshifts and Velocity Changes from 4D Seismic Analysis: A Case Study from the Norne Field. Master's thesis, Norwegian University of Science and Technology, Norway, Trondheim.

Fayemendy, C., Espedal, P. I., Andersen, M., Lygren, M., 2012. Time-lapse seismic surveying: A multi-disciplinary tool for reservoir management on Snorre. First Break 30, 49–55, https://doi.org/10.3997/1365-2397.2012017.

Fjær, E., Holt, R. M., Horsrud, P., Raaen, A. M., Risnes, R., 2008. Chapter 12 - Reservoir Geomechanics. In: Fjær, E., Holt, R. M., Horsrud, P., Raaen, A. M., Risnes, R. (Eds.), Petroleum Related Rock Mechanics 2nd Edition. Vol. 53 of Developments in Petroleum Science. Elsevier, pp. 391 – 433, https://doi.org/10.1016/S0376-7361(07)53012-8.

Gassmann, F., 1951. ber die Elastizitt Porser Medien. Viertel. Naturforsch. Ges. Zrich 96, 1–23.

Gjerstad, H. M., Steffensen, I., Skagen, J. I., 1995. The Norne Field - Exploration History & Reservoir Development Strategy. Offshore Technology Conference, 525–532, https://doi.org/10.4043/7924-MS.

Goto, R., Lowden, D., Smith, P., Paulsen, J. O., Aronsen, H., Osdal, B., 2004. Steered-streamer 4D case study over the Norne field. SEG Technical Program Expanded Abstracts 23, https://doi.org/10.1190/1.1839695.

Grude, S., Osdal, B., Landrø, M., 2013. Sea-bed diffractions and their impact on 4D seismic data. Geophysical Prospecting 61, 199–214, https://doi.org/10.1111/j.1365-2478.2012.01118.x.

Guilbot, J., Smith, B., 2002. 4-D constrained depth conversion for reservoir compaction estimation: Application to Ekofisk Field. The Leading Edge 21, 302–308, https://doi.org/10.1190/1.1463782.

Han, D., Batzle, M. L., 2004. Gassmann's equation and fluidsaturation effects on seismic velocities. Geophysics 69 (2), 398–405, https://doi.org/10.1190/1.1707059.

Hatchell, P. J., Bourne, S. J., 2005a. Measuring reservoir compaction using timelapse timeshifts. SEG Technical Program Expanded Abstracts 2005, 2500–2503, https://doi.org/10.1190/1.2148230.

Hatchell, P. J., Bourne, S. J., 2005b. Rocks under strain: Strain-induced time-lapse time shifts are observed for depleting reservoirs. The Leading Edge 24 (12), 1222–1225, https://doi.org/10.1190/1.2149624.

Hatchell, P. J., van den Beukel, A., Molenaar, M. M., Maron, K. P., Kenter, C. J., Stammeijer, J. G. F., van der Velde, J. J., Sayers, C. M., 2005. Whole earth 4D: Reservoir monitoring geomechanics. SEG Technical Program Expanded Abstracts, 1330–1333https://doi.org/10.1190/1.1817532.

Holt, R. M., Nes, O. M., Fjaer, E., 2005. In-situ stress dependence of wave velocities in reservoir and overburden rocks. The Leading Edge 24 (12), 1268–1274, https://doi.org/10.1190/1.2149650.

Jack, I., 2017. 4D seismic - Past, Present, and Future. The Leading Edge 36, 386–392, https://doi.org/10.1190/tle36050386.1.

Kearey, P., Brooks, M., Hill, I., 2002. Chapter 3 - Elements of Seismic Surveying. In: An Introduction to Geophysical Exploration. Blackwell Science Ltd, pp. 21–42.

Kragh, E., Christie, P., 2002. Seismic repeatability, normalized RMS, and predictability. Geophysics 21, https://doi.org/10.1190/1.1497316.

Landrø, M., 2001. Discrimination between pressure and fluid saturation changes from time lapse data. Geophysics, 836–844, https://doi.org/10.1190/1.1444973.

Landrø, M., 2015. Chapter 19 - 4D Seismic. In: Bjørlykke, K. (Ed.), Petroleum Geoscience: From Sedimentary Environments to Rock Physics. Springer Berlin Heidelberg, pp. 489–514, https://doi.org/10.1007/978-3-642-34132-8_19.

Landrø, M., Amundsen, L., 2018. Introduction to Exploration Geophysics with Recent Advances. Bivrost.

Landrø, M., Solheim, O. A., Hilde, E., Ekren, B. O., Strønen, L. K., 1999. The Gullfaks 4D seismic study. Petroleum Geoscience 5, https://doi.org/10.1144/petgeo.5.3.213.

Landrø, M., Stammeijer, J., 2004. Quantitative estimation of compaction and velocity changes using 4D impedance and travel-time changes. Geophysics 69 (4), 949–957, https://doi.org/10.1190/1.1778238.

Landrø, M., Strønen, L. K., Digranes, P., Solheim, O. A., Hilde, E., 2001. Time-lapse seismic as a complementary tool for in-fill drilling. Journal of Petroleum Science and Engineering 31 (2), 81 – 92, https://doi.org/10.1016/S0920-4105(01)00122-X.

MacBeth, C., Mangriotis, M. D., Amini, H., 2018. Review Paper: Post-stack 4D seismic time-shifts: Interpretation and evaluation. Geophysical Prospecting 67 (1), 3–31, https://doi.org/10.1111/1365-2478.12688.

Mann, R. L., Fatt, I., 1960. Effect of pore fluids on the elastic properties of sandstone. Geophysics 25 (2), 433–444, https://doi.org/10.1190/1.1438713.

Mavko, G., Chan, C., Mukerji, T., 1995. Fluid substitution: Estimating changes in VP without knowing VS. Geophysics 60 (6), 1750–1755, https://doi.org/10.1190/1.1443908.

Mavko, G., Mukerji, T., Dvorkin, J., 2009. Fluid effects on wave propagation, 2nd Edition. Cambridge University Press, p. 266346.

Mulders, F. M. M., 2003. Modelling of Stress Development and Fault Slip in and Around a Producing Gas Reservoir. Delft University Press. Doctoral Thesis, 288.

Norwegian Petroleum, 2019. Norwegian Ministry of Petroleum and Energy and the Norwegian Petroleum Directorate. https://www.norskpetroleum.no/en/facts/field/norne, Last accessed on 2019-03-30.

NPD, 2019. $CO_2$ storage atlas of the Norwegian Sea. Norwegian Petroleum Directorate, 1–60.

NPD factpages, 2019. Norwegian petroleum directorate. http://factpages.npd.no/factpages/Default.aspx?culture=no, Last accessed on 2019-05-28.

Osdal, B., Husby, O., Aronsen, H. A., Chen, N., Alsos, T., 2006. Mapping the fluid front and pressure buildup using 4D data on Norne Field. The Leading Edge 25, 1134–1141, https://doi.org/10.1190/1.2349818.

Petrel, 2017. Petrel Help Center. Last accessed on 2019-05-27.

Petrel Geophysics, 2016. Training and Exercise Guide. Schlumberger.

Petrowiki, 2019. https://www.petrowiki.org/Glossary:Bubblepoint Last accessed on 2019-06-02.

Pigott, J. D., Kang, M. H., Han, H. C., 2013. First order seismic attributes for clastic seismic facies interpretation: Examples from the East China Sea. Journal of Asian Earth Sciences 66, 34–54, https://doi.org/10.1016/j.jseaes.2012.11.043.

Randen, T., Pedersen, S. I., Sønneland, L., 2001. Automatic detection and extraction of faults from three-dimensional seismic data. SEG Technical Program Expanded Abstracts, 551–554.

Røste, T., Dybvik, O. P., Søreide, O. K., 2015. Overburden 4D time-shifts induced by reservoir compaction at Snorre field. The Leading Edge 34 (11), 1366–1374, https://doi.org/10.1190/tle34111366.1.

Røste, T., Stovas, A., Landrø, M., 2006. Estimation of layer thickness and velocity changes using 4D prestack seismic data. Geophysics 71 (6), S219–S234, https://doi.org/10.1190/1.2335657.

Simm, R., Bacon, M., 2014. Chapter 4 - Well to seismic ties. In: Seismic Amplitude: An Interpreter's Handbook. Cambridge University Press, pp. 38–57, https://doi.org/10.1017/CBO9780511984501.005.

Statoil, 1992. Completion report well 6608/10-2 PL128. Norwegian Petroleum Directorate,http://factpages.npd.no/pbl/wellbore_documents/1782_6608_10_2_COMPLETION_REPORT_AND_LOG.pdf, Last accessed on 2019-06-12.

Statoil, 1993. Completion report well 6608/10-3 PL128. Norwegian Petroleum Directorate,http://factpages.npd.no/pbl/wellbore_documents/1732_6608_10_3_COMPLETION_REPORT_AND_LOG.pdf, Last accessed on 2019-06-12.

Statoil, 2001. PL 128 - Norne Field Reservoir Management Plan.

Statoil ASA, 2004. Report: Annual reservoir development plan Norne and Urd field. Norwegian Petroleum Directorate.

Statoil ASA, 2006. Report: Annual reservoir development plan Norne and Urd field. Norwegian Petroleum Directorate.

Stewart, R. R., Huddleston, P. D., Kan, T. K., 1984. Seismic versus sonic velocities: A vertical seismic profiling study. Geophysics 49 (8), 1153–1168, https://doi.org/10.1190/1.1441745.

Swiecicki, T., Gibbs, P. B., Farrow, G. E., Coward, M. P., 1998. A tectonostratigraphic framework for the Mid-Norway region. Marine and Petroleum Geology 15, 245–276, https://doi.org/10.1016/S0264-8172(97)00029-9.

Telford, W. M., Geldart, L. P., Sheriff, R. E., 1990. Applied Geophysics, 2nd Edition. Cambridge University Press, https://doi.org/10.1017/CBO9781139167932.

Tura, A., Lumley, D., 1999. Estimating Pressure and Saturation Changes from Time Lapse AVO Data. SEG Technical Program Expanded Abstracts, 1655–1658, https://doi.org/10.4043/12130-MS.

Verlo, S. B., Hetland, M., 2008. Development of a field case with real production and 4D data from the Norne Field as a benchmark case for future reservoir simulation model testing. Master's thesis, Norwegian University of Science and Technology, Norway, Trondheim.

Wang, Z. Z., 2001. Fundamentals of seismic rock physics. Geophysics 66 (2), 398–412, https://doi.org/10.1190/1.1444931.

WesternGeco, 2007. Data processing report for Statoil block 6608/10 (Norne) ST0113, ST0103, ST0305, ST0409, ST0603 2006 4D processing.

White, R. E.and Simm, R., 2003. Tutorial: Good practice in well ties. First Break 21, 75–83.

Yilmaz, Ö., 2012. Chapter 1 - Fundamentals of Signal Processing. In: Seismic Data Analysis. Society of Exploration Geophysicists, pp. 25–158, https://doi.org/10.1190/1.9781560801580.ch1.

Appendix A

# Processing Flows

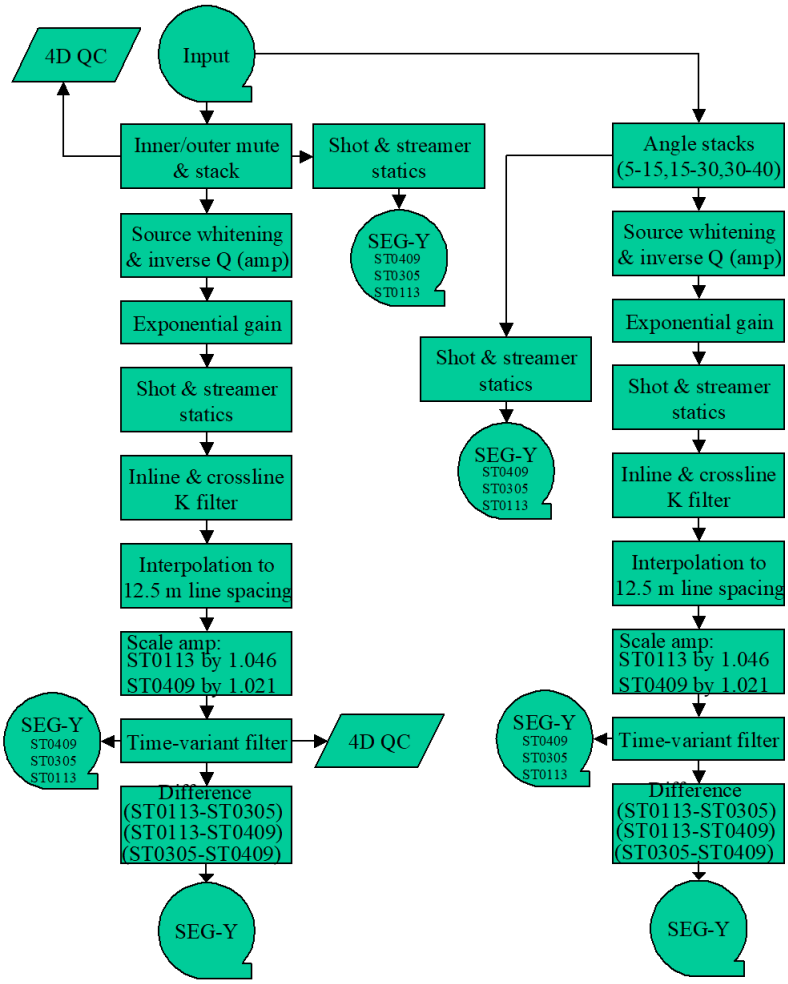


**Figure A.1:** The post-stack portion of the full seismic processing flow (WesternGeco, 2007)

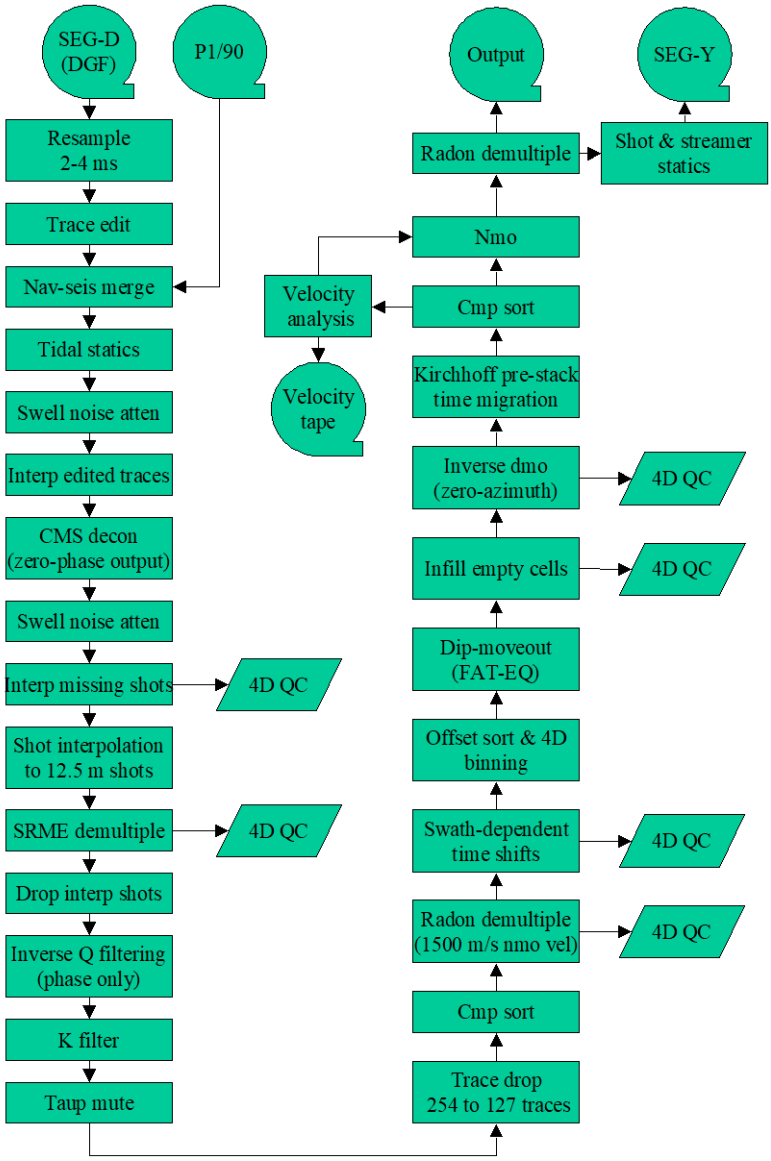


**Figure A.2:** The pre-stack portion of the full seismic processing flow (WesternGeco, 2007)

Appendix B

# Method 1: Time-shift and relative time-shift maps

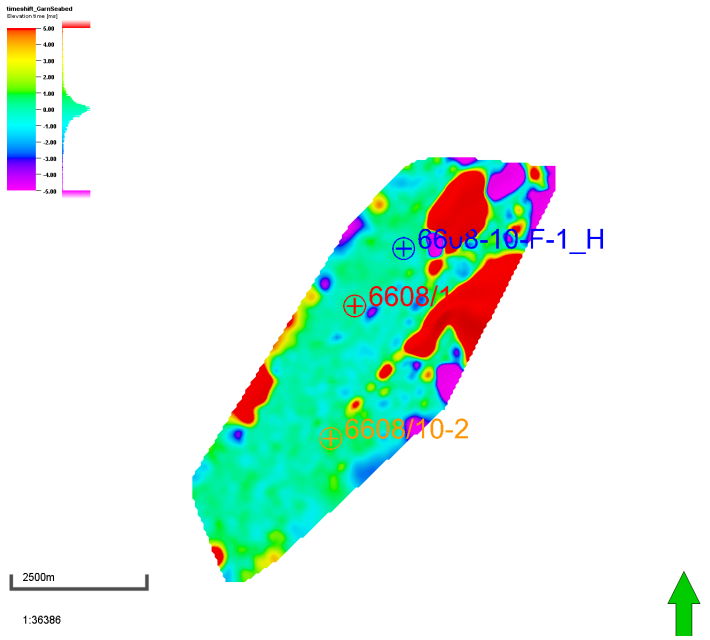


**Figure B.1:** Time-shift map generated using Method 1 from seabed down to Top Garn Fm. Big red and purple blobs show the noisy areas, which are introduced to the maps due to interpretation uncertainty. Small travel-time changes can be noted close to well locations, indicated by blue/light blue colors for negative time-shifts, and green/yellow colors for positive time-shifts

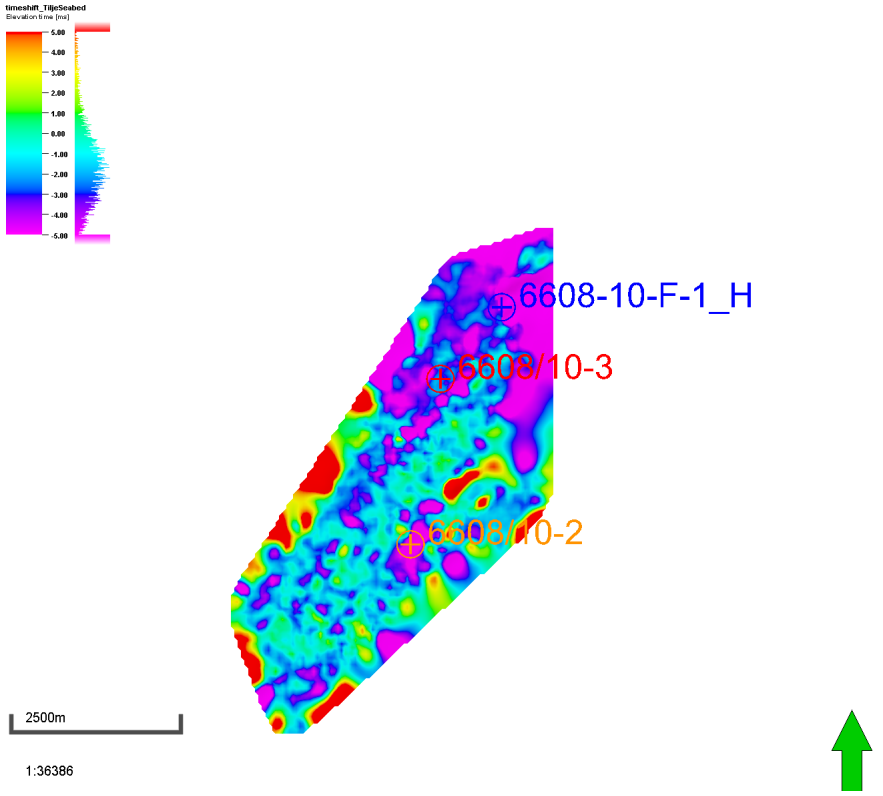


**Figure B.2:** Time-shift map generated using Method 1 from seabed down to Top Tilje Fm. Big red and purple blobs show the noisy areas, which are introduced to the maps due to interpretation uncertainty. Small travel-time changes can be noted close to well locations, indicated by blue/light blue colors for negative time-shifts, and green/yellow colors for positive time-shifts

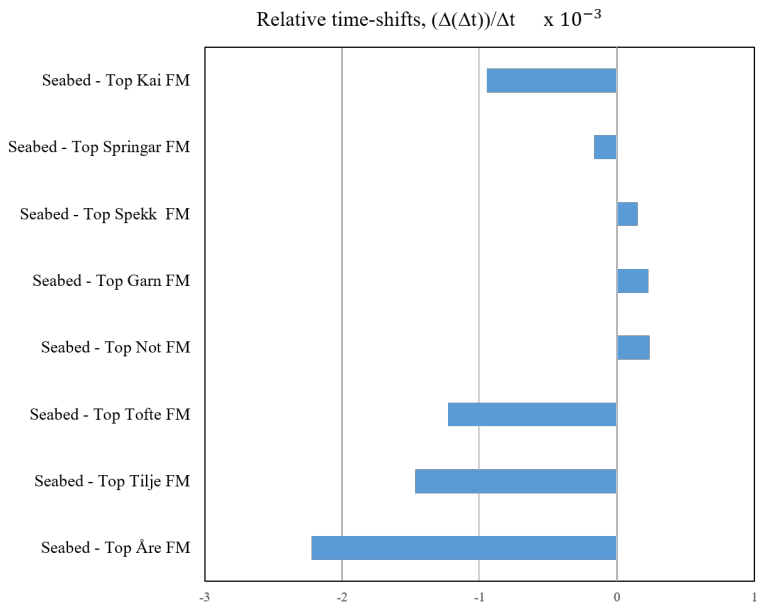


**Figure B.3:** Relative time-shift values, calculated using Method 1, for the intervals between seabed and top of each interpreted horizon in well 6608/10-3

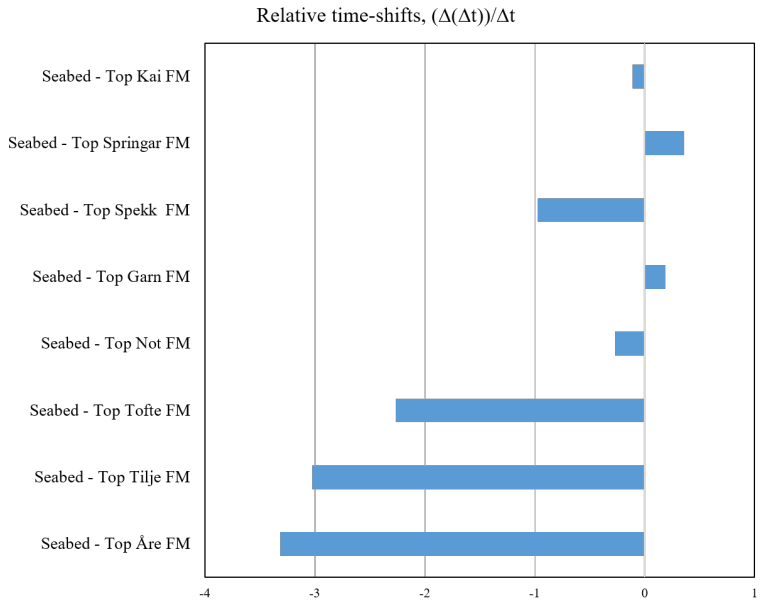


**Figure B.4:** Relative time-shift values, calculated using Method 1, for the intervals between seabed and top of each interpreted horizon in well 6608/10-2

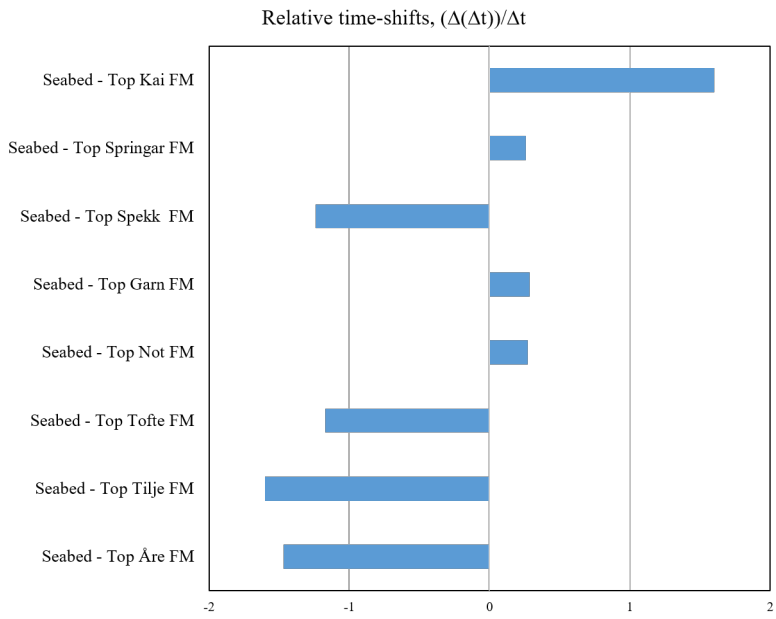


**Figure B.5:** Relative time-shift values, calculated using Method 1, for the intervals between seabed and top of each interpreted horizon in well 6608/10-F-1H

Appendix C

# Method 2: Time-shift and relative time-shift maps

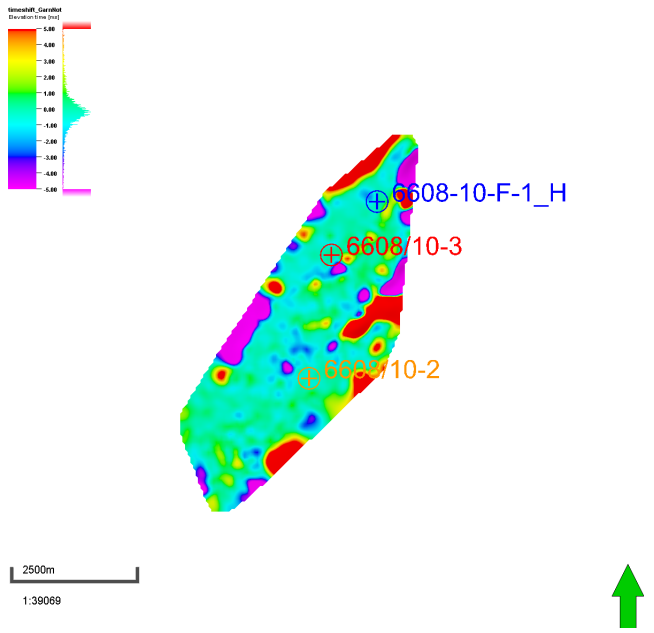


**Figure C.1:** Time-shift map generated using Method 2 for the interval between Top Garn Fm and Top Not Fm. Big red and purple blobs show the noisy areas, which are introduced to the maps due to interpretation uncertainty. Small travel-time changes can be noted close to well locations, indicated by blue/light blue colors for negative time-shifts, and green/yellow colors for positive time-shifts

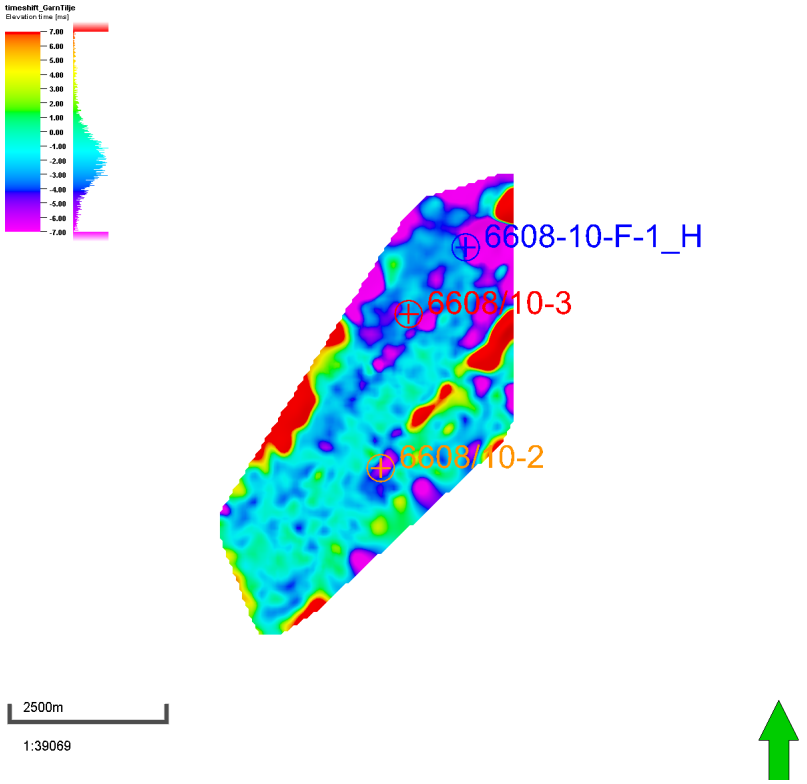


**Figure C.2:** Time-shift map generated using Method 2 for the interval between Top Garn Fm and Top Tilje Fm. Big red and purple blobs show the noisy areas, which are introduced to the maps due to interpretation uncertainty. Small travel-time changes can be noted close to well locations, indicated by blue/light blue colors for negative time-shifts, and green/yellow colors for positive time-shifts

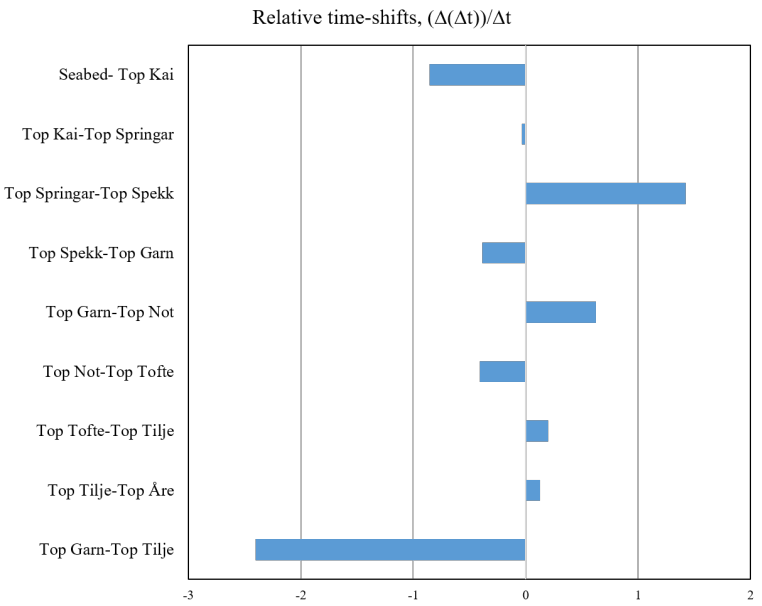


**Figure C.3:** Relative time-shift values, calculated using Method 2, for the intervals between individual horizons in well 6608/10-3

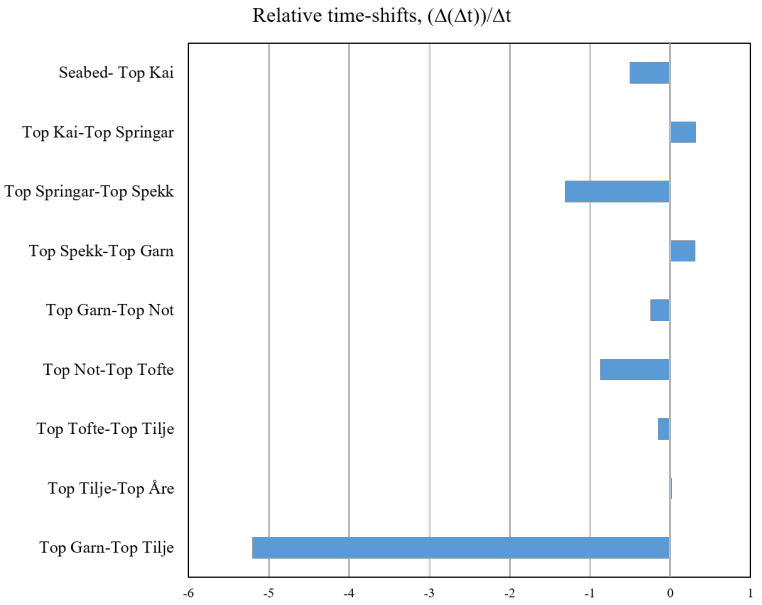


**Figure C.4:** Relative time-shift values, calculated using Method 2, for the intervals between individual horizons in well 6608/10-2

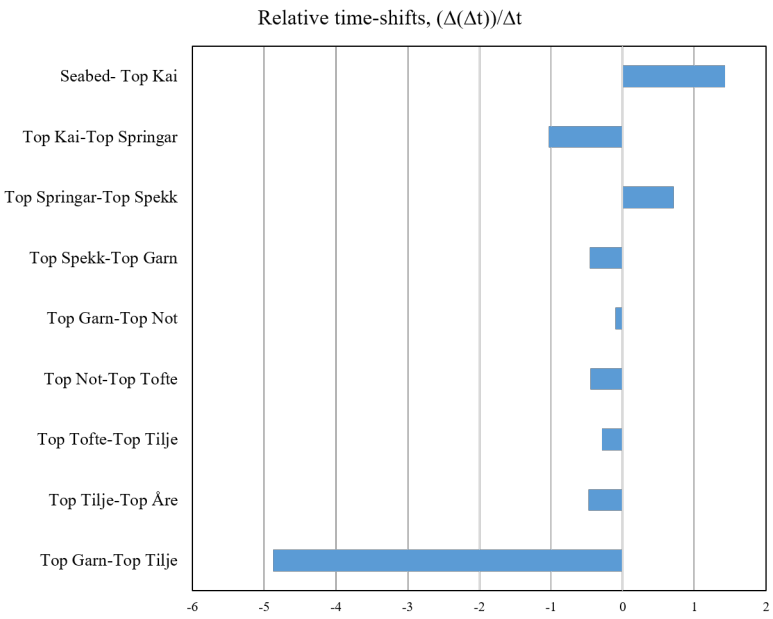


**Figure C.5:** Relative time-shift values, calculated using Method 2, for the intervals between individual horizons in well 6608/10-F-1H

Appendix D

# Cross-correlation time-shift maps

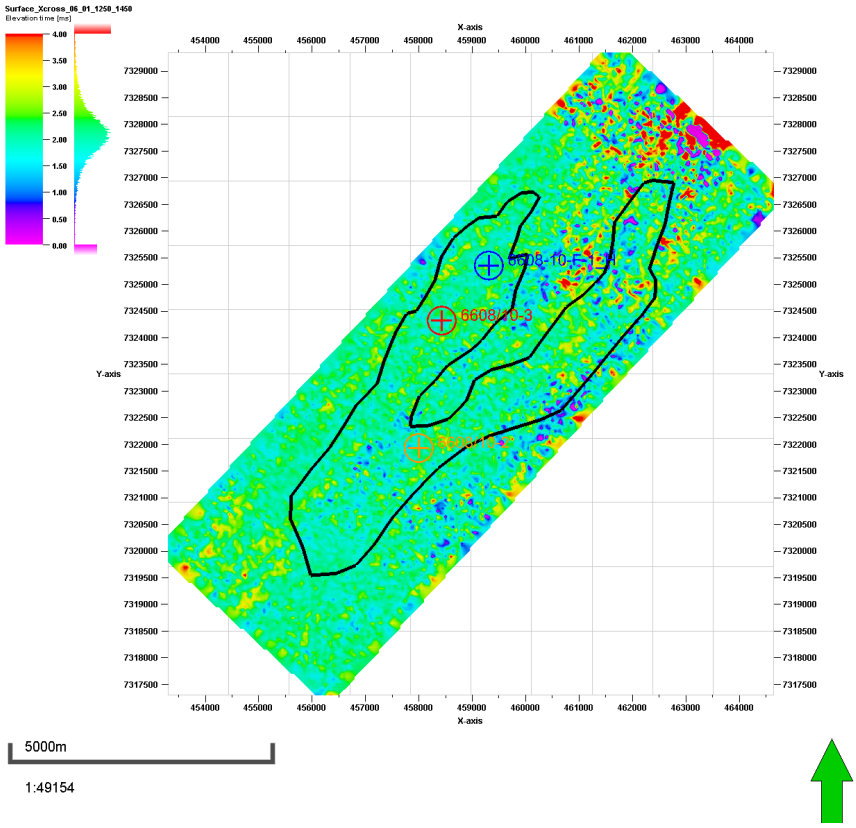


**Figure D.2:** Top view of time-shift map at 1350 ms level (approximately Top Kai Fm) generated using cross-correlation technique. Black coloured line delineates the reservoir shape

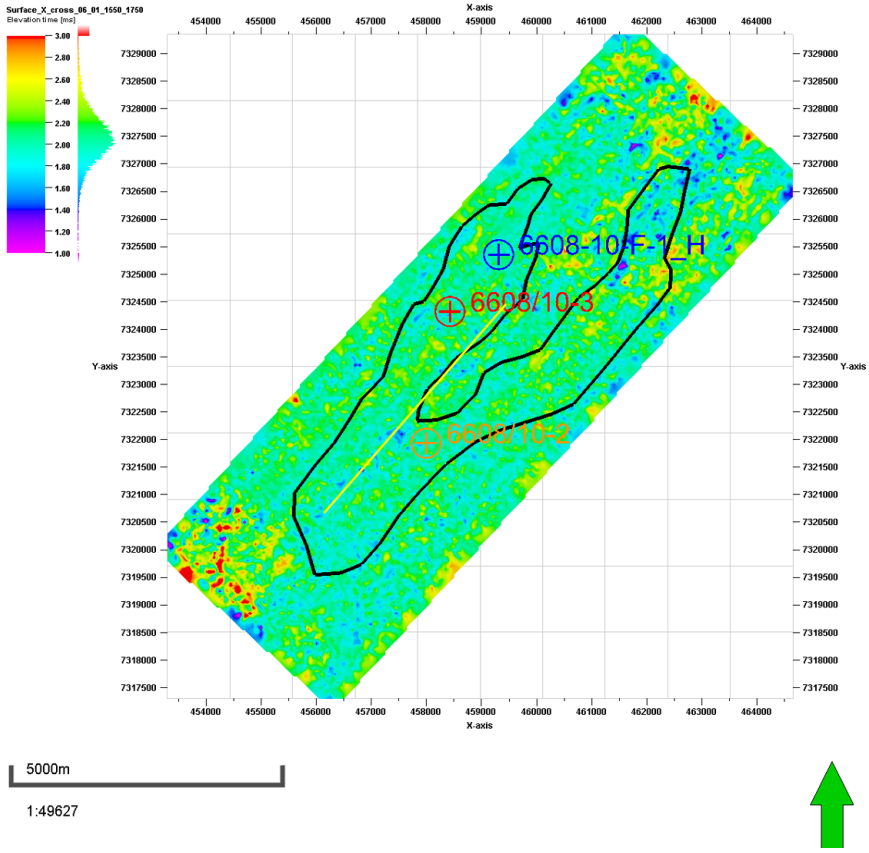


**Figure D.3:** Top view of time-shift map at 1650 ms level (faulted area) generated using cross-correlation technique. Black coloured line delineates the reservoir shape

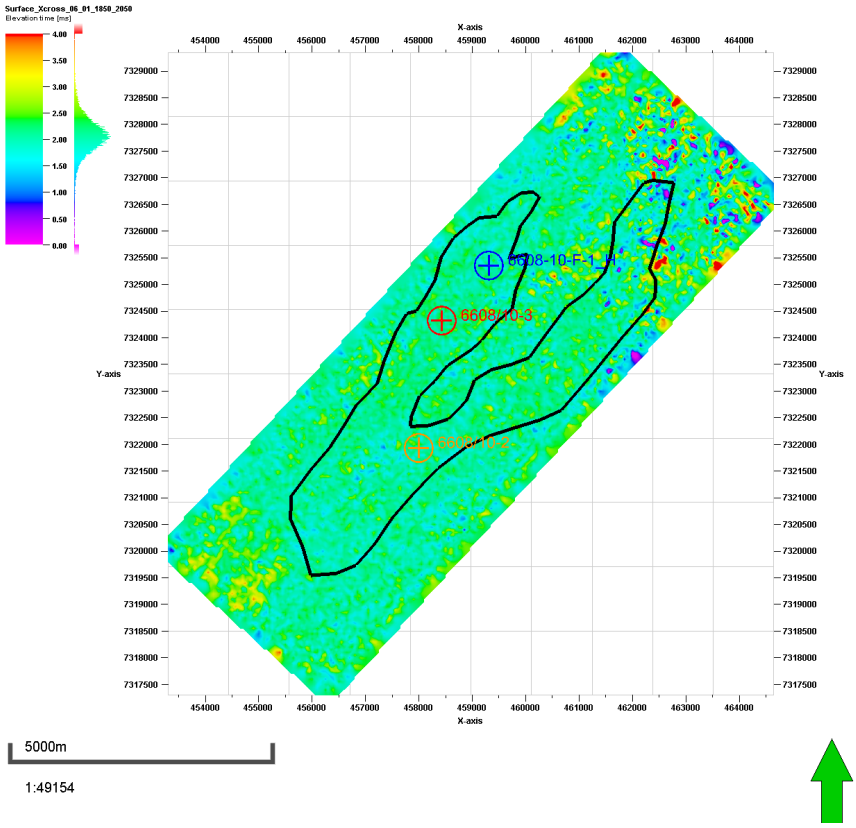


**Figure D.4:** Top view of time-shift map at 1950 ms level generated using cross-correlation technique. Black coloured line delineates the reservoir shape

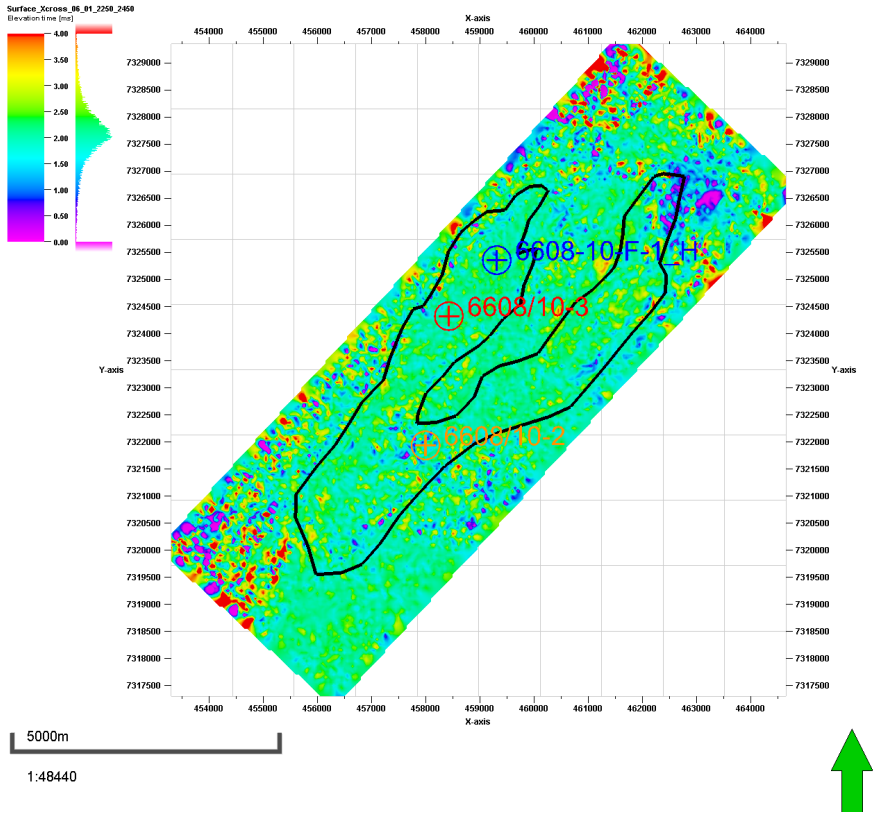


**Figure D.5:** Top view of time-shift map at 2350 ms level generated using cross-correlation technique. Black coloured line delineates the reservoir shape